ESA CONTRACT REPORT

Contract Report to the European Space Agency

Impact of EarthCARE products on Numerical Weather Prediction

July 2004

Author: Marta Janisková

Contributors: Angela Benedetti, Jean-Jacques Morcrette and Adrian M. Tompkins

Final report for ESA contract 15740/01/NL/GS

ESA Study Manager: J. Pedro V. Poiares Baptista

ECMWF
Shinfield Park
Reading
RG2 9AX
United Kingdom

For additional copes please contact: library@ecmwf.int

Series: ECMWF - ESA Contract Report

A full list of ECMWF Publications can be found on our web site under:
http://www.ecmwf.int/publications/

Contract Report to the European Space Agency

Impact of EarthCARE products on Numerical Weather Prediction

Author: Marta Janisková

*Contributors: Angela Benedetti, Jean-Jacques Morcrette
and Adrian M. Tompkins*

Final report for ESA contract 15740/01/NL/GS
ESA Study Manager: J. Pedro V. Poiares Baptista

European Centre for Medium-Range Weather Forecasts
Shinfield Park, Reading, Berkshire, UK

July 2004

Contents

Abstract

The ability of the numerical weather prediction (NWP) models to provide reliable forecasts depends on the quality of initial conditions, or analyses, as well as model deficiencies. While objective forecasting skill has improved at least one day per decade, the detailed prediction of weather parameters such as precipitation and cloud cover is less impressive and still subject to inaccurate description of the moist processes and their specification in the initial conditions for forecast.

More comprehensive evaluations of cloud-radiation interactions in NWP models with the aim of their improvements require consistent measurements of radiative fluxes, cloud fraction coverage, vertical structure of clouds and cloud/water ice contents within future satellite missions. The performance of the ECMWF model, including various model changes related to clouds and radiation, are discussed to illustrate the need for complementary datasets such as those proposed by the Earth Clouds, Aerosols and Radiation Explorer (EarthCARE). The data will be invaluable source of information for model validation, the improvement of physical parametrizations, and could be used as an input for data assimilation systems and their development.

Despite the major influence of clouds on the atmospheric water and energy balance, there is still no explicit cloud analysis in global systems. The cloud contribution to the satellite radiances is removed from the assimilation systems. The main reason lies in the difficulty to observe and model cloud variability in time and space. However, with the recent improvements in the representation of clouds and flexible data analysis systems (such as three- and four-dimensional variational assimilation - 3D-Var, 4D-Var), it is becoming possible to assimilate observations in cloudy situations.

An important step in the development of the assimilation of cloud-affected observations is introducing the cloud-radiation processes in the assimilating model. In addition to the existing linearized radiation model, a new diagnostic cloud scheme, which retains the most important features of the ECMWF nonlinear prognostic cloud scheme, while removing much of the complexity and many discrete transitions, has been developed together with its tangent-linear and adjoint versions. The new scheme improves on the current assimilation scheme for many aspects such as cloud cover and ice water content, both in the tropics and mid-latitudes, and precipitation in the tropics. The inclusion of this more complex cloud scheme within the existing linearized parametrizations improves the accuracy of the tangent-linear approximation. With its physical link between cloud properties and the thermodynamical control variables of temperature and humidity, the new scheme provides the opportunity to develop a system which can assimilate both cloud and precipitation observations.

One-dimensional variational (1D-Var) system have been used for preliminary studies on the 4D-Var of cloud related observations. 1D-Var experiments have been carried out using observations from the Atmospheric Radiation Measurement (ARM) Programme sites in order to show ability of 1D-Var to modify the model profiles of temperature and humidity when using measurements of both cloud properties and radiative fluxes. Another purpose of the study has been to examine the behaviour of the new parametrizations of moist atmospheric processes in 1D-Var assimilation and to assess situations when convective clouds are dominant.

Sensitivity of the radiation schemes to the temperature, humidity and cloud properties has been investigated using the adjoint technique. The study shows which variables can be modified when certain observations of the TOA radiation fluxes are used in data assimilation. It also indicates the vertical extent of the influence of such observations.

1 Introduction

Difficulties in representing clouds and aerosols in the Numerical Weather Prediction (NWP) models influence the quality of weather forecasts. Clouds are known to play a major role in the water and energy budgets of the Earth's atmosphere. In the NWP models, they are used to calculate the vertical profiles of solar and radiative heating, as well as the distribution of precipitation. The radiative properties of clouds and their ability to produce precipitation is also controlled by aerosols. Since the global models cannot resolve individual clouds explicitly, physical processes describing the formation and dissipation of clouds are implicitly taken into account through parametrization schemes. Passive remote sensing provides some information on the geographical distribution of clouds, aerosols and radiation, but very limited information on the vertical structure. Different models can usually adjust the radiative fluxes at the top of atmosphere to agree with satellite observations, but this is achieved through quite different vertical distributions of cloud. Therefore vertically resolved observations of clouds are needed for an evaluation of the parametrization of cloud processes and cloud-aerosol-radiation interactions in order to improve parametrization schemes of the models and consequently their ability to provide reliable weather forecasts.

In recent years, much effort at ECMWF has been put into improvement of physical parametrizations of the model and several studies have assessed the ECMWF model in simulating cloud related features of the atmosphere (Miller *et al.* 1999, Beesley *et al.* 2000, Chevallier *et al.* 2001, Hogan *et al.* 2001, Webb *et al.* 2001, Chevallier and Kelly 2002, Jakob 2002, Morcrette 2002, Teixeira and Hogan 2002, Tompkins 2002, Chevallier and Bauer 2003, Jung and Tompkins 2003, Lalaurette *et al.* 2003). The studies used a variety of observational sources, but mostly satellite observations (ERBE[1], CERES[2], ISCCP[3], ATOVS[4], SSM/I[5]) that only give TOA fluxes, total cloud cover and optical thickness, but cannot provide sufficiently accurate determination of cloud profiles and consequently heating profiles. Only few of those studies used measurements related to the vertical structure of clouds, but only over a number of limited locations (a few days from the LITE[6], the cloud radar measurements at Chilbolton, at the ARM[7] programme sites), since there are no such global observations available. However, the vertical profiles are important in controlling the radiative transfer processes in the atmosphere and in the simulations of clouds and their radiative effects. Despite the significant improvements in the description of cloud-radiation processes in the recent versions of the ECMWF operational model, a number of problematic aspects was identified. In order to deal with those problems and to improve the quality of forecast, a better description of the structure of the clouds compared to the current network is required. Such information will be available from the future satellite missions (EarthCARE[8], CloudSat, CALIPSO[9]).

A large part of forecasting deficiencies is connected with the imperfect assimilation of available observational data in the numerical prediction process. Accurate initial conditions required by NWP models rely on the quality of the observations and the quality of the assimilation schemes. Pressure, temperature, water vapour and wind information from conventional and satellite observations have been operationally assimilated at global NWP centres for a long time. Despite the major influence of clouds on the atmospheric water and energy balance, there is still no explicit cloud analysis in global systems. The cloud contribution to the satellite radiances is removed from the assimilation systems. In some meso-scale models, cloud analyses based on nudging techniques have been introduced (e.g. Macpherson *et al.* 1996, Lipton and Modica 1996, Bayler *et al.* 2000).

---

[1] Earth Radiation Budget Experiment
[2] Cloud and the Earth's Radiant Energy System
[3] International Satellite Cloud Climatology Project
[4] Advanced TIROS (Television Infrared Observation Satellite) Operational Vertical Sounder
[5] Special Sensor Microwave Imager
[6] Lidar In-space Technology Experiment
[7] Atmospheric Radiation Measurement
[8] Earth Clouds, Aerosols and Radiation Explorer
[9] Cloud-Aerosol Lidar and Infrared Pathfinder Satellite Observations

The main reason why global analysis systems do not include cloud information is that cloud processes contain small spatial and temporal scales not explicitly described by NWP models. These make it difficult to observe and model cloud variability in time and space. However, with the recent improvements in the representation of clouds and flexible data analysis systems (such as three- and four-dimensional variational assimilation - 3D-Var, 4D-Var), it is becoming possible to assimilate observations in cloudy situations. More accurate description of the structure of clouds will be provided by future satellite missions, among them EarthCARE. The inclusion of cloud observations in data assimilation should lead to an improved initial state of the dynamical and thermodynamical variables linked to the generation and dissipation of the clouds, which could in turn improve the quality of the forecasts.

The EarthCARE mission (European Space Agency 2004) has been specifically defined with the basic objective of improving the understanding of cloud-aerosol-radiation interactions so as to include them correctly and reliably in climate and numerical weather prediction models. The scientific objectives are:

- the observation of cloud distribution (cloud overlap), cloud-precipitation interactions and the characteristics of vertical motions within clouds;
- the observation of the vertical distributions of atmospheric liquid water and ice on a global scale, their transport by clouds and their radiative impact;
- the observation of the vertical profiles of natural and anthropogenic aerosols on a global scale, their radiative properties and interaction with clouds; and
- the retrieval of profiles of atmospheric radiative heating and cooling through the combination of the retrieved aerosol and cloud properties.

EarthCARE will meet these objectives by measuring simultaneously the vertical structure and horizontal distribution of cloud and aerosol fields together with outgoing radiation over all climate zones, having all instruments on a single satellite platform. The profile information can only be provided by active instruments, a lidar for aerosols and thin clouds and a high frequency (94GHz) Doppler radar for clouds. A multi-spectral imager is required to provide additional geographical coverage of aerosol and cloud optical property retrievals and a broad-band radiometer is required to measure radiances and to derive fluxes. A set of observations provided by EarthCARE will be then unique and will have a wide range of applications. It will be used for an improved understanding of energy and water fluxes in the atmosphere and of the mutual interactions of clouds, aerosols and radiation. This in turn will have direct application in improving numerical models for operational weather forecasting and for climate prediction. EarthCARE data will represent an important source of information for model validation, the improvement of physical parameterizations, and could be used as input for data assimilation systems and their development.

In this report evidence is given on the potential importance of EarthCARE like observations for NWP, together with the development and experimentation in order to be able to assimilate these data.

The recent changes related to cloud and radiation parametrizations in the ECMWF model are briefly described in Section 2. An assessment of the ECMWF model in simulating cloud related features is also given using several observational sources and a wide range of operational forecasts and research experiments.

In recent years, four-dimensional variational (4D-Var) data assimilation has become a powerful tool in transferring information from the irregularly distributed observations into initial conditions for a numerical forecast model. At ECMWF, 4D-Var system with incremental formulation (Courtier *et al.* 1994) is used operationally since November 1997 (Rabier *et al.*, 2000; Mahfouf and Rabier, 2000). This data assimilation system is flexible enough to allow the inclusion of new types of observations. The assimilation of cloud properties and radiation observations (cloudy radiances and radiative fluxes) requires a cloud scheme and a radiative transfer model as relevant observation operators defining the model counterpart of observations in the variational data

assimilation system. Moreover, an efficient computation of the gradient of the objective function during the minimization requires the linearized (tangent-linear and adjoint) versions of both the observation operators and the forecast model. The linearized radiation model has been developed during the previous ESA[10] contract (Janisková 2001, Janisková *et al.* 2002a). In the operational ECMWF data assimilation system, this radiation model is still combined with the linearized version of the simple diagnostic cloud scheme (Slingo 1987), which has a number of weaknesses preventing the assimilation of cloud related observations. To improve the description of cloud processes in the linearized model, a new scheme, which retains the most important features of the ECMWF nonlinear prognostic cloud scheme, while removing much of the complexity and many discrete transitions, has been developed together with the tangent-linear and adjoint versions (Tompkins and Janisková 2004). This scheme is described in Section 3. The section also provides a validation of the nonlinear version of the scheme, an examination of the accuracy of the linearization of the new scheme and an evaluation of impact of including this scheme into the existing linearized physical package.

Section 4 describes one-dimensional variational (1D-Var) experiments which have been carried out using observations from the ARM Programme sites. The aim of these studies is to show ability of 1D-Var to modify the model profiles of temperature and humidity when using measurements of both cloud properties and radiative fluxes. Another purpose of the study has been to examine behaviour of the developed parametrizations of moist atmospheric processes (convection scheme - Lopez and Moreau 2004, cloud scheme - Tompkins and Janisková 2004) in 1D-Var assimilation of such observations and to assess situations when convective clouds are dominant.

A sensitivity of the radiation schemes to the temperature, humidity and cloud properties has been investigated using the adjoint technique in Section 5. This study provides information on the meteorological variables to which the radiation schemes are the most sensitive. It also shows which variables would be modified and over which vertical extent, if observations of the top of atmosphere (TOA) radiation fluxes were used in data assimilation.

---

[10]European Space Agency

2   Cloud and radiation processes in the ECMWF forecast model and their validation

The current operational forecast model describes the state of the atmosphere in spectral space up to wavenumber 511 corresponding to a grid-length of about 40 km. It uses a semi-Lagrangian advection scheme together with a linear Gaussian grid. The vertical dimension is discretized over 60 layers using a hybrid coordinate.

The physical package is based on Gregory *et al.* (2000). Two prognostic equations describe the time evolution of cloud condensate and cloud fraction in the prognostic cloud scheme initially developed by Tiedtke (1993). The modifications to the original formulation of this scheme are given by Jakob and Klein (2000) and Jakob (2000). The broadband radiation scheme includes the Rapid Radiative Transfer Model (RRTM; Mlawer *et al.* 1997, Morcrette 1998,Morcrette *et al.* 1998) for the infrared and the Fouquart and Bonnel (1980) scheme (with six spectral bands) for the shortwave radiation. At the surface, the Tiled ECMWF Scheme for Surface Exchange over Land (TESSEL) described by van den Hurk *et al.* (2000) is used.

2.1   The radiation schemes

The shortwave radiation scheme was originally developed by Fouquart and Bonnel (1980) and subsequently revised by Morcrette (1991) for use in the ECMWF model. It uses the photon-path-distribution method to separate the parametrization of the scattering processes from that of molecular absorption. Upward and downward fluxes are obtained from the clear sky and cloudy reflectances and transmittances of the atmospheric layers. To perform the spectral integration, the solar spectral interval is discretized into subintervals in which the surface reflectance is considered as constant. The cloud optical properties are based on Ebert and Curry (1992) for ice clouds and on Fouquart (1987) and Smith and Shi (1992) for water clouds. All cloudy fluxes are computed from cloud optical thicknesses derived from the liquid and ice cloud water content weighted by a 0.7 inhomogeneity factor following Tiedtke (1996). The shortwave radiation scheme was modified to increase the spectral resolution. The model used four spectral intervals with transmission functions based on statistical models. This was replaced by a six band code using transmission functions derived from a line-by-line code (Dubuisson *et al.* 1996). Part of the requirement for a new scheme stemmed from an earlier change in model vertical resolution, which raised the model top from 10 to 0.2 hPa, and improvements in the surface scheme. The Rayleigh scattering optical thickness is now solar-zenith angle dependent and all optical properties have been recomputed for the six new bands.

The previous emissivity based longwave radiation scheme (Morcrette 1991) used at ECMWF has been replaced by the Rapid Radiation Transfer Model (RRTM; Mlawer *et al.* 1997) in June 2000. The scheme is based on a two-stream solution of the longwave transfer. The ECMWF version of the RRTM longwave radiation scheme (Morcrette *et al.* 1998) also includes a maximum-random overlap assumption but keeps the cloud fraction and cloud optical thickness as two separate quantities. In RRTM, the cloud optical thickness is defined as a function of spectrally varying mass absorption coefficients and relevant cloud water and ice paths. This quantity is then used within the actual cloudy fraction of the layer.

2.2   Cloud parametrization scheme

The ECMWF prognostic cloud scheme developed by Tiedtke (1993) was implemented in the operational model in April 1995. The scheme represents both stratiform and convective clouds, and their time evolution is defined through two large-scale budget equations for cloud water content and cloud fractional cover. This scheme links the formulation of clouds to large-scale ascent, diabatic cooling, boundary layer turbulence, and their dissipa-

tion to adiabatic and diabatic heating, turbulent mixing of cloud air with unsaturated environmental air, and precipitation processes. It is therefore strongly coupled to the other physical parametrizations described in the ECMWF model. Precipitation processes are represented differently for pure ice clouds and for mixed phase and pure water clouds. The rain and snow formed are removed from the atmospheric column immediately, but can evaporate and interact with the cloud water in the layers they pass through. The precipitation process in ice clouds is treated as a source for cloud ice in the layer below, whereas ice settling into clear-sky is converted into snowfall. For mixed phase and pure water clouds a parametrization describing the conversion of cloud droplets into raindrops is taken from Sundquist (1978). It represents both the collision process and the Bergeron-Findeisen mechanism. Evaporation of rain/snow is described by a scheme following Kessler (1969) and only takes place when the given mean relative humidity is below a threshold value. The new precipitation/evaporation method developed by Jakob and Klein (2000) explicitly accounts for the vertical distribution of cloud layers and allows the cloud overlap assumption to be applied consistently with the radiative computations.

In the last two years, the cloud scheme was extensively modified. The numerical implementation of the scheme was upgraded, such that all the cloud related processes (sources and sinks) are assumed to occur simultaneously in order to assure that no precipitation could form, if a process such as evaporation would remove all liquid water over a timestep. The new solution also ensures that the total water and moist static energy is conserved. A number of additional changes include the treatment of ice sedimentation, identified by Jakob (2002) as a key parametrization. This treatment was modified to assume that large ice particles fall according to Heymsfield and Donner (1990) with dependency on ice mixing ratio q_i as $V = Kq_i^{0.16}$, where the constant K assumes a reduced value of 2.3. Small ice particles are given a residual non-zero fall-speed of 0.15 m s^{-1}. Other cloud physics changes included the cloud top entrainment process which was reformulated in terms of total water and dry static energy, and solved implicitly. The cumulus subsidence-induced cloud water advection process was also implicitly solved, along with the cloud erosion by turbulent mixing term. Finally, changes were made in the way supersaturation was handled, which is now calculated at semi-Lagrangian arrival point profiles.

2.3 Validation of clouds and radiative fluxes at ECMWF

In recent years much effort at ECMWF has been put into the improvement of physical aspects of the model and several studies have assessed the ECMWF model in simulating cloud related features of the atmosphere. Systematic errors in the ECMWF forecasting system were recently described using a wide range of operational forecasts and research experiments in the study of Jung and Tompkins (2003).

2.3.1 Summary of the previous studies

There have been a number of detailed studies that have examined the cloud related parameters of the ECMWF model. The studies use a variety of observational sources. A recent summary by Lalaurette *et al.* (2003) shows a clear reduction in European cloud cover biases after the implementation of the Tiedtke (1993) scheme in 1995. International Satellite Cloud Climatology Project (ISCCP) cloud cover observations were used to validate the cloud cover in the ERA15 reanalysis by Jakob (1999), who identified an underestimation of summer-time cloud cover over Eurasia, extratropical oceans and also in stratocumulus regions in the range of 10 to 15 %, while cloud cover was too high in trade cumulus areas by about the same amount. The lack of stratocumulus is a common deficiency of many models (e.g. Teixeira and Hogan 2002, Tompkins 2002). Klein and Jakob (1999) pointed out the tendency of the ECMWF model to overestimate the optical depth of low clouds in mid-latitudes, while ice clouds appeared to be underrepresented. ISCCP data were also used in the study of Tselioudis and Jakob (2002), where the statistics was separated into different dynamical regimes for mid-latitudes clouds.

They found again a general overestimation of cloud optical depth, and associated underestimation in cloud cover, particularly in subsidence regimes. High clouds were too thick while the cloud top pressure was too low. Low cloud in subsidence regimes had too small cloud cover, and was optically too thick. Webb *et al.* (2001) also used ERBE and ISCCP data to highlight a lack of mid-level clouds in the Tropics.

In series of studies, Chevallier *et al.* (2001), Chevallier and Kelly (2002), and Chevallier and Bauer (2003) used model fields to simulate radiances observed by various satellite platforms, and concluded that generally cloud systems were correctly located in the short term forecasts. However, they highlighted an overestimation of cloud liquid water, especially in the Tropics, and an underestimation of ice, mainly in mid-latitudes. They again emphasized the lack of stratocumulus.

The ability of the short-term forecasts to correctly locate clouds was also identified by Mace *et al.* (1998), Klein and Jakob (1999), Miller *et al.* (1999), Hogan *et al.* (2001) and Morcrette (2002) using both space-borne lidar, ISCCP clouds and ground based radar observations. The studies have shown that cloud in mid-latitude winter is strongly dynamically forced, and the dynamical fields are well represented by the system.

2.3.2   *Influence of cloud and radiative processes in the recent model*

The systematic model errors of the ECMWF model have been recently examined for four month atmospheric climate runs in the study of Jung and Tompkins (2003), where an assessment of the ECMWF model in simulating cloud related features of the atmosphere has also been given. The integrations were carried out using the model cycle 26r1 (which was operational since 29 April 2003 up to October 2003) at resolution of T_L95L60 and covered the summer and winter seasons of 1987 and 1988 partly because of the availability of verification data. Here, the study of Jung and Tompkins (2003) is extended by showing statistics for one year experiments starting in August 2000, using a wider range of up-to-date observations. To give an indication of the improvements and changes in the cloud and radiation parameterizations, a comparison is made between the ERA-40 cycle 23r4, which became operational in June 2000, and the current cycle 28r1.

The model radiation diagnostics are compared to the top of the atmosphere (TOA) shortwave albedo and longwave net fluxes, which are both derived from Cloud and the Earth's Radiant Energy System (CERES) products (Wielicki *et al 1996*). The total cloud cover (TCC) is compared to the D2 product of ISCCP (Rossow and Schiffer 1991, Rossow and Garder 1993, Rossow and Schiffer 1999). Total column water vapour and liquid water path (LWP) amounts are compared to SSM/I retrievals (version 5 of Wentz 1997). No critique is made of the quality of the retrieved observations, which are simplicially assumed to represent "truth".

The first field to be examined is total cloud cover (Fig. 1) , which reveals a number of obvious problematic features. The cloud simulation for the period is the almost complete lack of stratocumulus clouds off the western coast of the Americas and Africa. Compared to he ISCCP D2 data, the cloud cover error exceeds 30 % in places, and is over 10 % for a significant region. Most of the mid-latitude winter hemisphere suffers from too little cloud. Note that in contrast to the earlier study (Jung and Tompkins 2003), the underestimation of the cloud cover over the Eurasian continent is much reduced. This highlights the danger of using just one or two seasons to validate the model climate. All these systematic biases in cloud cover were identified in the previous studies discussed above, indicating that the asymptotic biases also affect the short-term forecast performance. Although many alterations were made to the convective and cloud cover schemes between cycles 23r4 and 28r1, the cloud cover climate has not undergone substantial improvement. In fact, the underestimation in the south mid-latitudes and the stratocumulus regions has slightly deteriorated.

Retrievals for September 2000 from SSM/I are compared to the ensemble mean model for the liquid water path (Fig. 2). The liquid water path (LWP) biases with respect to SSM/I information are broadly consistent with the cloud cover comparison with ISCCP data, both in terms of geographical location and the sign of biases.
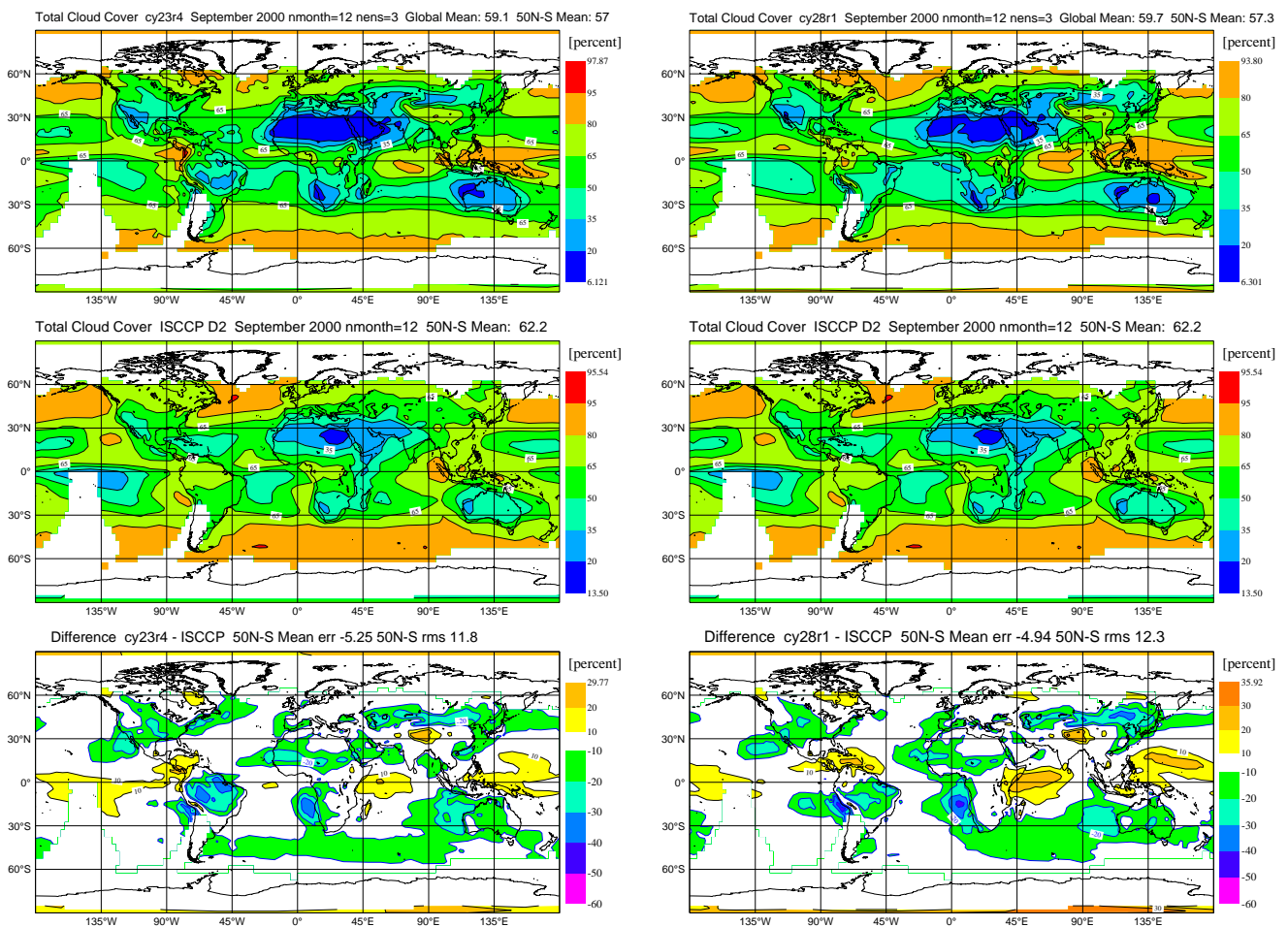
Figure 1: Mean cloud cover (%) for September 2000 for the model (upper panel), ISCCP observations (middle panel), and the difference between model and observations (lower panel). Left: results for the model cycle 23r4, right: results for the cycle 28r1.

Likewise the LWP is overestimated in the deep convection regions, while it is severely underestimated in the stratocumulus regions. The model fails to represent the contrast between the trade and stratocumulus regimes. However, comparing cycles 23r4 and 28r1 reveals a dramatic improvement over the past 2 years, with the excessive cloud water in the trades substantially reduced and the bias in mid latitudes also showing signs of improvement. In agreement with the cloud cover data though, it is possible to see that the stratocumulus regions have slightly deteriorated.

The TOA infrared fluxes are compared to CERES observations for September 2000 (Fig. 3-4). In agreement with the cloud cover and LWP statistics, the shortwave and longwave radiation budgets have also improved. In particular the decreased of total column liquid water in the trades led to an improved shortwave radiation budget (Fig.4). The infrared fluxes (Fig. 3) indicate that the Tropics and ocean regions are too opaque, consistent with the excessive cloud cover in these regions. On the other hand, the increase in deep convective activity over the tropical continents has led to a reduction in longwave radiation biases there.

Despite the significant improvements, a number of problematic aspects in the model climatology was noted. The description of stratocumulus clouds off the west coasts of the continents should be improved when the current dry mixing is replaced by a boundary layer scheme that is based on a moist, non-local parcel model
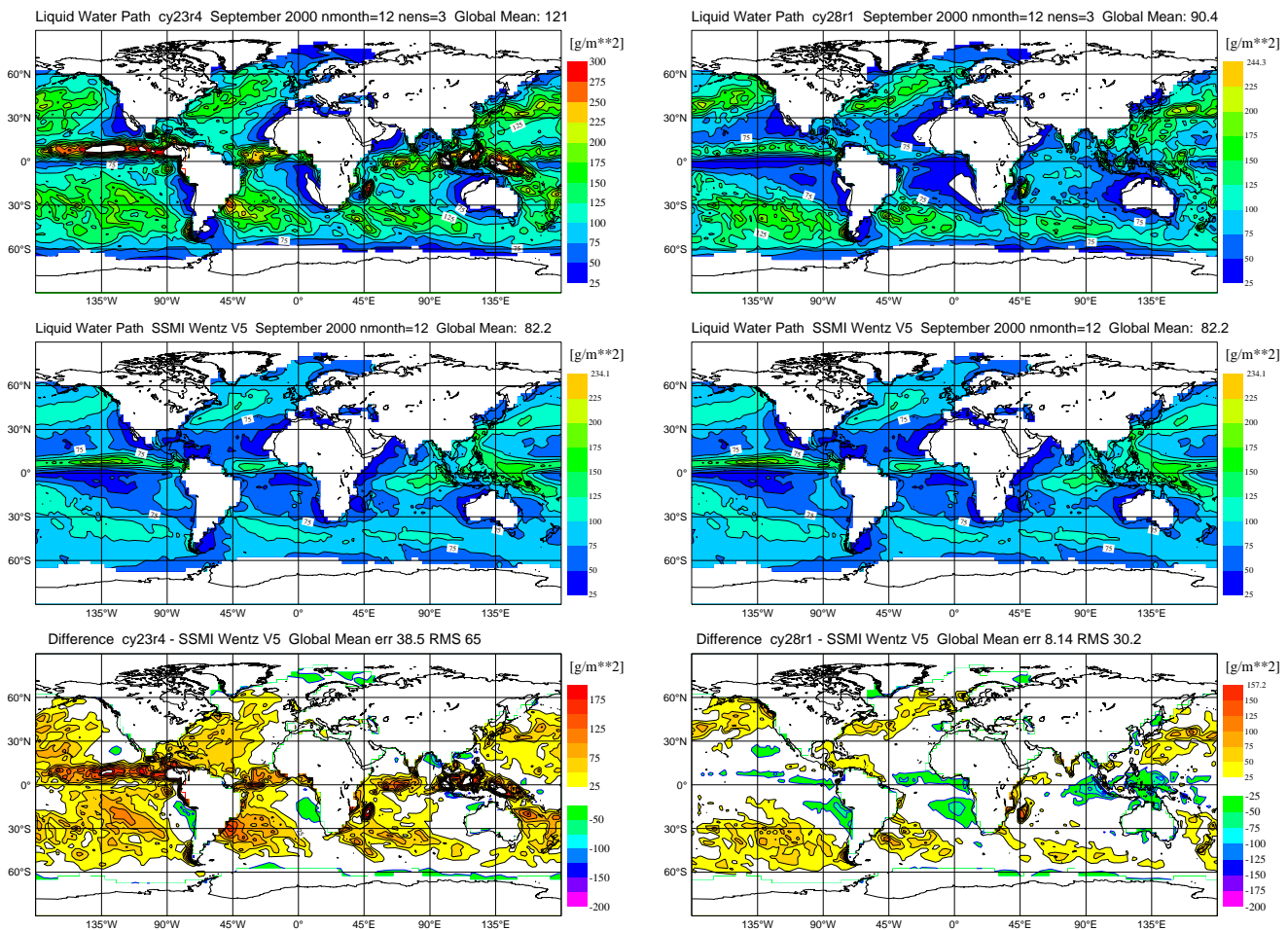
Figure 2: Cloud liquid water path (kg m^{-2}) for September 2000 for the model (upper panel), observations retrieved from SSM/I (middle panel), and the difference between model and observations (lower panel). Left: results for the model cycle 23r4, right: results for the cycle 28r1.

concept. The model cloud scheme is also under development to introduce a simple statistical framework to represent the subgrid fluctuations of humidity and their effect on cloud cover, and to combine this with a separate ice variables. This will hopefully allow the mid-latitude climate to be improved. In order to allow more comprehensive evaluations of cloud-radiation interactions in NWP models, and hence to improve their parametrization, it is important that future satellite missions will generate consistent measurements of radiative fluxes, cloud fractional coverage and cloud water/ice contents.

2.3.3   Comparisons with field experiments datasets

In the previous section, the validation of the cloud parametrizations in global circulation models has been done against the satellite observations that only give TOA fluxes, total cloud cover and optical thickness, but cannot provide sufficiently accurate determination of cloud profiles and consequently energy heating profiles. There are no such global datasets, which would simultaneously provide the vertical profiles of clouds and aerosol characteristics together with vertical temperature and humidity profiles and the TOA radiances. However, the vertical profiles are important in controlling the radiative transfer processes in the atmosphere and in the simulations of clouds and their radiative effects.
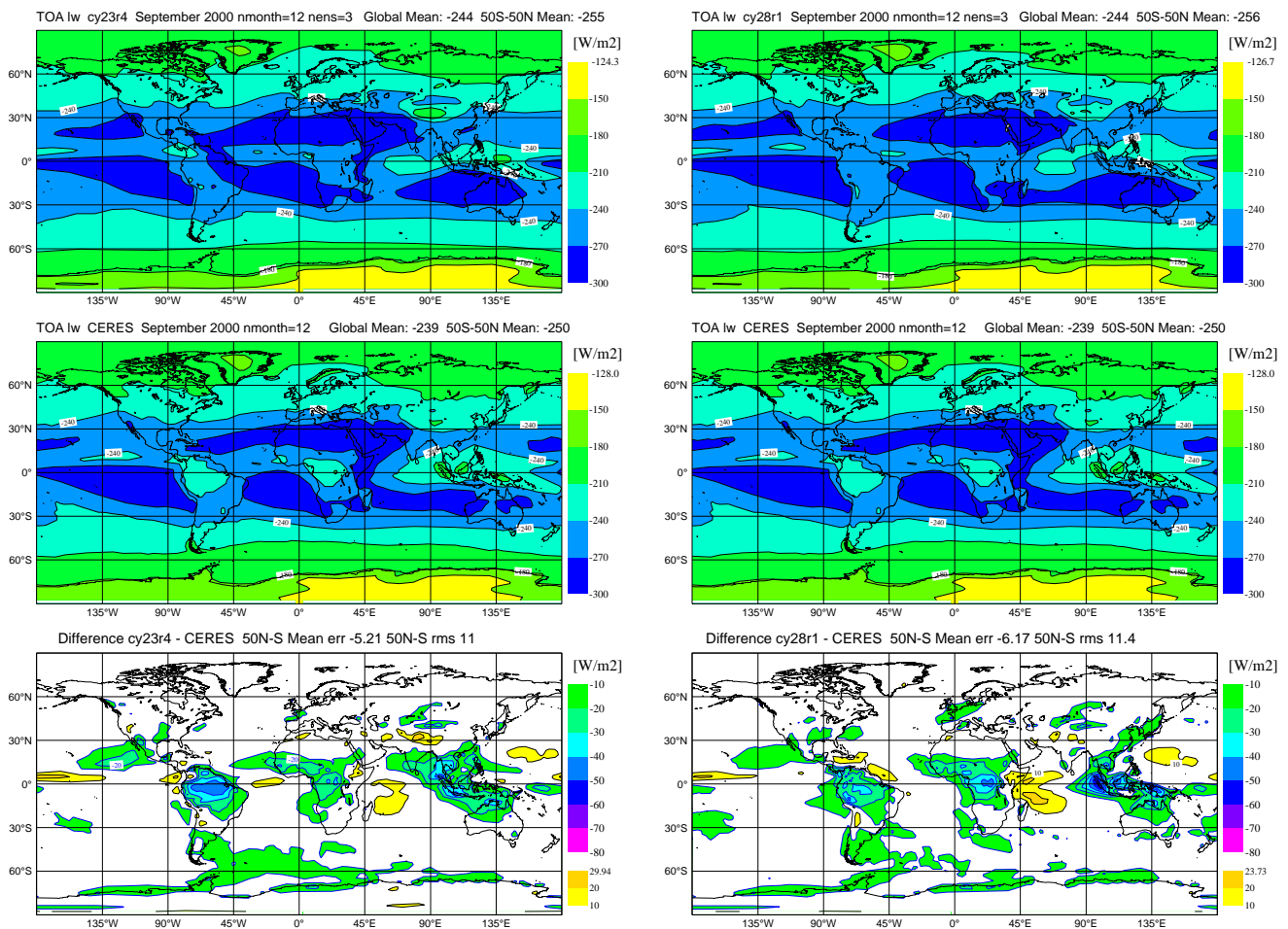
Figure 3: Outgoing longwave radiation ($W\ m^{-2}$) for September 2000 based on the model (upper panel) and CERES estimates (middle panel) along with differences between the model and observational data (lower panel). Left: results for the model cycle 23r4, right: results for the cycle 28r1.

The vertical structure of clouds is only available from the specific field experiment datasets, as those of the Atmospheric Radiation Measurement (ARM) programme and of the CloudNET project collecting data from the different sites with the cloud radar measurements (Chilbolton, Cabauw, Palaiseau). The regular comparison of the different models, among them also of the ECMWF forecast model, is being done by the CloudNET project. Figure 5 (obtained from the web page - http://www.met.rdg.ac.uk/radar/cloudnet/quicklooks/index.html) shows a comparison of cloud cover derived from a 94 GHz radar over Chilbolton (U.K.) during May and October 2003 with those from ECMWF short-range forecasts. It is evident that the model is able to correctly capture the major cloud events in those periods although errors in the details are clearly visible. This figure shows the potential of the use of space-borne radar to derive vertical cloud fraction distributions for model comparison.

The above comparisons of the model to data are only a small sample of the possibilities that both the new remotely sensed data and the short-range forecast approach to evaluation of model clouds could provide . This approach will gain importance with the use of data provided by space-borne radar systems which will form part of missions, as CloudSat, CALIPSO and also EarthCARE.
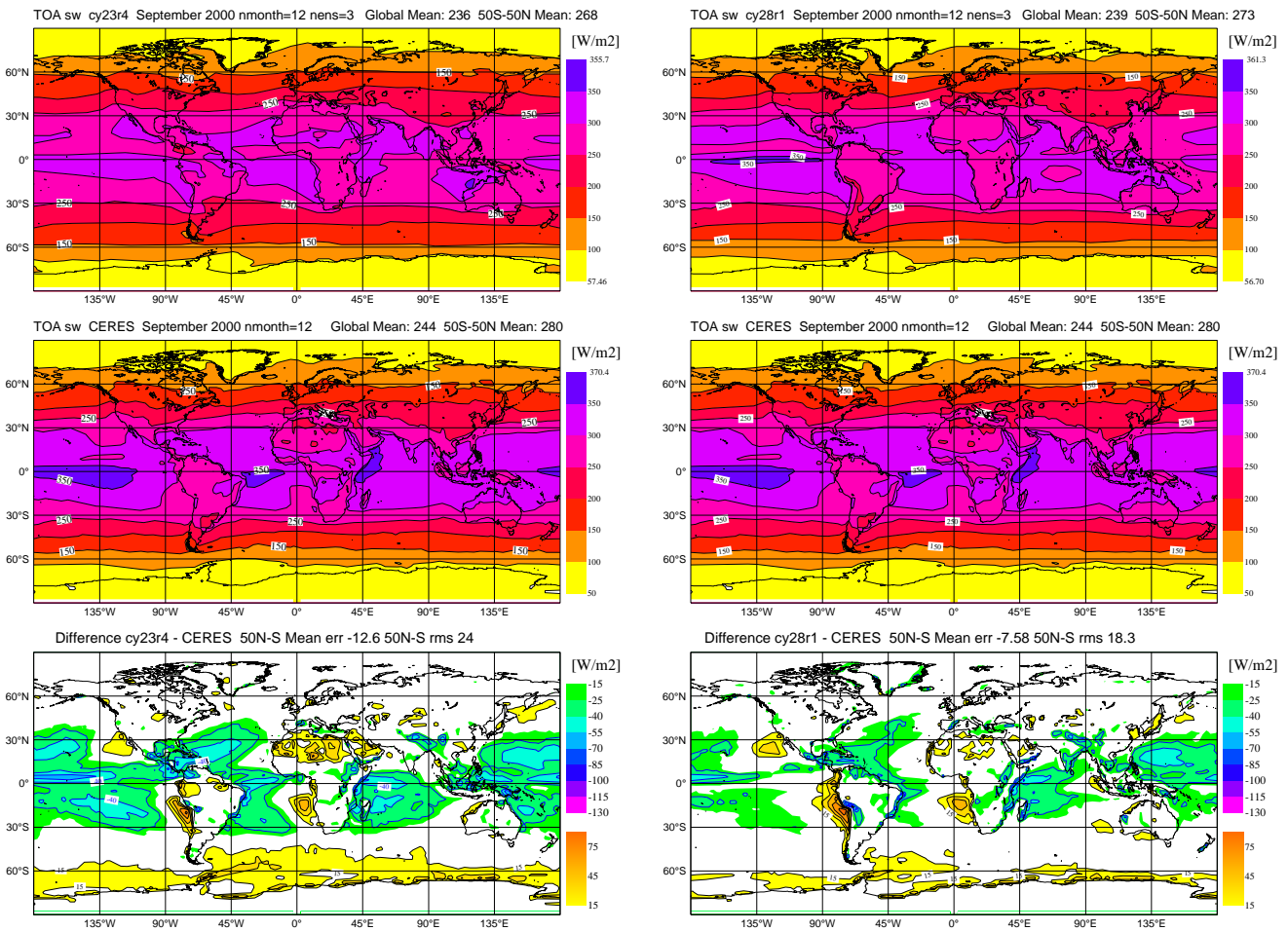
Figure 4: Top of atmosphere absorbed shortwave radiation ($W\,m^{-2}$) for the period June-August 1987 based on the model (upper panel) and ERBE estimates (middle panel) along with differences between the model and observational data (lower panel). Left: results for the model cycle 23r4, right: results for the cycle 28r1.

May 2003

MODEL

OBSERVATION

October 2003

MODEL
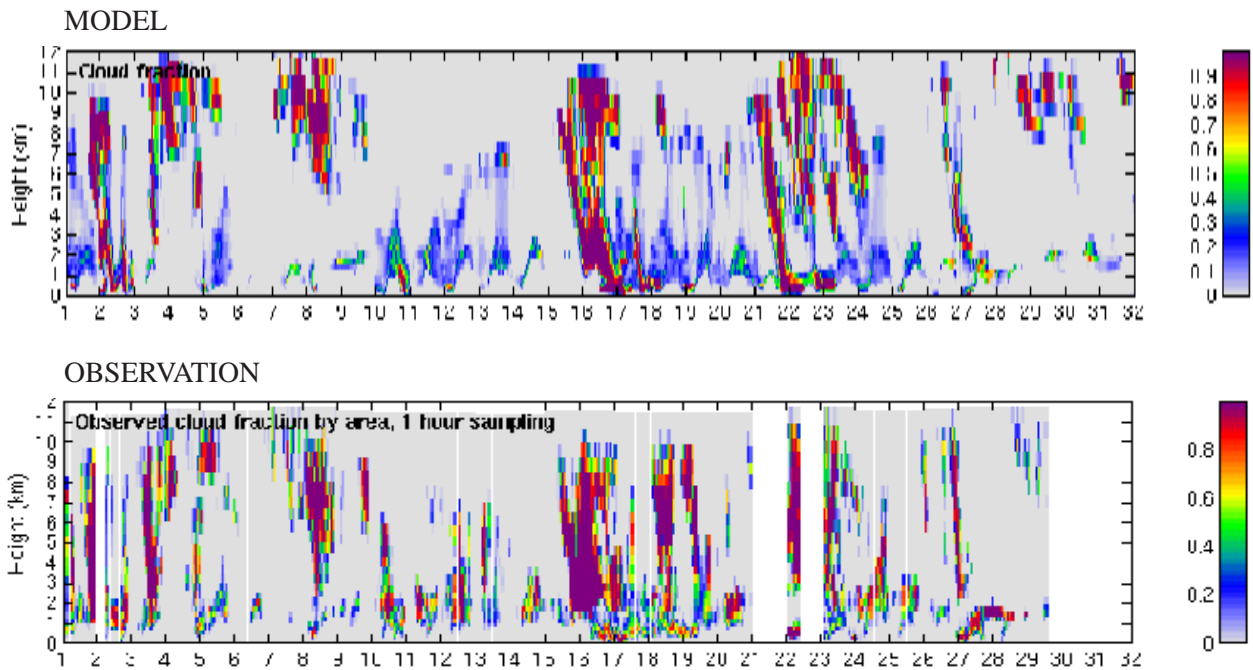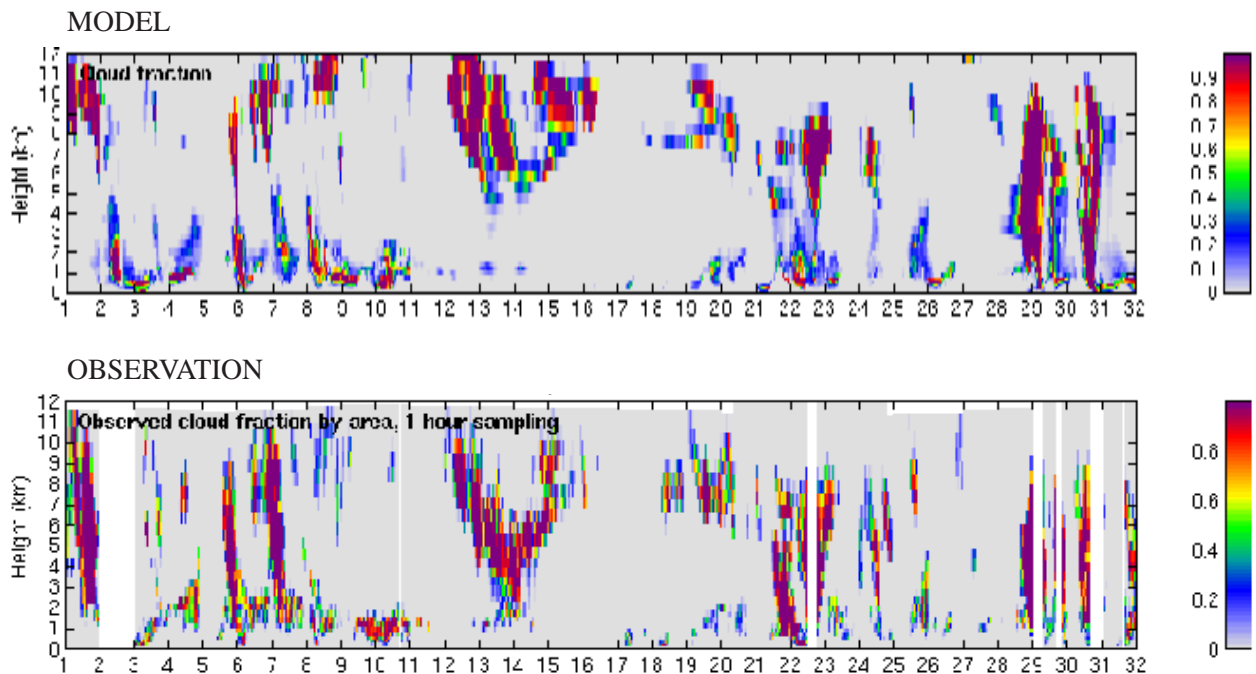
OBSERVATION

Figure 5:   Comparison of the ECMWF cloudiness profiles for the forecast range of 12 to 36 hours against radar estimates at Chilbolton during May and October 2003. The white areas in the panels for observations represent missing data.

3 Linearized radiation and cloud schemes

The assimilation of cloud properties and radiation observations (cloudy radiances or radiative fluxes) requires a cloud scheme and a radiative transfer model as relevant observation operators defining the model counterpart of observations in the variational data assimilation system. Moreover, an efficient computation of the gradient of the objective function during the minimization requires the linearized (tangent-linear and adjoint) versions of both the observation operators and the forecast model. Therefore, the linearized cloud scheme and radiation schemes accounting for cloudiness have been developed at ECMWF (Janisková *et al.* 2002a).

3.1 The linearized radiation schemes

The linearized radiation scheme developed for data assimilation purposes describes longwave and shortwave, clear-sky and cloudy radiation transfer. The scheme must be computationally efficient to be called at each time step and at the full spatial resolution for an improved description of the cloud-radiation interactions during the assimilation period.

The linearized code for the shortwave radiation scheme has been derived from the ECMWF original nonlinear scheme developed by Fouquart and Bonnel (1980) and revised by Morcrette (1991). The nonlinear scheme is reasonable fast for application in 4D-Var and has, therefore, been linearized without a priori modifications. The only modification with respect to the nonlinear model is using two spectral intervals with transmission functions (instead of six intervals used in the nonlinear model) in order to reduce the computational cost.

The complexity of the RRTM radiation scheme for the longwave part of the spectrum makes accurate computations expensive. In the variational assimilation framework, simplifications were made to reduce its computational cost. A combination of artificial neural networks (Chevallier *et al.* 2000) and pre-computed Jacobians of the longwave radiation flux with respect to global mean averaged temperature and water vapour profiles (Chevallier and Mahfouf 2001) has been defined for the linearized longwave radiation scheme. The flux perturbation is approximated by:

$$dF(z_i) = \sum_k \left[a_k(z_i)dF_k(z_i) + F_k(z_i)da_k(z_i) \right] \tag{1}$$

$$
\begin{array}{cccc}
\swarrow & \searrow & \swarrow & \searrow \\
\text{NL model} & \text{Jacobian} & \text{neural} & \text{TL model} \\
 & \text{matrices} & \text{networks} &
\end{array}
$$

A neutral network version of the ECMWF longwave radiative transfer model is significantly faster (seven times) than the operational longwave radiation code with a comparable accuracy. Using pre-computed Jacobians averaged globally is justified by the fact that the variability of the clear-sky Jacobians does not play an essential role when computing total sky (i.e. including) fluxes as shown by Chevallier and Mahfouf (2001).

3.2 The linearized cloud scheme

The current linearized diagnostic scheme, which is used in 4D-Var, has recognized weaknesses: the cloud liquid water is proportional to the saturation vapour pressure and can be inconsistent with the cloud cover; the rainfall generation is simply the result of removing super-saturation and is therefore independent of the cloud variables. Rainfall evaporative processes are currently inhibited. A new simplified cloud scheme and its tangent-linear and adjoint versions (Tompkins and Janisková 2004) have been developed to allow the use of cloud related observations in the ECMWF 4D-Var system. The main advantages of the new scheme are better consistency between the cloud cover and cloud mass and a link of rainfall generation to cloud characteristics. There are

also distinct similarities with the current and planned cloud parametrizations, so a better fit can be expected of the linearized simplified model to the nonlinear one.

3.2.1 Description of the scheme

The new scheme can be divided into a number of components. The cloud cover and in-cloud liquid water content consists of two sources, stratiform and convective cloud. The stratiform and convectively detrainment cloud water are combined to derive the mean in-cloud water content, which is subsequently used to calculate the precipitation production. The precipitation flux is assumed to fall out within one timestep, and is allowed to evaporate during the descent. These four processes of stratiform cloud generation through large-scale motions, convectively generated cloud, precipitation generation and evaporation were shown by Fillion and Mahfouf (2003) to dominate the sensitivity of the prognostic Tiedtke (1993) scheme. A simplified scheme based on this reduced set of processes should then be able to reproduce the sensitivity of the full complex prognostic scheme.

(a) Stratiform cloud properties

The new scheme is based on statistical ideas, which assume a probability density function (PDF) to describe the subgrid-scale fluctuations of total water and/or temperature. This allows the in-cloud liquid water and cloud cover to be determined by integrating the saturated portion of the grid box. In this scheme, the uniform distribution is used to describe the PDF of subgrid-scale fluctuations for simplicity and for consistency with the full forecast model's scheme, which uses the same assumption for the clear sky vapour fluctuations Tiedtke (1993).

One of the two parameters specifying the uniform distribution can be determined from the control variables of temperature and humidity, combined to give the relative humidity. For the closure, a diagnostic assumption is made for the total water variance, or equivalently the distribution width W. Knowledge of the relative humidity and the distribution width exactly specifies the uniform distribution and the cloud cover and water content can subsequently be diagnosed.

Given a cloud fraction C_{strat}, the grid mean specific humidity is an appropriately weighted combination of the clear sky value $r_{sat} - \frac{1}{2}W(1 - C_{strat})$ and the saturated value r_{sat} in the cloudy region (again assuming no supersaturation can exist), which leads to the following relationship for C_{strat}:

$$C_{strat} = 1 - \sqrt{\frac{2r_{sat}(1 - RH)}{W}}. \tag{2}$$

In order to specify a reasonable but simple form for the distribution width W, the asymmetric nature of cloud formation is taken into account. This implies that a lower variance is required for high relative humidities, and this is included in a very simplified manner by reducing the distribution width linearly from its maximum value of $2r_{sat}(1 - RH_{crit})$ when $RH = RH_{crit}$, a critical relative humidity for cloud formation, to its minimum value when $RH = 1$, which is determined by a constant parameter κ. The width of the uniform distribution W is thus given by

$$W = 2r_{sat}(1 - RH_{crit} - \kappa(RH - RH_{crit})). \tag{3}$$

The relationship between cloud cover and relative humidity is shown in Fig. 6 for various values of κ. When $\kappa = 0$, the relationship reduces to the form used by Sundqvist *et al.* (1989).

The grid-mean cloud water mass mixing is obtained by integrating the uniform PDF across the cloudy region to give $r_{lstrat} = \frac{W}{2}C^2$, which substituting the definition for W again gives:

$$r_{lstXrat} = r_{sat}C_{strat}^2(1 - RH_{crit} - \kappa(RH - RH_{crit})) \tag{4}$$
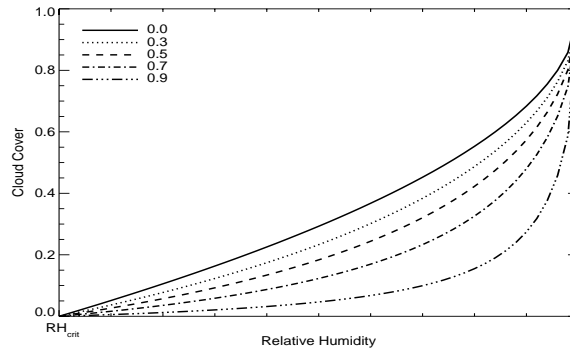
Figure 6: Cloud cover versus relative humidity for various values of κ (see legend).

Thus it is clear that both the stratiform cloud cover and mass mixing ratio will be sensitive to the choice of the parameters κ and RH_{crit} which are defined as:

$$\kappa = MAX[0, 0.9(\sigma - 0.2)^{0.2}], \tag{5}$$

$$RH_{crit} = 0.7\sigma(1 - \sigma)(1.85 + 0.95(\sigma - 0.5)), \tag{6}$$

where σ is the vertical coordinate of the pressure divided by the surface pressure. These functions, depicted graphically in Fig. 7, were chosen on pragmatic grounds, and were designed to tackle the deficient mid-level cloud amount relative to observations noted with the previous diagnostic scheme which used a constant critical relative humidity for cloud formation throughout most of the troposphere. The implemented profile of κ reduces from 0.86 through most of the lower troposphere towards zero in the upper troposphere. This, combined with the profile of RH_{crit}, implies that stratiform clouds are initiated at drier relative humidities in the mid troposphere and that the variance is largest at and above the tropopause region.

(b) Convective contribution

One of the most significant sources of cloud in the tropics and mid-latitude summers in the Tiedtke (1993) cloud scheme is the detrainment from deep convection (e.g. Teixeira 2001). This information will also be provided by the convection scheme specifically developed for the data assimilation (Lopez and Moreau 2004). The detrained cloud water is added to the diagnostic stratiform component given above. For the cloud cover, the assumption is adopted from Tiedtke (1993) that convective clouds randomly overlap existing stratiform cloud, and the source term is solved implicitly (after Eq. 37 in Tiedtke, 1993). Thus the convective cloud cover
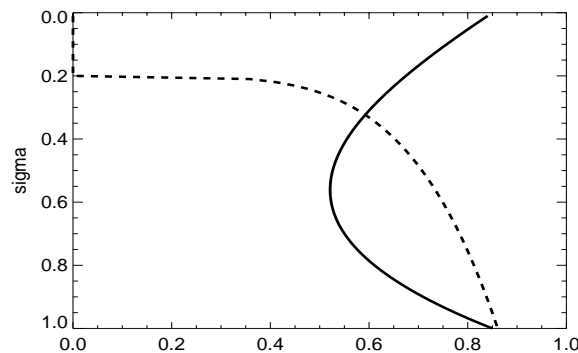
Figure 7: RH_{crit} (solid) and κ (dashed line).

contribution (C_{conv}) is given by

$$C_{conv} = (1 - C_{strat})(1 - e^{\frac{-D\Delta t}{\rho}}), \qquad (7)$$

where D is the mass detrainment rate, ρ is the density, and Δt is the timestep.

Unlike the prognostic Tiedtke scheme, no memory exists for cloud water between consecutive timesteps. Thus the additional assumption is made that any convectively detrained cloud water that is not converted to precipitation during the timestep, evaporates. This is necessary to prevent convectively active regions from artificially drying during the forward integration.

(c) Precipitation production

The generation of both snow and rain are parametrized as auto-conversion terms. The functional form adopted is based on Sundqvist *et al.* (1989) as

$$\frac{dr_l}{dt} = r_l c_0 \left(1 - exp \left[- \left(\frac{r_{cl}}{r_{cl}^{crit}} \right)^p \right] \right), \qquad (8)$$

where r_{cl}^{crit} is the critical value of the in-cloud water content at which precipitation generation becomes efficient, set to 0.5 g kg^{-1}. The other variables c_0 and p are constants, given the values $3 \times 10^{-4}\Delta t$ and 2, respectively. Note that once the cloud water mass significantly exceeds r_{cl}^{crit}, the rate equation becomes quasi-linear, approximating $r_l c_0$.

The local modifications of c_0 and r_{cl}^{crit} by Tiedtke (1993) to take into account the Bergeron-Findeisen or collection processes are not included here. To compensate for the neglected processes in this simplified scheme, c_0 has been increased by a factor of three to obtain a sensitivity that reproduces as closely as possible the sensitivity of the operational prognostic scheme.

A detailed investigation of the tangent-linear approximation for the new scheme revealed that the linearized scheme developed noise during the integration coming from the auto-conversion function which describes the portion of cloud water converted to precipitation. Therefore the linearized version of the function had to be modified by reducing the size of perturbation close to threshold values, which constrain the amount of created precipitation to be between zero and a defined maximum (see Tompkins and Janisková 2004).

(d) Rainfall evaporation

As with the Tiedtke (1993) scheme, precipitation falls to the surface within one timestep and evaporates during its descent. To retain this important term, the new scheme also bases it on the Newtonian relaxation formulation of Kessler (1969) (see Eq. 35 of Tiedtke 1993). For simplicity, the diagnostic scheme uses a maximum overlap assumption for the precipitation fraction (the proportion of a grid cell through which precipitation is falling).

The scheme partially accounts for the overlap of precipitation with the subgrid clear sky distribution of humidity fluctuations, which we recall are uniformly distributed. Thus, instead of using the mean humidity throughout the whole clear sky region to calculate the rate at which rainfall evaporates, the new scheme uses the mean humidity only in the clear-sky portion through which the rainfall is falling, denoted C_{pre}^{clr}. Consistent with the maximum overlap assumption, this is taken to be the most moist C_{pre}^{clr} fraction of the clear sky. Using the uniform distribution, the humidity used to calculate evaporation in Eq. 35 of Tiedtke (1993) is given by

$$r_{pre}^{clr} = r_{sat} - \frac{C_{pre}^{clr}(r_{sat} - r_v)}{(1 - C)^2}. \qquad (9)$$

The significant advantage of this new formulation is that it parametrizes the evaporative processes smoothly without switches or discrete transitions used in the operational Tiedtke (1993) scheme.

3.2.2 Validation of the scheme

(a) 1D tests

The new cloud scheme (*NEWDIAG*) has been tested by comparing physical tendencies of thermodynamical quantities, calculated for a series of input temperature and humidity profiles, to those produced by the complex prognostic scheme (*OPERPROG*) used in the forecast model. The performance of *NEWDIAG* scheme is also compared with the existing operational 4D-Var diagnostic cloud scheme (*OPERDIAG*). This was conducted over the Atmospheric Radiation Measurement (ARM) programme sites located at South Great Plains (SGP) in North America and the two tropics sites based at Nauru and Manus in the Tropical Western Pacific (TWP). This initial test concentrated on the performance of the cloud schemes in a strongly constrained environment where the background thermodynamic fields are not permitted to diverge. In this way serious biases in the underlying cloud scheme physics may be identified.

The mean cloud cover from each scheme is shown in Fig. 8 for the different situations at the ARM sites. At the SGP site, the *NEWDIAG* scheme (Fig. 8a) produces a considerable improvement, with upper level cloud cover almost identical to the prognostic scheme. The new scheme is also able to reproduce the cloud fraction structure at the tropical sites (Fig. 8b, c), with peaks in the lower and upper level cloud fractions due to its direct link to convection through the detrainment term. The *OPERDIAG* produces too much cloud throughout the mid troposphere, with a flat featureless profile. A comparison of the liquid water and ice mass mixing ratios (not shown) revealed that the new diagnostic scheme reproduces the ice and liquid water profiles of the prognostic model reasonable well. In comparison to *NEWDIAG*, the present operational diagnostic scheme is obviously deficient, especially in the Tropics.
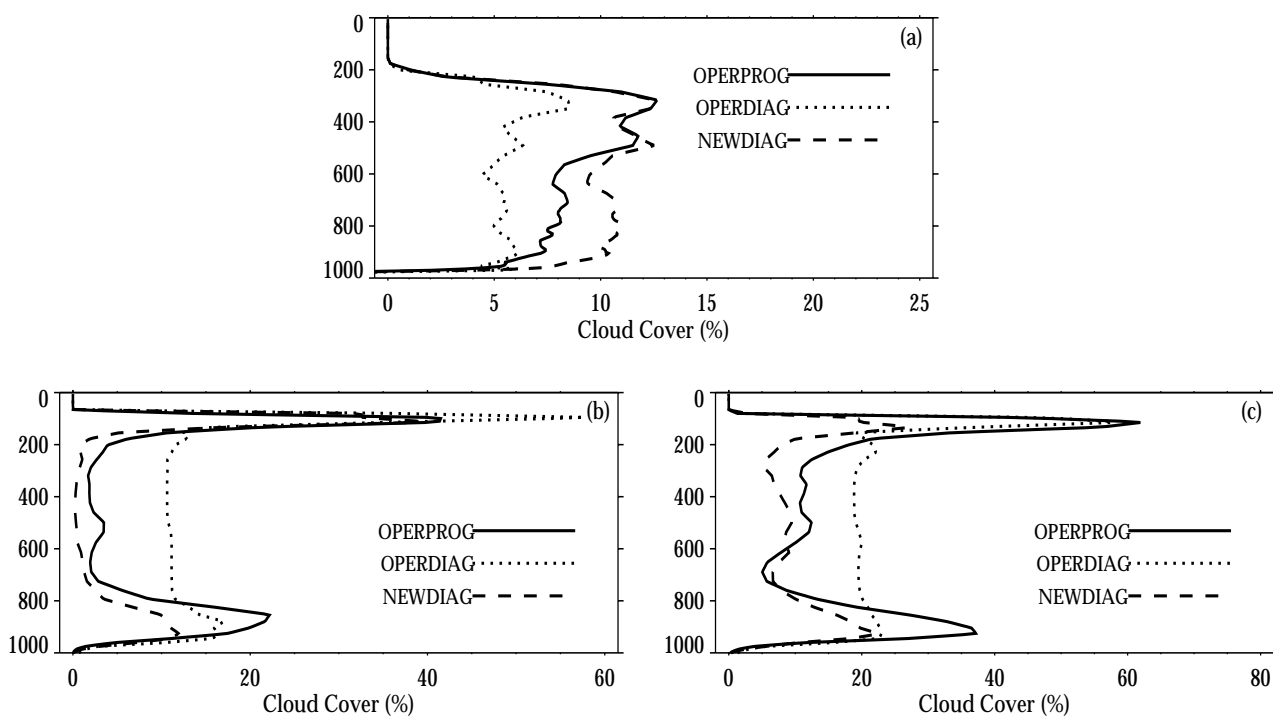
Figure 8: Mean cloud fraction over the ARM SGP site during January 2001 (a), the ARM TWP Nauru site during March 2001 (b) and the ARM TWP Manus site during May 2001 (c), predicted by the operational prognostic scheme (OPERPROG), 4D-Var operational diagnostic scheme (OPERDIAG) and the new diagnostic scheme (NEWDIAG). The lower right panel gives the mean cloud fraction for this period.

To gain a more systematic view of the impact of the new scheme, Fig. 9 gives mean biases and root mean

square errors in radiative quantities, calculated as a monthly mean for the whole of 2001 at the ARM SGP site. The observations used for the comparison are the net solar and infra-red fluxes at the top of atmosphere and surface. The TOA radiometric measurements are derived from geostationary satellite data (GOES-8 over the SGP site and GMS-5 over the tropical locations). This comparison is conducted for the new diagnostic scheme and the fully prognostic scheme, and shows that for all statistics, the new scheme gives an improved fit to the observations during winter, when cloud is mostly synoptically forced. When convective activity predominates during the late spring and summer months, the full prognostic scheme, with its ability to sustain anvil cloud in dry conditions, outperforms the diagnostic model. Overall, the two schemes are comparable, although it should be emphasized again that the thermodynamic fields are not free to evolve when using the diagnostic model.
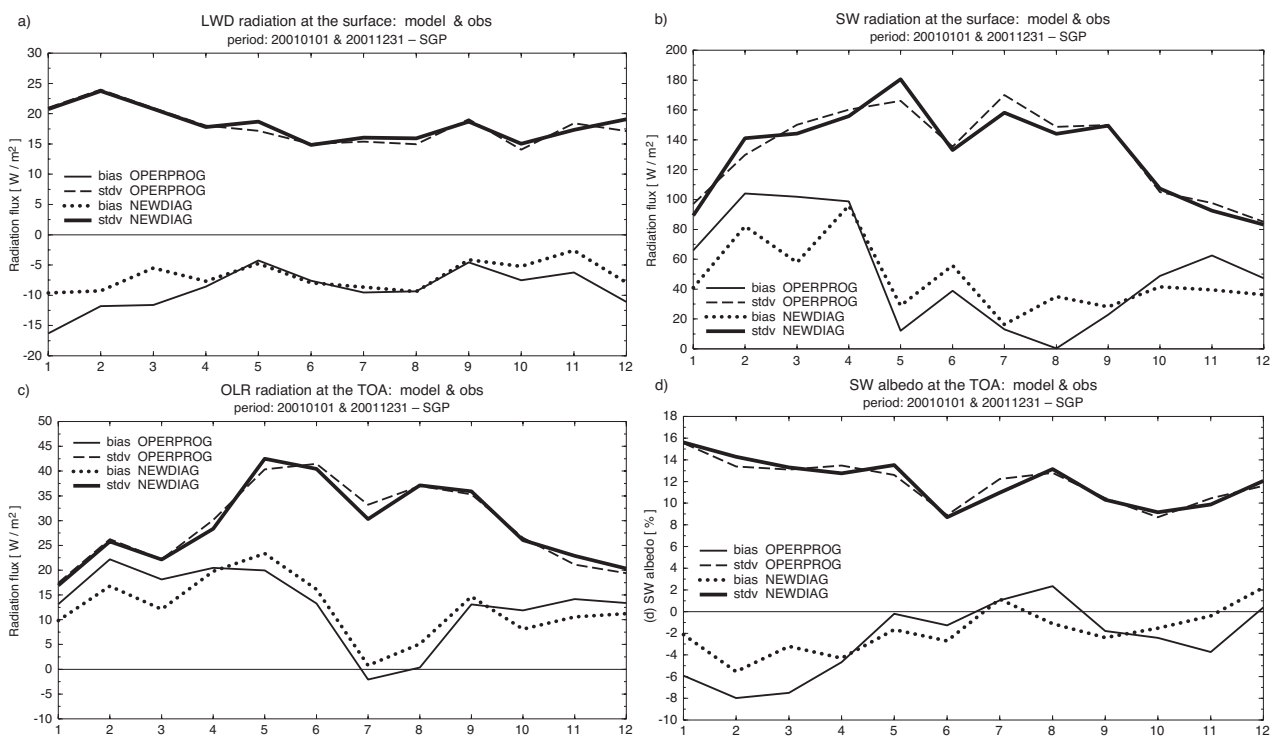
Figure 9: Monthly mean statistics for the year of 2001 at the ARM SGP site for (a) surface downward longwave radiation, (b) surface net shortwave radiation, (c) TOA outgoing longwave radiation and (d) shortwave albedo.

(b) Global forecasts

As a further test, a series of 12 hour global model integrations were executed, with the full prognostic scheme used in operational forecasts replaced in turn by the nonlinear versions of the current operational assimilation diagnostic cloud scheme, and then by the new scheme described here. Two weeks of forecasts were conducted at T159L60 resolution (120 km horizontal resolution and 60 vertical levels), for the first two weeks of March 2001. The choice of resolution was initiated by the fact that the linearized model with the physical processes, for which the new scheme was developed, is run at T159 in the current inner-loop integration of 4D-Var. Using the default model as a reference, the new scheme improves on the current assimilation cloud scheme for many variables such as cloud cover and ice water content, both in the tropics and mid-latitudes. In particular the new scheme addresses the overriding weakness of the current operational linearized physics package, which produces almost no large-scale precipitation (and associated perturbations of control variables) in the tropics (Fig.10). Instead the new scheme almost perfectly replicated both the pattern and quantity of tropical precipitation.

The total column cloud water for the three cloud schemes at the same 12 hour range is examined in Fig.11. The existing scheme *OPERDIAG* clearly produces too little cloud condensate in mid-latitudes, while cloud water is
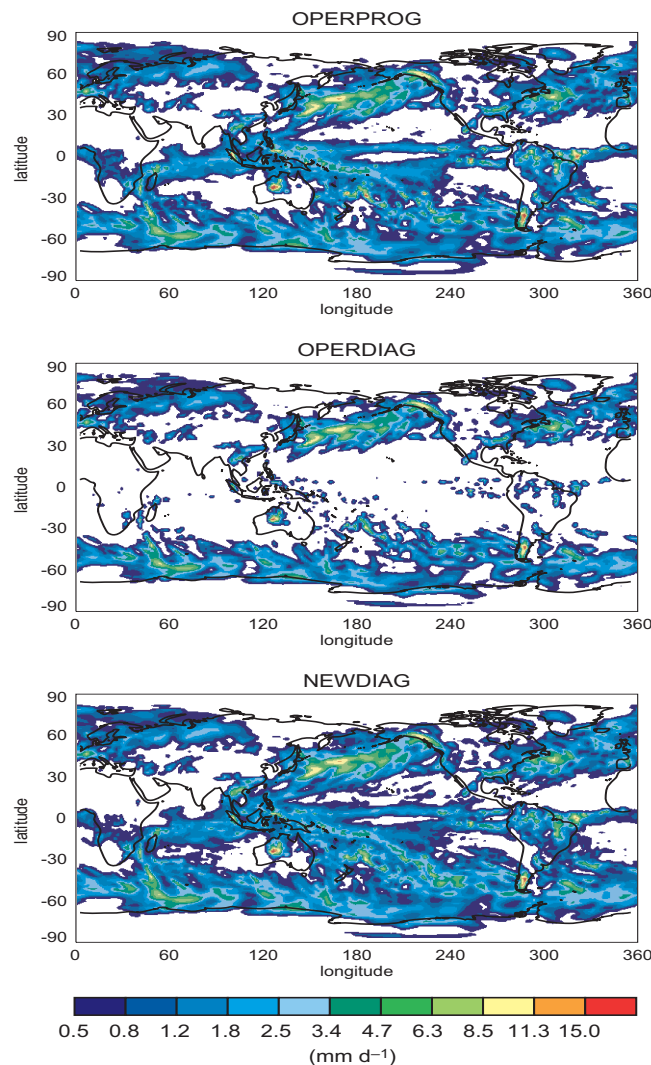
Figure 10: 12 hour accumulated large-scale precipitation averaged over 14 forecasts at T159 resolution for the three cloud schemes.

widespread through out the tropics. The new diagnostic scheme better predicts the location of the cloud water, and as with the other variables, the *NEWDIAG* is found to match *OPERPROG* more closely. The peak cloud water contents in the extra-tropics match well. It is notable that the new scheme does increase the cloud water in some areas of the tropics, which is due to an increase in upper level ice cloud with respect to the Tiedtke scheme (not shown). It is arguable that this is beneficial since previous investigations by Chevallier and Kelly (2002) indicate that the *OPERPROG* scheme produces too little upper level ice.

The forecasts were also examined at a range of 24 hours, to verify that the conclusions drawn would be robust if the assimilation window were to be extended in the future. No significant departure in the forecast behaviour were noted at this extended range (not shown).

3.2.3 Validation of the tangent-linear approximation

The linearized versions (tangent-linear and adjoint) of the cloud scheme described above have been developed. After the standard validation of the tangent-linear and adjoint codes (Taylor formula and adjoint identity), the linear evolution of the model with new cloud parametrization has been studied. Comparisons were made
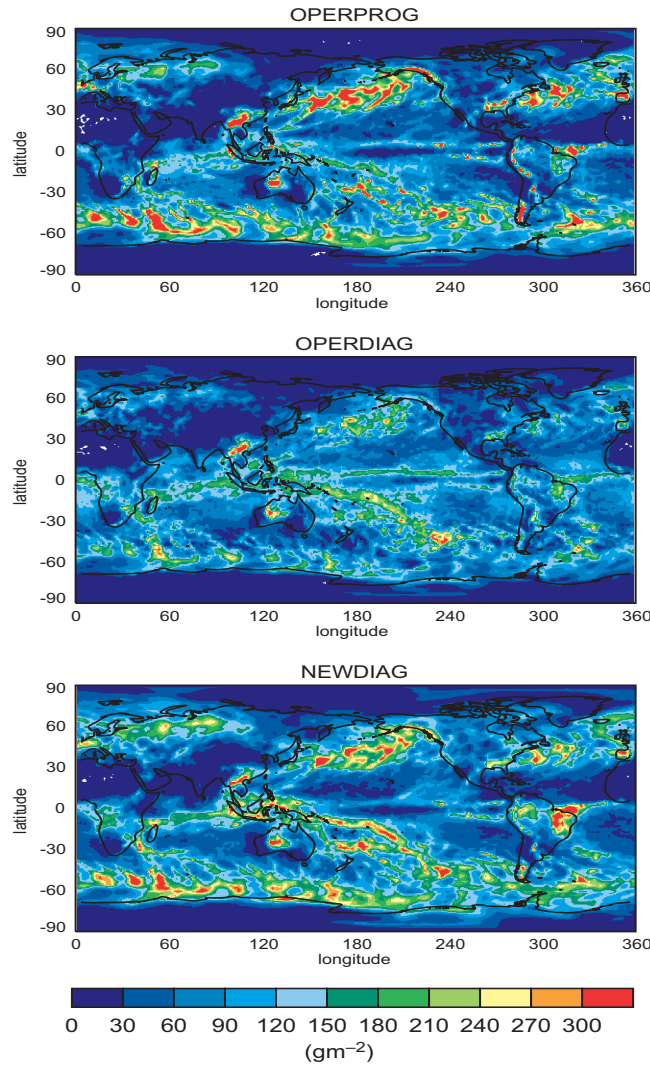
Figure 11: Total column cloud water (liquid + ice) averaged over 14 forecasts at T159 resolution at the 12 hour forecast range for the three cloud schemes.

between the evolution over 12 hours of analysis increments $\delta\mathbf{x}$ ($\delta\mathbf{x} = \mathbf{x}^a - \mathbf{x}^b$, where $\mathbf{x}^a$ represents analysis and $\mathbf{x}^b$ background field) with the simplified tangent-linear model $M'(\delta\mathbf{x})$ and the finite differences between two nonlinear forecasts ($M(\mathbf{x}^a) - M(\mathbf{x}^b)$) using the full nonlinear physical package, starting from the different initial conditions. Experiments are performed for three cases to sample the seasonal cycle (15 December 2000, 15 March 2001, 15 June 2001) using the model resolution T159L60 of the ECMWF global spectral model, mimicking an inner-loop integration of the operational 4D-Var system.

In the following evaluations, the impact of the cloud scheme is examined using mean absolute errors between the tangent-linear and nonlinear integrations as:

$$\varepsilon = \overline{\left| [M(\mathbf{x}^a) - M(\mathbf{x}^b)] - M'(\mathbf{x}^a - \mathbf{x}^b) \right|} \tag{10}$$

where M is the forecast model starting either from the analysis $\mathbf{x}^a$ or from the background $\mathbf{x}^b$ and M' is the tangent-linear model starting from the initial conditions $\mathbf{x}^a - \mathbf{x}^b$. The results are evaluated as a relative impact (in %) as:

$$\eta = \frac{\varepsilon_{exp} - \varepsilon_{ref}}{\varepsilon_{ref}} \cdot 100\ \% \tag{11}$$

where ε_{exp} and ε_{ref} are absolute mean errors for experimental and reference runs, respectively.

Figure 12 summarizes the relative impact $-\eta$ (with the minus sign added such that positive values indicate an improvement) coming from including the new diagnostic cloud scheme to the operational set of linearized physical parametrizations. In this figure, ε_{ref} represents the absolute mean error of the TL model with the set of operational linearized physics using the radiation schemes (*oper*) described by Janisková *et al.* (2002a). The experimental run (*new_cloud*) includes the linearized version of the new cloud scheme. The results are presented for temperature, specific humidity and zonal wind at various geographical domains. Including the cloud scheme in the linear model improves globally the fit to the nonlinear model for each evaluated variable. The largest improvement is achieved in the Tropics for temperature and zonal wind and in North20 for specific humidity. A small negative impact is mainly observed for zonal wind in South20. The ability of the TL model to approximate the finite differences is necessarily dependent on the meteorological situation, but the largest improvements are generally in the Tropics, with the exception of specific humidity for which the improvement is globally uniform.
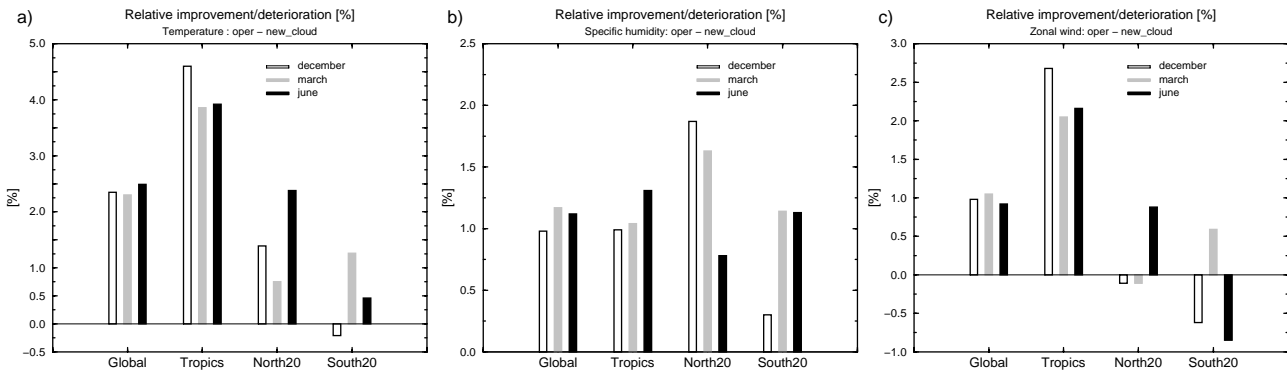
Figure 12: The improvement/deterioration of the tangent-linear (TL) model when using the new linearized cloud scheme in place of the current operational diagnostic scheme for the geographical domains of: Tropics: 20N-20S, North20: 20N-90N, South20: 20S-90S and globally. The results are presented as the percentage improvement for (a) temperature, (b) specific humidity and (c) zonal wind. The comparisons are made for 15 December 2000 (white bar), 15 March 2001 (grey bar) and 15 June 2001 (black bar).

For a detailed presentation of the impact coming from the cloud scheme, zonal mean values of error differences ($\varepsilon_{new\_cloud} - \varepsilon_{oper}$) are displayed in Fig. 13 for temperature and specific humidity, just for the situation of 15 March 2001. Negative values are associated with an improvement of the experimental TL model (*new_cloud*) with respect to the reference one (*oper*) since they correspond to a reduction of the error ε. The new cloud scheme reduces the global mean error by 2.3 % for temperature and by 1.2 % for specific humidity. Such values, while apparently limited, usually translate into a significant enhancement of forecast skill on implementation into the 4D-Var system. The improvement is significant over the whole Tropics and in the lower troposphere, as demonstrated in Fig. 13c, which presents error differences for temperature at model level L49 (~ 850 hPa) in the tropical domain (30S - 30N). At this level the relative improvement is as large as 7.8 %, despite the fact that the TL integration was performed with a simple convection scheme (i.e., no perturbation of the detrainment term), since the new scheme can generate precipitation when the relative humidity is less than 100 %. The areas of error reduction correspond to the regions with the most improvement observed in the 3D forecast validation (section 3.2.2 b). It is probable that evaporation processes, which were neglected in the previous version of the linearized large-scale condensation scheme (Mahfouf 1999) contribute to an improvement of the tangent-linear approximation of the simplified model to the full nonlinear model (in finite differences) when using the new cloud scheme.

Figure 14 showing the vertical profiles η of relative reduction or increase of error differences (Eq.11) provides

a) Error difference: new_cloud - oper: -4.5 %
Temperature - 15/03/2001 12 h t+12

b) Error difference: new_cloud - oper: -1.8 %
Specific humidity - 15/03/2001 12 h t+12

c) Error difference (level 49): new_cloud - oper: -7.8 %
Temperature - 15/03/2001 12 h t+12
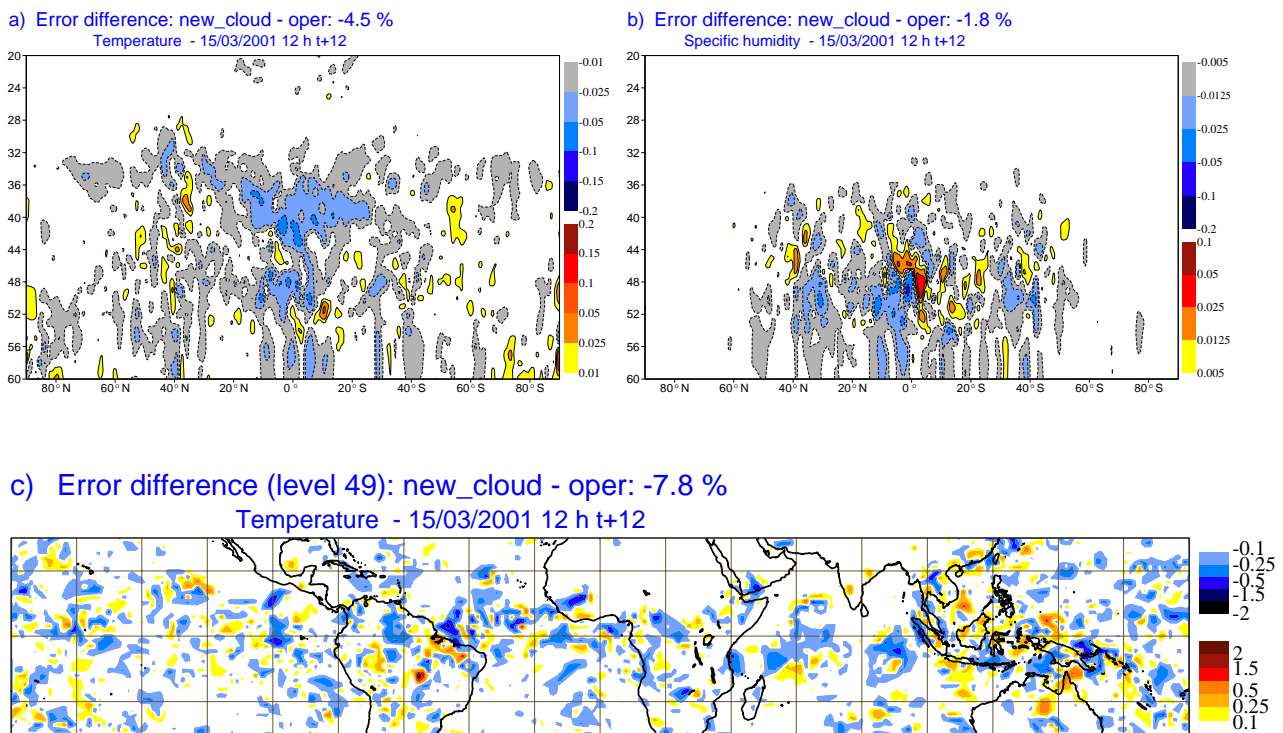
Figure 13: Influence of the tangent-linear (TL) cloud scheme on the evolution of temperature (a) and specific humidity (b) increments in zonal mean. Results are presented as the error differences (in terms of fit to the nonlinear model with full physics) between the TL model with operational linearized physics including new radiation schemes and the TL model with new cloud scheme. (c) presents the same, but for temperature at the model level L49 ($\sim$ 850 hPa) and in the tropical domain (30S - 30N). 12-hour forecast for the situation of 15 March 2001, 12 UTC, units: K for temperature, g.kg^{-1} for specific humidity.

a more detailed examination of the influence of the *NEWDIAG* scheme on the vertical profiles, both globally and for the Tropics only. The new cloud scheme has a positive impact for temperature in the whole profiles (improvements up to 6 % globally and up to 9 % in the Tropics). For the zonal wind, the error is mostly reduced below the model levels L48 - L49 ($\sim$ 800 hPa). The improvements for humidity are up to 2.5 % both, globally and in the Tropics. There is an increase in error difference for specific humidity at L31 - L34 ($\sim$ 200 - 300 hPa), where the absolute mean error ε (not shown) is quite small (0.02 - 0.03 g.kg^{-1}). This is likely to be a result of differing ice microphysics used in the two schemes. The lower end of the peak marking the deterioration is at exactly the temperature (250 K) at which the operational prognostic scheme discretely switches its physics from the Sundqvist-based auto-conversion for the mixed phase, to a sedimentation-based form for the pure ice phase. The new diagnostic scheme, using auto-conversion throughout the troposphere to ensure a smooth scheme, is unable to reproduce the behaviour caused by this discrete change in physics.

Overall, the inclusion of new cloud scheme into the operational set of the linearized physics, except for the isolated deterioration described above, improves the accuracy of the tangent-linear approximation of the simplified model to the full nonlinear model (in finite differences).
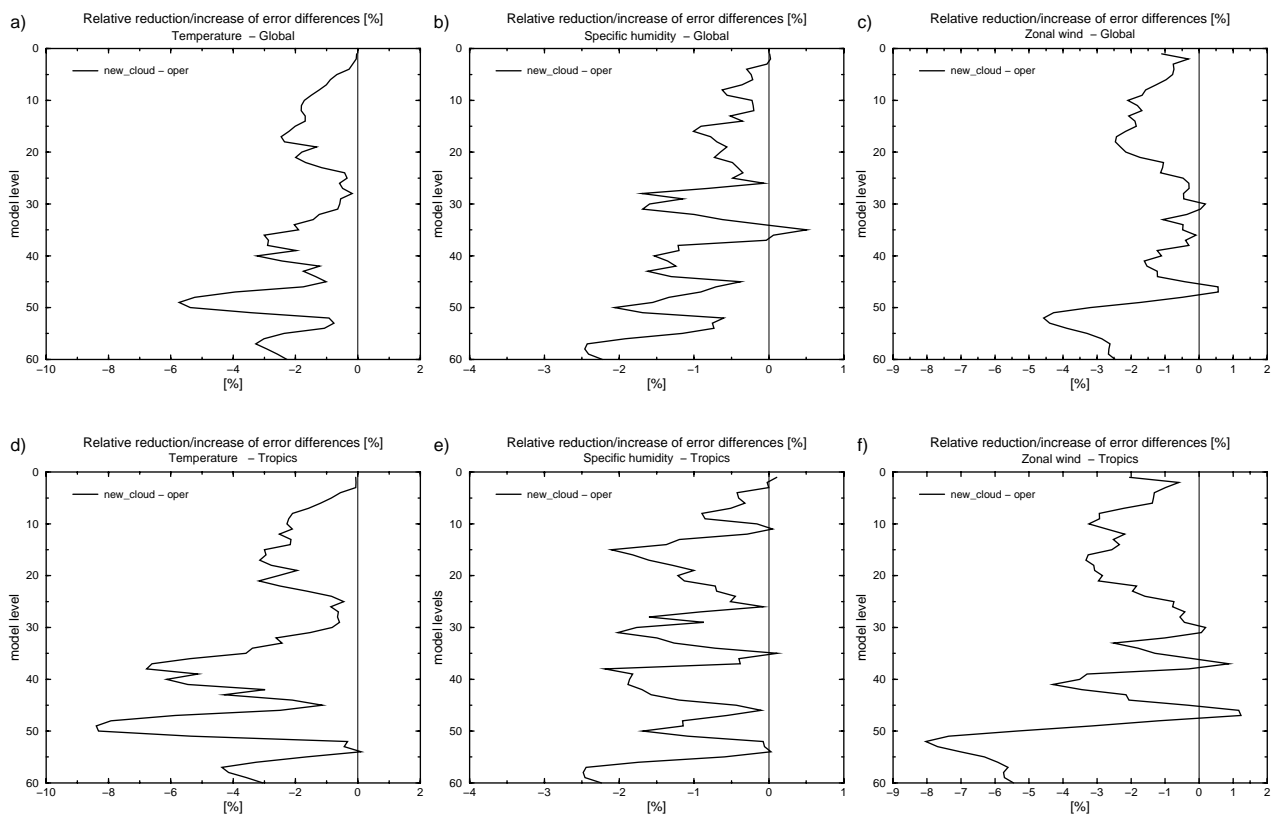
Figure 14: Vertical profiles of relative decrease (negative values) or increase (positive values) of error differences as a percentage for temperature (a,d), specific humidity (b,e) and u wind component (c,f). Results are shown for global statistics (top panels) and only the Tropics (bottom panels). The results show the impact of adding the new cloud scheme to the operational linearized model and are presented for the 12-hour forecast on the 15th March 2001, 12 UTC.

4 Data assimilation experiments

Data assimilation forms a crucial component of any forecast system, aiming to provide the forecast model with the most accurate initial conditions using all available information on the atmospheric state in an optimal way. At ECMWF the operational data assimilation system used since November 1997 (Rabier *et al.* 2000, Mahfouf and Rabier 2000) is an incremental four-dimensional variational system (4D-Var) described by Courtier *et al.* (1994). The goal of 4D-Var is to define the initial atmospheric state $(\mathbf{x}(t_0))$ such that the distance between the model trajectory and the observations is minimum over a given period $[t_0, t_n]$. The model trajectory $\mathbf{x}(t)$ is constrained to fit the observations $\mathbf{y}$ by adjusting the initial conditions. The misfit to observations $\mathbf{y}$ and to background (or first-guess) model state $\mathbf{x}^b$ is measured by an objective cost function $\mathscr{J}$, that is being minimized during the assimilation process:

$$\mathscr{J}(\mathbf{x}_0) = \frac{1}{2}(\mathbf{x}_0 - \mathbf{x}_0^b)^T \mathbf{B}^{-1}(\mathbf{x}_0 - \mathbf{x}_0^b) + \frac{1}{2}\sum_{i=0}^{n}(H_i[\mathbf{x}(t_i)] - \mathbf{y}_i^o)^T \mathbf{R}_i^{-1}(H_i[\mathbf{x}(t_i)] - \mathbf{y}_i^o) \tag{12}$$

The above function consists of two terms: the background objective function which measures the distance between the initial state of the model $\mathbf{x}(t_0)$ and the background $\mathbf{x}^b$ using the covariance matrix $\mathbf{B}$ of the background error, and the observation objective function which measures the distance between the model trajectory and the corresponding observations using the covariance matrix $\mathbf{R}$ of the observation error. Observation and model errors are assumed to be unbiased and mutually uncorrelated.

4.1 1D-Var experiments

1D-Var systems may be used for preliminary studies on the 4D-Var. The principle of the 1D-Var is similar to that of 4D-Var, but the control vector $\mathbf{x}$ represents a single column only and the time dimension is not included.

4.1.1 The 1D-Var method

(a) General description

Let $\mathbf{x}$ be the vector representing an atmospheric state described by its temperature T, humidity q and surface pressure p_s (control variables in the 1D-Var). The goal of 1D-Var is to define the atmospheric state $\mathbf{x}$ such that the distance between a background profile (short-term forecast) and observations is minimum. The model is constrained to fit the observations by adjusting its initial conditions. Then the minimization problem consists in finding the optimum profile $\mathbf{x}$ which minimizes the objective function:

$$\mathscr{J}(\mathbf{x}) = \frac{1}{2}(\mathbf{x} - \mathbf{x}^b)^T \mathbf{B}^{-1}(\mathbf{x} - \mathbf{x}^b) + \frac{1}{2}\sum_{i=1}^{n}\left(\frac{F_i(\mathbf{x}) - F_{o_i}}{\sigma_{o_i}}\right)^2 \tag{13}$$

where $\mathbf{B}$ is the covariance matrix of the background error taken from the operational ECMWF 4D-Var (described in more details in Section 4.1.1(c)). $\mathbf{x}^b$ is the background vector (short term forecast profile). F_{o_i} represents a set of observations i ($i = 1, \cdots, n$) with observation errors σ_{o_i} (including errors of representativeness). $F_i(\mathbf{x})$ is an observation operator providing the model equivalent of observations F_{o_i}. In this study, $F_i(\mathbf{x})$ includes the shortwave and longwave radiation schemes together with the cloud and convection schemes, as well as radar reflectivity model. The minimization requires an estimation of the gradient of the objective func-

tion:

$$\nabla \mathscr{J}(\mathbf{x}) = \mathbf{B}^{-1}(\mathbf{x} - \mathbf{x}^b) + \sum_{i=1}^{n} \mathbf{F}_i^T \left[\frac{F_i(\mathbf{x}) - F_{o_i}}{\sigma_{o_i}^2} \right] \tag{14}$$

The transpose of the observation operator $\mathbf{F}^T$ can be obtained explicitly through the Jacobian matrix computed in finite differences by a perturbation method. Such approach is affordable due to the low dimension of the control vector in 1D-Var. Using the adjoint of the tangent-linear physical processes to compute $\mathbf{F}^T$ reduces significantly the computational cost. An estimation of the gradient of $\mathscr{J}$ is done using a limited memory quasi-Newton optimization routine (M1QN3), which requires an estimation of the gradient of the objective function at each iteration (Gilbert and Lemaréchal 1989).

(b) Observation operator

The assimilation of cloud properties and radiation observations (cloudy radiances or radiative fluxes) requires a cloud scheme and a radiative transfer model as relevant observation operators defining the model counterpart of observations in the variational data assimilation system. Moreover, an efficient computation of the gradient of the objective function during the minimization requires the linearized (tangent-linear and adjoint) versions of both the observation operators and the forecast model. Therefore, the linearized cloud scheme (Tompkins and Janisková 2004) and radiation schemes accounting for cloudiness have been developed at ECMWF (Janisková *et al.* 2002a).

A brief description of the linearized code for the *shortwave and longwave radiation schemes* is given in Section 3.1. The linearized *cloud scheme* is described in more details in Section 3.2. In addition to these schemes, the observation operator *H* consists of a simplified convection scheme (Lopez and Moreau 2004) providing the detrained cloud water as an input to convective contribution of the cloud scheme. The radar forward model is used to convert model fields into reflectivities (Benedetti and Janisková 2004).

(i) Convection scheme. In the simplified convection scheme, all types of convection (shallow, mid-level, and deep) are treated in the same way. In particular, the link between the model control variables and the cloud base mass flux (the so-called closure assumption) is expressed through a single formulation that depends on the release of convective available potential energy (CAPE) in time. In contrast with the operational convection scheme used in the forecast model, the equations that describe the vertical evolution of the updraught mass flux and of the updraught thermodynamic characteristics (dry static energy and total water), are uncoupled. The uncoupling allows the removal of the iterative calculations involved in the operational code for updating the cloud base mass flux, thereby leading to an easier development of the adjoint code.

Convection is assumed to be activated only if the bulk convective updraught vertical velocity remains positive at cloud base. The updraught is assumed to originate from the surface only if its initial vertical velocity is positive, which is calculated from the surface heat fluxes using the formulation of Holtslag and Moeng (1991). The initial temperature and specific humidity departures of the updraught from the environment are assumed to be proportional to the surface sensible and latent heat fluxes. If convection cannot be initiated from the surface, the convective ascent may originate from higher levels provided relative humidity exceeds 80%, in which case the initial vertical velocity of the updraught is somewhat arbitrarily set to 1 m s^{-1}. Regardless of whether the updraught originates from the surface or from higher up, the vertical evolution of its kinetic energy is computed following Simpson and Wiggert (1969), which involves the buoyancy as well as the entrainment of environmental air into the updraught. The convective ascent is assumed to stop at the level where updraught vertical velocity becomes negative.

Simplified calculations of downdraughts and convective momentum transport based on the operational scheme (Tiedtke 1989) are also included in the new parametrization. More importantly, the precipitation formation rate is made proportional to the updraught cloud water content as in Tiedtke (1989).

(ii) Radar reflectivity model. The radar backscattering cross-section derived from the radar return power can be related to the amount of solid precipitation (rain and snow) and the amount of cloud ice/water content that the radar signal encounters in its path. The forward modeling of this radar signal can be performed by assuming a size distribution of the scatterers and by computing their optical properties. Here it is assumed that all rain/snow/cloud ice and water particles are spherical. Their optical properties are computed using the Mie solution at the frequency of interest and as functions of temperature, and then integrated by assuming a Marshall-Palmer distribution for the precipitation-sized particles and a modified-gamma distribution for the cloud particles. The radar reflectivity factor is proportional to the integral of the backscattering cross-section over the size distribution. A variable commonly used to describe the radar return is the equivalent radar reflectivity, hereafter indicated with the symbol Z, which represents the radar reflectivity factor that an equivalent volume of spherical water droplets would be associated with. If the target particles are in a solid phase, it is necessary to convert the raw reflectivity factor into an equivalent reflectivity. This is done in the forward model assuming a fixed density for the snow (ρ=0.1 g cm^{-3}) and cloud ice (ρ=0.9 g cm^{-3}). In presence of intense precipitation, the radar signal is attenuated. By computing the total optical depth and the path–integrated attenuation, the attenuated profile of reflectivity can be computed. To speed up computations, all reflectivity values are collected in a look-up table and organized according to the values of temperature and cloud liquid/ice water and precipitation contents. A bilinear interpolation is then applied to extract the reflectivity value corresponding to the given model temperature and hydrometeor contents. A special treatment of the melting layer is also included in the computation of the look-up table, although is only applied at exactly 0°C. The reflectivity values contained in the look–up table were verified against those derived from other forward models and those derived from simple Z-R/LWC relationship. Comparisons show that the current forward model is reliable within a few dBZs. Research to better quantify forward modeling errors is currently underway.

(c) Background error statistics

The background error covariance matrix **B** provides to the variational analysis the appropriate information about the 1D (vertical) statistical structure of the forecast errors. The covariance matrix of the background error **B** is taken from the operational ECMWF 4D-Var system (Rabier *et al.* 1998, Derber and Bouttier 1999). The vertical correlations have been computed statistically using the National Meteorological Center method (Parrish and Derber 1992) from differences between 48-h and 24-h forecasts. No cross correlations between the background errors of specific humidity and temperature are considered. The standard deviation of temperature over the vertical are about 1 K up to around 200 hPa, then they grow in the stratosphere up to 4.5 K. The standard deviation for specific humidity has been empirically specified by Rabier *et al.* (1998) as a function of temperature and specific humidity profiles. The vertical profile has a maximum around 850 hPa, an exponential decrease above and lower values in the boundary layer. An example of vertical profile of standard deviations for temperature and humidity is illustrated on Fig. 15.

4.1.2 *Experimental framework*

1D-Var experiments have been carried out using data from the Atmospheric Radiation Measurement Program (ARM - Stokes and Schwartz, 1994). Measurements of both cloud properties and radiative fluxes, which are available on a routine base, have been used in these feasibility studies. The aim of these studies has been to show the ability of 1D-Var to modify dynamical variables, temperature and specific humidity, since an important aspect of the cloud assimilation is to achieve a consistency between cloud parameters and dynamics. Experiments have shown that when dynamical fields are inconsistent with the cloud profiles, the analyzed cloud information is lost within a few model time steps. The control vector of the assimilation system should therefore consist of dynamical variables (temperature, humidity and wind). Another purpose of the study has been to examine the behaviour of the new moist parametrization schemes (cloud and convection) in 1D-Var
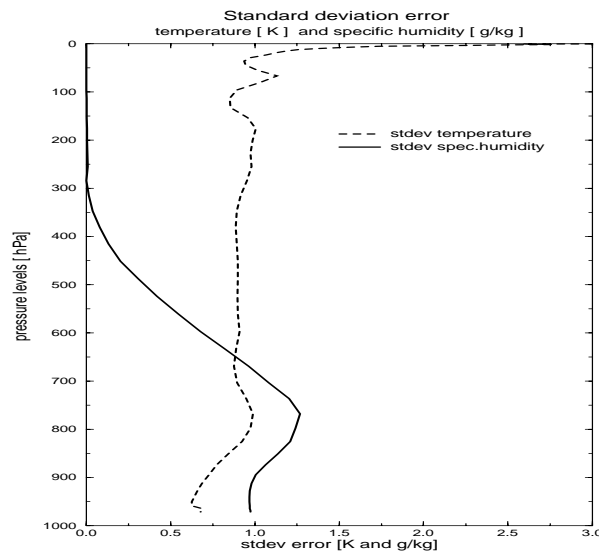
Figure 15: Vertical profiles of typical values of the standard deviation of the ECMWF model background errors for temperature (dashed line) and specific humidity (solid line). Units are in K and g kg^{-1} respectively.

assimilation of the cloud related observations and to assess situations where convective clouds are dominant.

(a) Background profiles

The background temperature and specific humidity profiles were taken from the 12-hour forecast of the ECMWF model with T511 spectral truncation (corresponding to approximately 40 km) and 60 vertical levels. The profiles represent mean values for the the nearest grid-points around the different ARM sites. These profiles of T and q, along with surface pressure, p_s, tendencies, and surface quantities are first used in the moist physics routines (simplified convection and cloud schemes described above) to compute cloud properties (cloud cover, ice and liquid-water contents) and precipitation fluxes. A radar observational operator is then applied to the model fields to obtain the equivalent reflectivity. The radiative transfer model is employed to compute the shortwave and longwave radiation fluxes from the background variables and cloud properties.

Several months of the year 2001 have been retrieved from the ECMWF archive for 1D-Var experiments. In this report, results for the months of January and May 2001 are presented.

(b) Observations

The assimilation experiments were carried out using observations taken at the ARM Southern Great Plains site (36.6°N - 97.5°W) during January 2001 and at the two ARM sites located in the tropical Western Pacific, at Naurus (0.5°S - 167°E) and Manus (2°S - 147°E), during January and May 2001, respectively. Measurements from the observational systems located at the ARM sites used directly in the experiments are the surface downward longwave radiation (LWD), the total column water vapour (TCWV) and the cloud radar reflectivity profiles. 1D-Var retrievals were compared against some independent observations, which were not assimilated, such as cloud-liquid water path (LWP), the surface downward shortwave radiation (SWD), the top of atmosphere radiation fluxes, and the temperature and humidity profiles from the radiosoundings. A comparison was also made with the vertically integrated water vapour derived from the humidity information in the radiosoundings. The TCWV derived from the radiosonde is slightly smaller than the MWR-derived value (Morcrette, 2001).

The LWD and SWD are measured by pyrgeometers and pyranometers (SIRS - Solar Infrared Radiation Sta-

tions). The radiation fluxes at the top of atmosphere are derived from geostationary satellite data: GOES-8 over an area encompassing the ARM-South Great Plains (SGP) site and GMS-5 covering both Manus and Nauru islands of the Tropical West Pacific (TWP) sites. The total column water vapour (TCWV) and cloud liquid water path (LWP) are derived from the Microwave Radiometer (MWR). The cloud radar reflectivity profiles are taken from the Multi-Mode Cloud Radar (MMCR) and only those measurements at the Southern Great Plains (SGP) site are used in our experiments.

All observations are averaged over 1-hour intervals as described by Morcrette (2001). For reflectivities, observations are screened at lower levels to exclude saturated values. For radiative fluxes, the averaging is carried out taking all values after rejecting the few unrealistic values. The same procedure has been applied to the measurements from the Microwave Radiometer. The measurements of the total column water vapour and liquid water path are sometimes contaminated by precipitation and the presence of condensation on the optics. The wet index is thus marked on the figures presenting the results from 1D-Var assimilation experiments in order to indicate when those measurements have not been assimilated because they are unreliable.

(c) Observation errors

The observation errors for the radiation measurements are usually defined as 5 W.m^{-2} for the longwave radiation and 10 W.m^{-2} for the shortwave radiation (BSRN standard - Ohmura *et al.*, 1998). However, experiments have shown (see Janisková *et al.*, 2002b) that errors larger by a factor 2 should be used in order to better combine use of the radiation and moisture observations.

LWP and TCWV are derived from MWR radiances. Errors on the retrievals from brightness temperatures are not provided. Therefore they have been specified somehow arbitrarily. The observation error for LWP measurements has been assigned as large as 50 % of the observed value. For the observation error of TCWV, the error specification defined for the assimilation of SSM/I (Special Sensor Microwave Imager) has been used (Gérard and Saunders, 1999):

$$\sigma_{TCWV_{obs}} = 7.27 \cdot 10^{-2} \, TCWV_{obs} + 1.63 \tag{15}$$

For the MMCR observations, preliminary tests have shown that the model gives values of reflectivity which are consistently higher than the MMCR observations when rain is present. The nominal dynamic range of the MMCR is between -40 and 20 dBZ. However, the signal might be already saturated at reflectivities between 8 and 10 dBZ due to the gradually slower clipping in the receiver. After several discussions with some of the MMCR experts (E. Clothiaux, P. Kollias, K. Moran, private communication), it was decided to only use reflectivity observations between -40 and 8 dBZ and above 1 km elevation to minimize the clipping effect of the range correction. Plans for the future include the monitoring of heavy rainy situation using independent data sets such as rain gauge observations, and the black-listing of the observations in dubious, i.e. heavy-precipitating, conditions. In such occurrences, it appears sensible to apply a larger error to the observations. Currently, the error on observed reflectivities is fixed to 1dBZ (approximately 25%) at all levels.

4.1.3   1D-Var on ARM SGP observations

Assimilation experiments with the new cloud and convection linearized schemes were carried out using observations taken at the ARM Southern Great Plains site (36.6°N - 97.5°W) during January 2001. This site was chosen because of the wealth of passive and active sensor observations that are routinely collected and processed, including radar reflectivities from the MMCR combined with lidar cloud boundaries observations from the Micropulse Lidar that represent the enhanced cloud product ARSCL[11] (Clothiaux *et al.* 2000).

---

[11]Active Remote Sensing of CLouds

Several combinations of observations were assimilated to explore the benefits deriving from profiling versus integrated measurements and from the synergy of both. Specifically the following set of experiments were performed:

- assimilation of reflectivity profile only (hereafter, AN_1);

- assimilation of total column water vapor and longwave downward (LWD) radiative flux at the the surface (hereafter, AN_2);

- combined assimilation of reflectivity, TCWV and LWD (hereafter, AN_3).

The combination of observations used in AN_3 was chosen to reproduce an "upside-down" satellite configuration such as that of EarthCARE where the observations from the active sensors will be perfectly co-located with the passive radiation measurements.

In these experiments, the observation operator H consists of all schemes described in section 4.1.1(b), i.e. two simplified parametrizations of moist atmospheric processes - cloud and convection schemes, a radar model for the computation of reflectivities and a radiative transfer model. Since an adjoint version of the radar model has not yet been developed, the transpose of the observation operator was obtained explicitly through the Jacobian matrix computed in finite differences by a perturbation method.

Results for January 2001 are shown in Figs. 16-20. Panels (a)-(c) of Figure 16 show a comparison of the first guess (b) and the 1D-Var retrieved radar reflectivity (c) versus the MMCR observations (a) for the AN_1 experiment. The 1D-Var analysis is closer to the observations for most of the profiles. Focusing on the first days of the month, it can be seen that the 1D-Var shows skills in increasing the reflectivity at lower levels. A reduction in reflectivity consistent with the observations is shown by the analysis at upper levels around 6-7 January. Less effective is the reduction around 10 January, when the observations indicate no clouds while the model first guess has large values of the reflectivity. Good agreement between analysis and observations is shown on 16-17 January where the cloud patterns are well adjusted to the observations. Major adjustments from the 1D-Var are also evident toward the end of the month (27-28 January). Panel (d) of the same figure displays the reflectivity time series from the AN_2 analysis: it is clear that the assimilation of TCWV and surface LWD radiation does not impact the reflectivity as dramatically. Some improvement with respect to the first guess can, however, be seen at the beginning of the month and around 22-23 January where the first guess shows cloudiness throughout the middle and lower troposphere contrary to the ARSCL reflectivities, and the analysis AN_2 correctly shows a decrease in clouds. The AN_3 analysis is very similar to AN_1 and hence is not shown here.

Figure 17 shows the average bias profile (first guess minus observations and analysis minus observations) over the whole month. The reduction in bias is quite dramatic when assimilating reflectivity only or reflectivity together with the surface LWD radiation flux and TCWV, confirming what seen in the time series plots. The bias in reflectivity gets slightly worse when only surface measurements are used. The standard deviation is, however, decreased with respect to the first guess indicating that the inclusion of an observational constraint acts to control the number of extreme cases and, hence, reduces the variability with respect to the observations.

The difference in TCWV between the first guess departures (absolute value of first guess minus observations) and the analysis departures (absolute value of analysis minus observations) for the three assimilation experiments is shown in Figure 18. The TCWV observations are only avaliable for non-rainy situations. By definition, a positive value of this quantity indicates that the analysis is closer to the observations than the first guess. The differences for AN_1 are mostly positive, indicating that the cloud reflectivity observations had a positive impact in reducing the distance between independently retrieved TCWV and the model background TCWV during
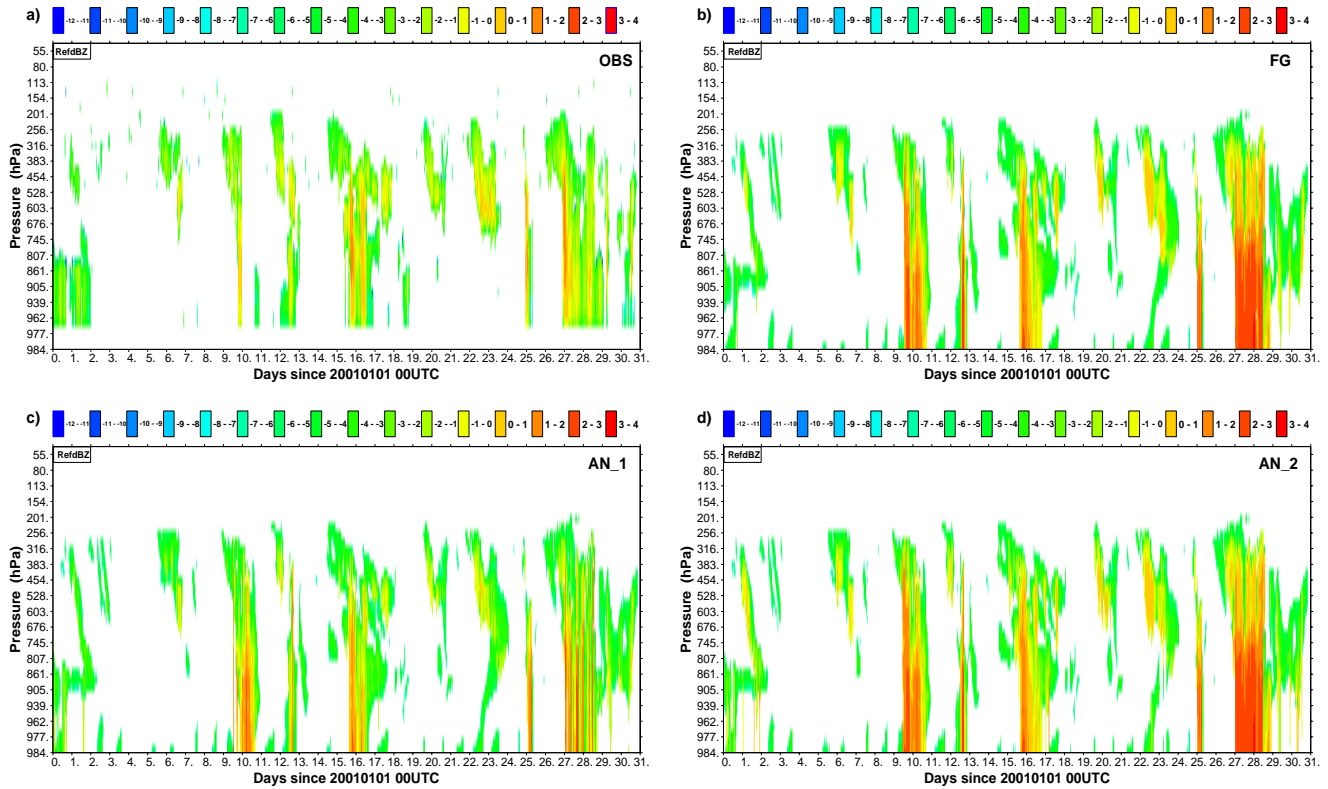
Figure 16: SGP site radar reflectivity (dBZ/10) for January 2001: (a) MMCR observations, (b) model first guess, (c) 1D-Var retrieval, when assimilating reflectivity only (AN_1), and (d) 1D-Var retrieval when assimilating TCWV and surface LWD flux (AN_2). See text for explanations.
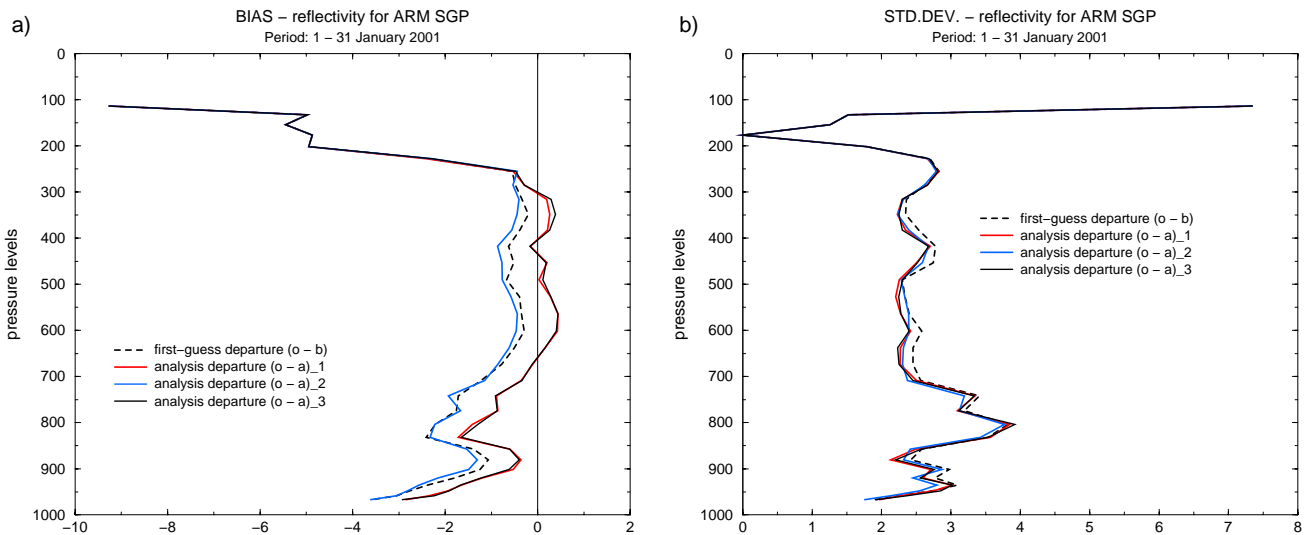
Figure 17: Profiles of radar reflectivity bias averaged over the whole month and the standard deviation: first-guess departures (dashed black line), analysis departures when only the reflectivity profile is assimilated (AN_1, red line), analysis departures when only surface LWD flux and TCWV are assimilated (AN_2, blue line) and analysis departures when reflectivity is assimilated in conjuction with surface LWD flux and TCWV (AN_3, black line).

cloudy days. Analysis AN_2 which includes the TCWV observations provides, not surprisingly, the most dramatic improvements in terms of TCWV, especially for clear sky days. However, the combination of TCWV, surface LWD flux and reflectivity has an overall good impact in all-sky situations benefiting both from the information on in-cloud moisture that can be derived from the reflectivity profile and from the clear-sky TCWV information.
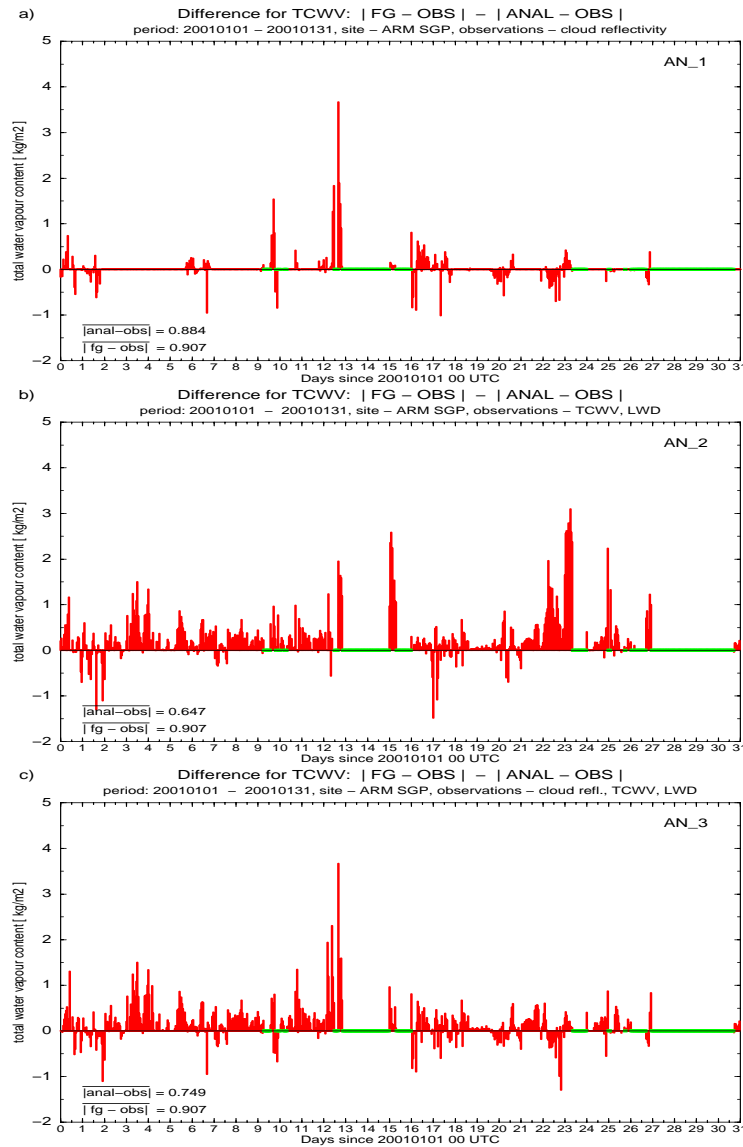
Figure 18: Time series of TCWV differences (in $kg.m^{-2}$) between absolute value of the first guess minus observation and absolute value of the analysis minus observation for January 2001 at the SGP site: (a) analysis AN_1, (b) analysis AN_2, and (c) analysis AN_3. Values of absolute mean differences over the whole month are reported in the lower left corner of the plots.

These results confirm the good behavior of the 1D-Var and show that after an assimilation of a given type of measurements the analysis is closer to those observations. This results is to be expected if convergence in the 1D-Var is achieved. Less intuitive is the way the profiles of temperature and moisture are modified in the minimization itself in order to adjust the initial first guess to the observations. Comparison with independent radiosonde observations were conducted to address this point. Profiles of relative humidity bias and standard deviation averaged over a month are shown in Fig. 19. The dashed black line represents the first guess depar-

tures (radiosonde observations minus first guess) while the solid red, the solid blue and the solid black lines represent the analysis departures (radiosonde observations minus analysis) for the three experiments AN_1, AN_2, and AN_3, respectively. Here, the benefits of combining observations is well visible. The AN_1 analysis produces a relative humidity profile which is closer to the observations (lower bias) and has a smaller standard deviation mostly in the middle and upper troposphere. The AN_2 analysis has a neutral or slightly negative impact above 750 hPa and positive below. This result can be linked to the increased sensitivity of the downward radiation flux to specific humidity and temperature closer to the surface (see Janisková *et al.* 2002a). The experiment where all three types of observations were assimilated retains the benefits from both previous analyses and shows improvements with respect to the first guess at all levels. In the monthly averages, the overall impact of the assimilation is not large in absolute value. However, on a daily basis, there can be large difference in the first guess departures and analysis departures of relative humidity. It is also important to remember that even small changes on relative humidity can induce large differences in supersaturation and lead to cloud formation/suppression.
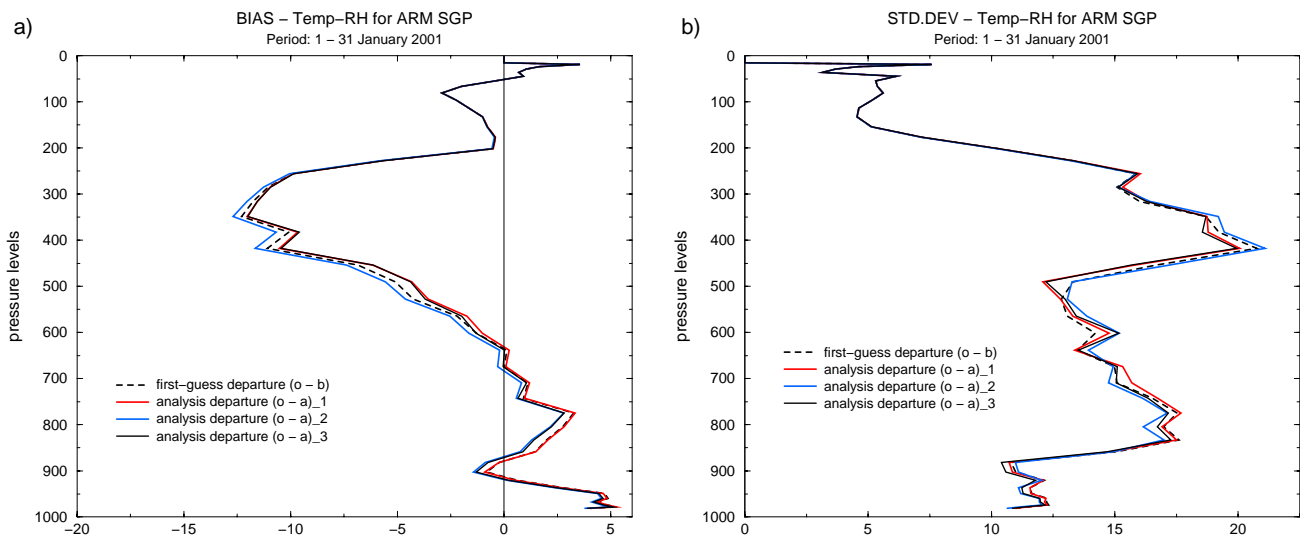
Figure 19: Profiles of relative humidity bias and standard deviation (in %) with respect to radiosounding observations for the first-guess (dashed black line) and 1D-Var retrieved profiles (red, blue, and black lines) for January 2001 at the SGP site. See text for explanations.

Figure 20 shows the impact of the assimilation on the longwave radiative fluxes at the surface (left column) and at the top of the atmosphere (right column). While the surface LWD flux is not an independent measurement for AN_2 and AN_3, the longwave radiation flux at TOA represents an independent source to validate the outcome of the different analyses. As previously, the impact is quantified in terms of the difference between the absolute value of the first-guess departure and the analysis departure. When assimilating reflectivity only, there is no improvement with respect to the fist guess in either the surface and the TOA longwave radiation fluxes. This could be related to the cloud optical properties not being correctly modified through the inclusion of reflectivity observations. On the contrary, the assimilation of TCWV and LWD flux has a positive impact: the surface flux is almost perfectly adjusted and the TOA flux is generally improved. Analysis AN_3 shows an intermediate behavior with improvements in both the surface and TOA longwave radiation fluxes that can be ascribed to the constraint provided by both the TWCV and the surface LWD flux.

Assimilation of radar reflectivities appears to be promising and will be further explored in the near future. Verification with independent observations showed advantages and deficiencies of including profiling versus integrated measurements. It was shown that the synergy of different cloud observations is the most beneficial
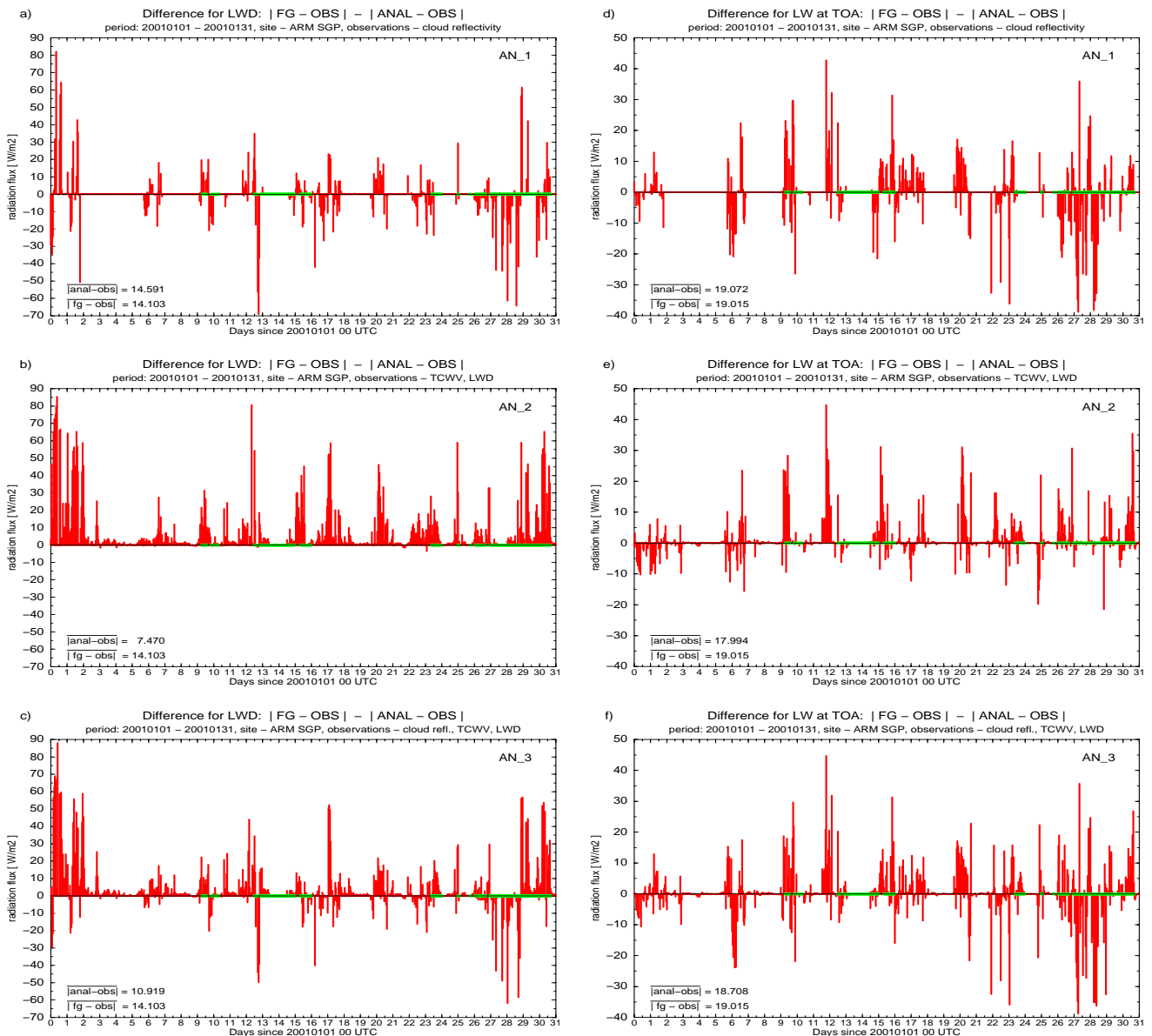
Figure 20: Time series of the differences between absolute value of the first guess minus observation and absolute value of the analysis minus observation for the downward longwave radiation at the surface in $W.m^{-2}$ (a-c) and for the outgoing longwave radiation at the TOA in $W.m^{-2}$ (d-f). Results are respectively displayed for the three experiments AN_1, AN_2 and AN_3.

toward improving the performance of the cloud assimilation system. Further improvements in the model will also facilitate the use of new satellite observations that will become available in the near future from missions such as EarthCARE, CloudSat and CALIPSO.

4.1.4   1D-Var on ARM TWP observations

Feasibility studies in a 1D-Var framework have been carried out to examine situations where convective clouds are dominant. The diagnostic cloud scheme, which was used in the previous 1D-Var experiments with cloud-

radiation observations (Janisková 2001, Janisková *et al.* 2002b), has several weaknesses, particularly prevalent in the tropics. These weaknesses did not allow us to perform assimilation experiments over the tropical areas or for the periods with predominant convective activity. The description of cloud processes was improved in the new diagnostic cloud scheme developed by Tompkins and Janisková (2004) and described in section 3.2. The capability of this scheme combined with the simplified convection scheme (Lopez and Moreau 2004) and radiation schemes (Janisková *et al.* 2002a) to assimilate observations from the Tropical Western Pacific (TWP) sites of ARM has been assessed.

Only observations of total column water vapour and downward longwave radiation at the surface were used since the cloud radar reflectivities were often not available or they were not reliable over the TWP sites. Experiments presented here were performed over the ARM TWP C2 site (Nauru) during January 2001 and TWP C1 site (Manus) during May 2001. Two different sides and two different periods were selected to investigate the potential of 1D-Var system in two different tropical regimes. As the tangent-linear and adjoint versions of all schemes being part of the observation operator H do exist, a computation of the gradient of the objective function during the minimization was done in an effective way using the adjoint technique.

(a) Results for the ARM TWP Nauru site

The TWP Nauru site is located at 0.5° S - 167° E and is drier than the other TWP site. There are usually two peaks in cloud cover, at around 900 and 100 hPa, corresponding to shallow and deep convection, respectively. There are nearly no mid-level clouds since the atmosphere is quite dry there. Figure 21 displays the cloud cover for the month of January 2001 obtained using the different cloud schemes (operational prognostic scheme - *OPERPROG*, operational diagnostic scheme - *OPERDIAG*, new diagnostic scheme - *NEWDIAG*). From this figure, it can be seen that the *OPERDIAG* somewhat exaggerates upper level cirrus cloud cover and produces too much clouds throughout the mid troposphere, with a flat featureless profile, when compared to the more complex *OPERPROG*. These weaknesses in the *OPERDIAG* prevented 1D-Var experimentation over the tropical site in earlier studies. The new cloud scheme is able to reproduce the general cloud fraction structure, with peaks in the lower and upper cloud fraction due to its direct link to convection through the detrainment term and therefore it can be used in data assimilation. The analyzed cloud cover obtained after 1D-Var assimilation of the ARM observations using the *NEWDIAG* scheme is displayed in Fig. 21d showing mostly an increase in the lower cloud fraction. How this modification in cloud fraction is connected with changes in temperature and humidity profiles is presented in Fig. 23-25. The impact of modified temperature, humidity and cloud characteristics on the radiation fluxes is shown in Fig. 22.

Improvement versus deterioration of the analysis with respect to the first guess after 1D-Var assimilation of ARM observations are summarized for the surface and the TOA radiation fluxes in Fig. 22. The results are presented as the differences between the absolute value of the first guess minus observation and the absolute value of the analysis minus observation for the downward longwave radiation at the surface (a), the downward shortwave radiation at the surface (b), the outgoing longwave radiation at the TOA (c) and the shortwave radiation albedo at the TOA (d). Positive values indicate an improvement of the analysis with respect to the first guess when compared to the observations. On the left corner of the figure, there are values of the absolute mean differences between analysis and observation, as well as between the first guess and observation for the whole period. As the downward longwave radiation was one of the assimilated observations, significant improvement of the resulting analysis is not surprising. Improvements in the analyzed downward radiation at the surface and the outgoing longwave radiation at the TOA with respect to the first guess is more rewarding since observations of those fluxes were not used in the assimilation and they represent independent observations. From the set of radiation fluxes verified in our experiments, the shortwave radiation albedo at the TOA is the only radiation flux not improved by 1D-Var.

Figure 23 shows a comparison of the first guess and analysis against the observations (obs_rs - radiosonde,
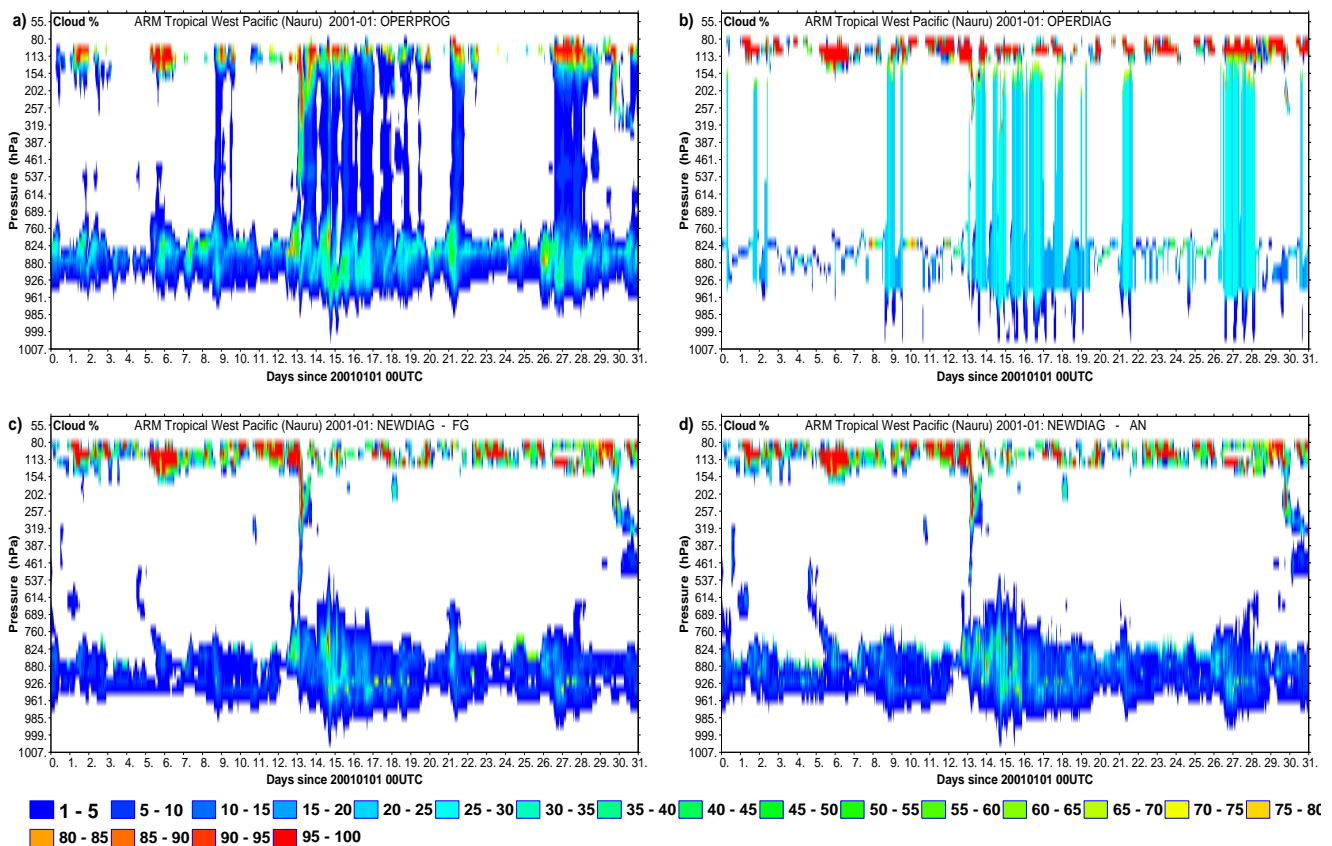
Figure 21: Time series of the cloud cover (%) over the ARM TWP C2 site (Nauru) during January 2001 predicted by: (a) the operational prognostic scheme (OPERPROG), (b) 4D-Var operational diagnostic scheme (OPERDIAG) and (c) the new diagnostic scheme (NEWDIAG) used in 1D-Var experiments. (d) shows analyzed cloud cover after 1D-Var assimilation of ARM observations.

obs_mr - microwave) of the total column water vapour. The wet index marked in the figures (in green) means that the MWR observation was not used (either it was unreliable or unavailable). It is clear that 1D-Var succeeded not only to get closer to the radiation observations, but also to improve the humidity analysis as it appears from the analyzed TCWV. The mean absolute difference between the analysis and observation for the whole month (2.314 kg m^{-2}) is lower than the difference between the first guess and observations (3.805 kg m^{-2}). During the periods when the modified humidity after 1D-Var assimilation led correctly to increased TCWV, the fractional cloud cover was also increased (Fig. 21). Such modifications occurred for several periods of January 2001 and they appear to be more significant on 1 and 6 January, the second half of 16 January, from 24 to 25 January and on 30 January 2001. On the contrary, the decreased TCWV correspond also to the decreased cloud cover as seen especially at the end of 13 and beginning of 14 January, the second half of 17 January and on 22 January 2001. In some of these periods of larger modifications in the cloud fraction corresponding to the improved TCWV, the fit of analysis to independent observations of radiation fluxes was also improved (Fig. 22). This is observed for the downward shortwave radiation at the surface on 6, 13, 16 and 22 January 2001, and for the upward longwave radiation at the TOA on 6 January, in period of 24-25 January and on 30 January 2001.

The results for the liquid water path are presented in Fig. 24. Despite the fact that the cloud LWP was not assimilated in 1D-Var, the analyzed values got significantly closer to the microwave observations. The situations with larger improvement corresponds to those cases, when the fit of analyzed TCVW to the observations was
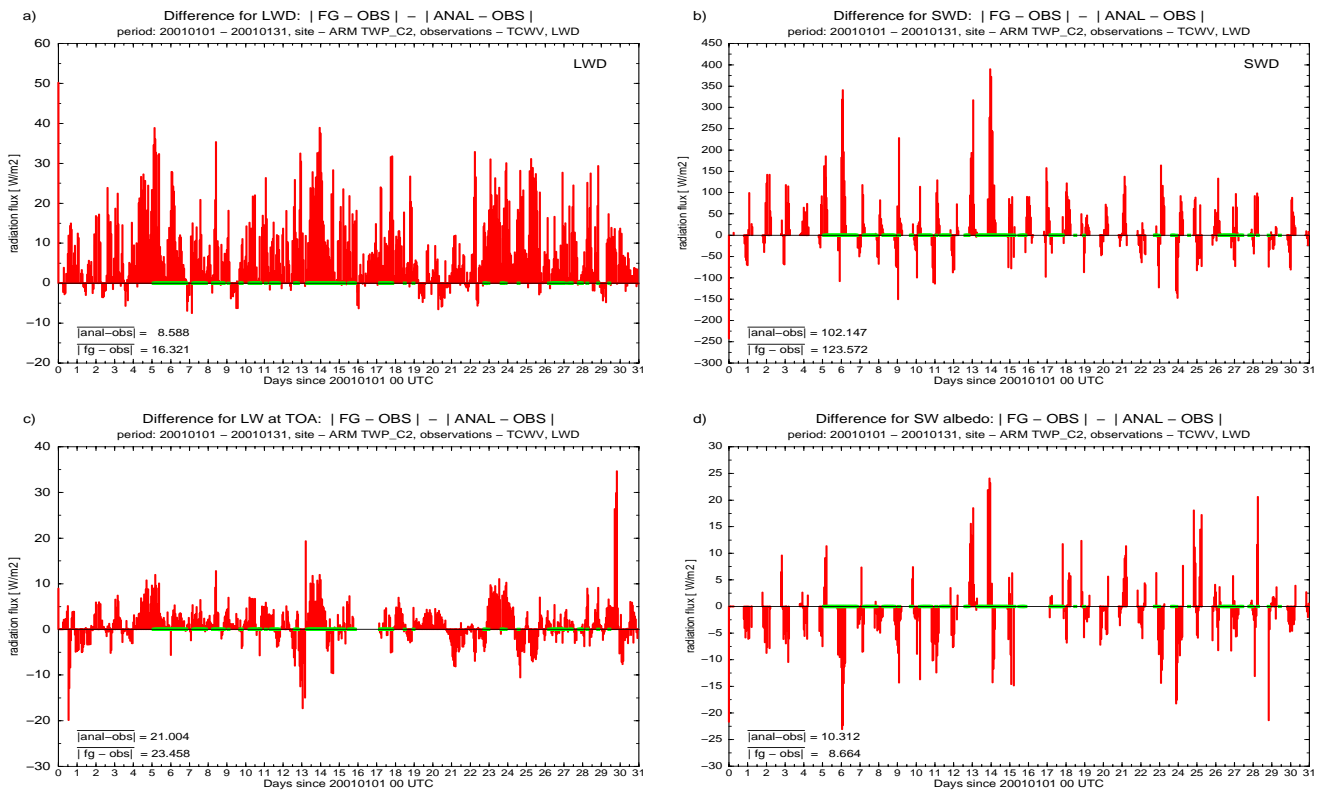
Figure 22: Time series of the differences between absolute value of the first guess minus observation and absolute value of the analysis minus observation for the downward longwave radiation at the surface (a), the downward shortwave radiation at the surface in (b), the outgoing longwave radiation at the TOA (c) and the shortwave radiation albedo at the TOA (d) over the ARM-TWP Nauru site during January 2001. The radiation fluxes are in $W.m^{-2}$. Average values of absolute mean differences over the whole month are reported in the lower left corner of the plots.
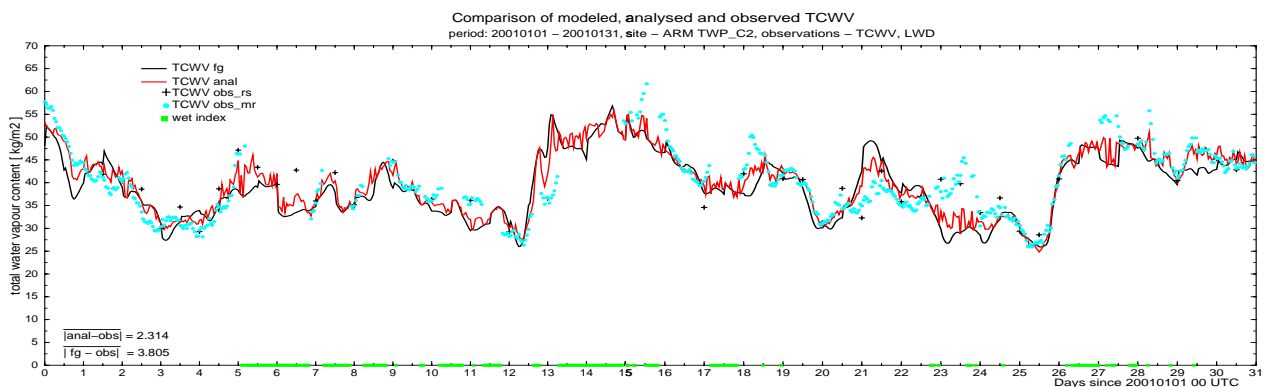
Figure 23: Comparison of the first guess and analysis against observations (obs_rs - radiosonde, obs_mr - microwave) of the total column water vapour ($kg.m^{-2}$) over the ARM-TWP Nauru site for the period of January 2001. Values of absolute mean differences between analysis and observations (obs_mr), as well as between the first guess and observations over the whole month are reported in the lower left corner of the plot.

also improved. One can find them, for instance, on 2 January and at the beginning of 3 January, on 16 January, from 22 to 26 January and on 30 January 2001.

As mentioned at the beginning of section 4.1.4, the cloud radar reflectivities are often not available or not
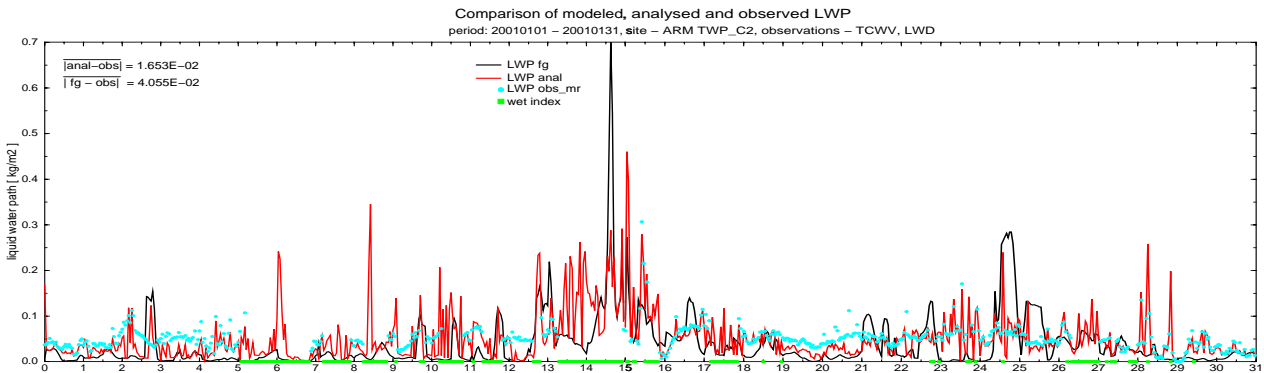
Figure 24: *Comparison of the first guess and analysis against observations (obs_mr - microwave) of the liquid water path* ($kg.m^{-2}$) *over the ARM-TWP Nauru site for the period of January 2001. Values of absolute mean differences between analysis and observations, as well as between the first guess and observations over the whole month are reported in the upper left corner of the plot.*

reliable at the ARM TWP sites. The only observations, that can provide information on the vertical structure of the modifications created by 1D-Var, are radiosonde observations. The background and analyzed profiles of temperature and humidity have been compared against radiosonde observations, which were not used for the assimilation. It can be seen that 1D-Var reduces bias (except few levels) and standard deviation for relative humidity (Fig. 25). The results are neutral for temperature (not shown). This indicates that, similarly as in the extratropics, it is mainly the specific humidity representation which is improved by the 1D-Var retrieval.
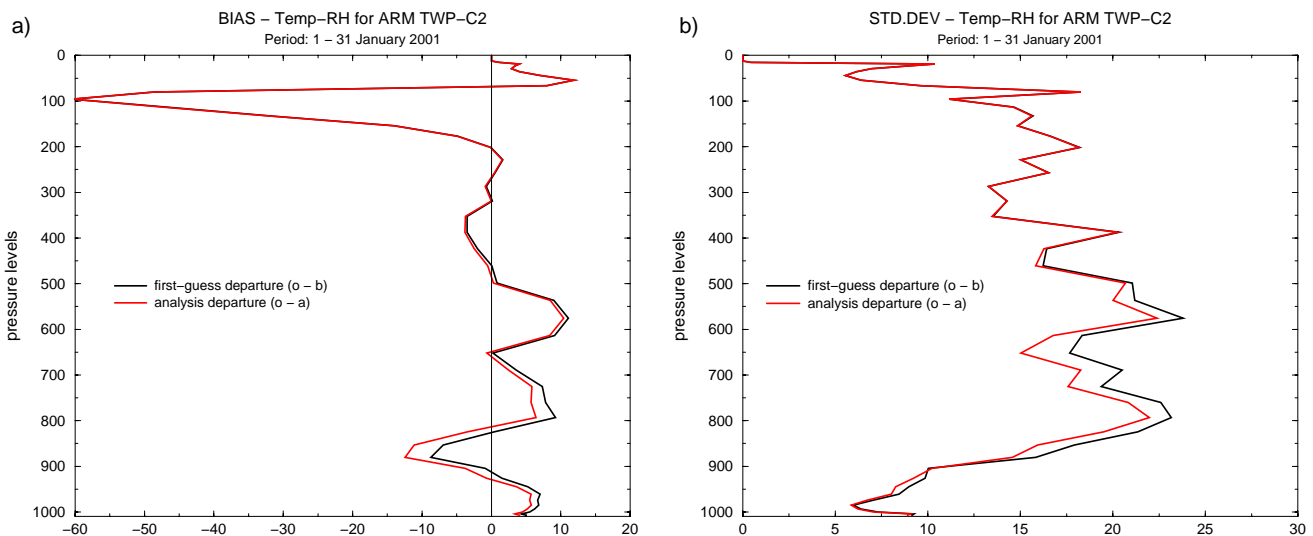
Figure 25: *Profiles of relative humidity bias and standard deviation (in %) with respect to radiosounding observations for the first-guess (black line) and 1D-Var retrieved profiles (red line) for January 2001 at the TWP Nauru site.*

(b) Results for the ARM TWP Manus site

The atmosphere over the TWP Manus site, which is located at $2°$S - $147°$E, is more humid and convection is usually more vertically developed. The deficiencies of the current operational diagnostic scheme *OPERDIAG* are even more obvious there than at the TWP Nauru site as seen on Fig. 26, which presents the time series of the cloud cover for the month of May 2001. In the presence of deep convection, the *OPERDIAG* has the cloud cover throughout the mid-troposphere fixed directly to the convective precipitation amount, which

mostly produces the uniform cloud cover of around 30 %. This cloud cover does not respond to the evolving thermodynamical conditions in a reasonable way and the data assimilation with such scheme might lead to an improper modifications of the temperature and humidity profiles. Though the *NEWDIAG* produces a cloud cover which is not perfect when compared to *OPERPROG*, the general structure of cloud fraction is preserved. Moreover, the experiments also showed (Tompkins and Janisková 2004) that the new scheme produces an authentic replication of the prognostic scheme's profile of both ice and liquid, with the peak in mid-level cloud water. These features are important for the assimilation in deep convective regions. The prevailing feature of the analyzed cloud cover (Fig. 26) is its reduction, though some increase in the cloud fraction was also observed, for instance on 2, 7 and 11 May 2001.
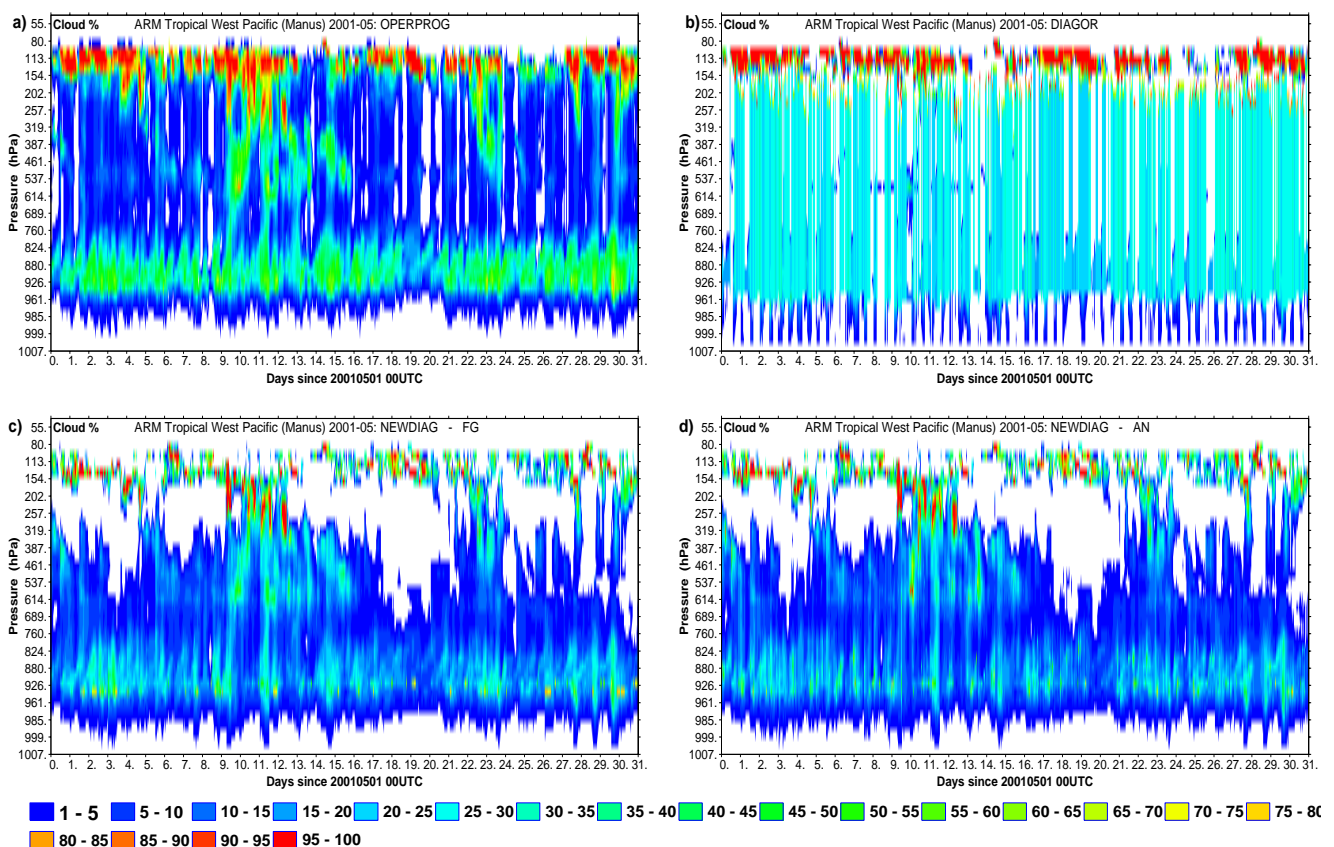
Figure 26: As Fig. 21, but over the ARM-TWP Manus site for the period of May 2001.

The difference in the surface and the TOA radiation fluxes between the first guess departures and the analysis departures is shown on Fig. 27. Here, contrary to the TWP Nauru site, the only radiation flux which is not improved after 1D-Var assimilation is the outgoing longwave radiation at the TOA. The overall slight deterioration of this flux comes from the period of three days - 10, 12 and 13 May 2001, where the shortwave radiation at the surface and the TOA is not improved either. As seen in Fig. 28, those are periods with very few TCWV observations. In this case, the temperature and humidity profiles were only adjusted through the downward longwave radiation observation, which can create an ambiguity on the retrieval. Indeed, when the TCWV observations in the middle of the period of 12-13 May 2001 exist, the analysis with respect to all compared radiation fluxes is improved. Though the TCWV observations are also absent on 1 May 2001, the analysis of radiation fluxes was improved here. This indicates that if only LWD is used as observation, the analysis can be arbitrarily either improved or deteriorated.

Comparison of the first guess and analysis against the microwave and few radiosonde observations (present
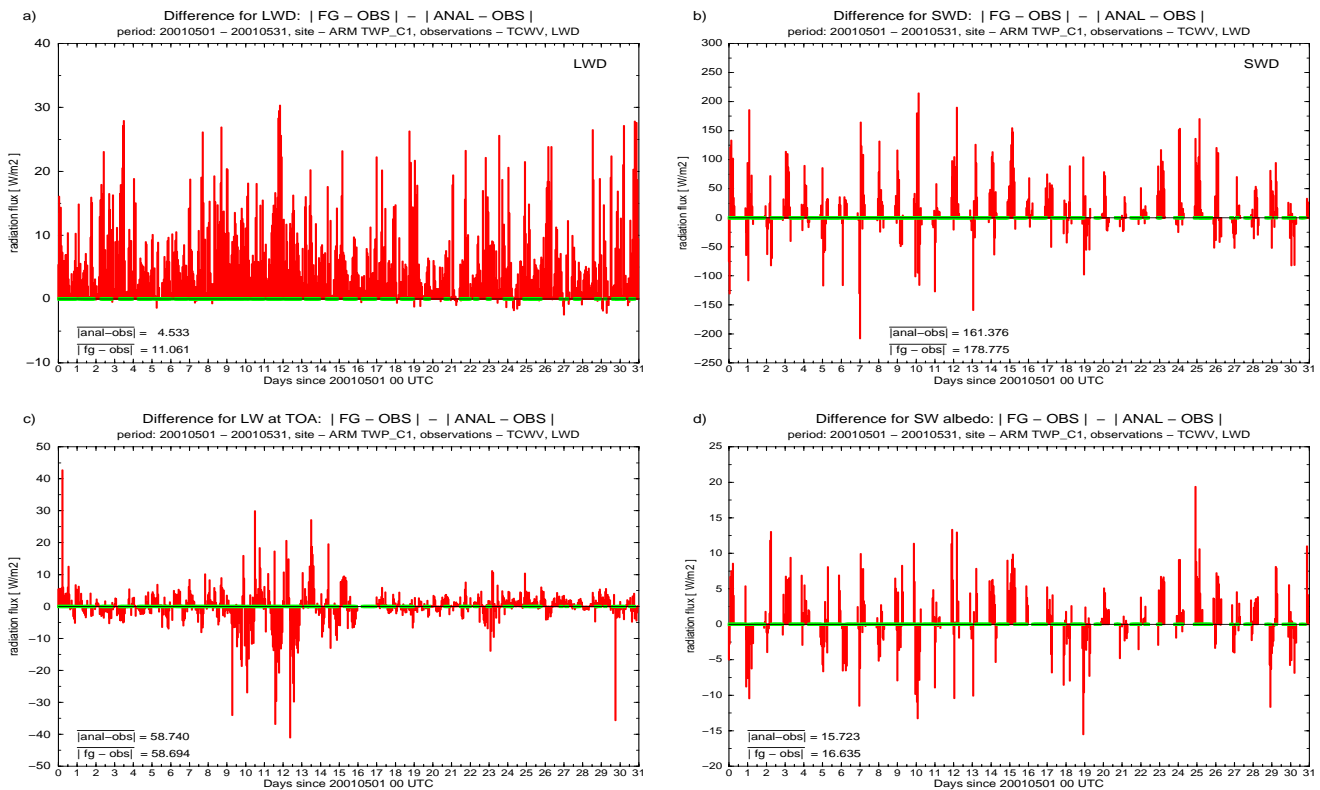
Figure 27: As Fig. 22, but over the ARM-TWP Manus site for the period of May 2001.

mostly in the second half of month) is shown on Fig. 28. The MWR observations were also missing or discarded quite often in the first half of month, since they were contaminated by precipitation and the presence of condensation on the optics, as indicated by wet index on the figure. Since TCWV measurements are assimilated in our experiments, the analysis provides a better fit to the observations. The mean absolute difference between the first guess and observations (3.164 kg m^{-2}) is reduced to 2.307 kg m^{-2} for the analysis.
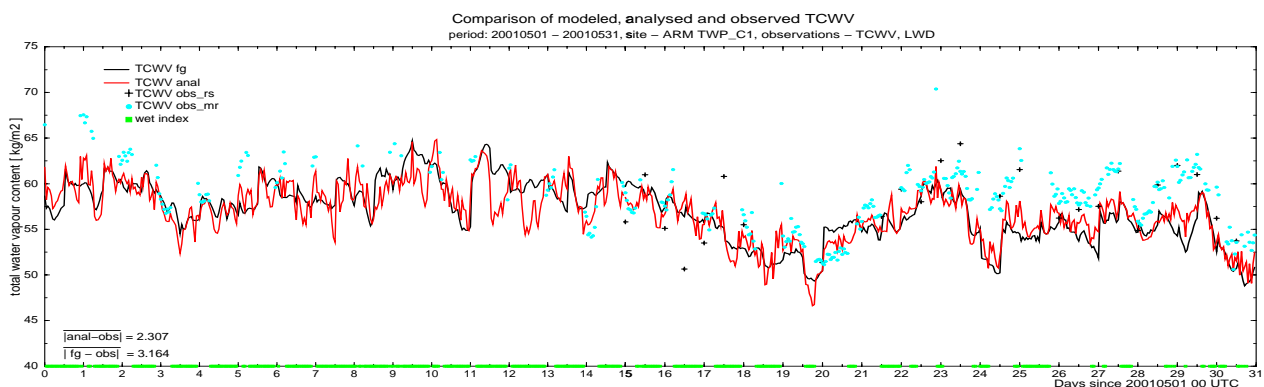
Figure 28: As Fig. 23, but over the ARM-TWP Manus site for the period of May 2001.

The liquid water path is improved after 1D-Var assimilation of LWD and TCWV observations (Fig. 29), though less significantly than over the TWP Nauru site. Periods with a large correction of the LWP correspond to the situations when the fit of the analyzed TCWV to the observations was also more improved. Such positive corrections of moisture are observed during the first 8-9 hours of 4 May 2001, overnights of 14 and 15 May 2001,

as well as during 21 May 2001. In all these situations, the shortwave radiation fluxes, either at the surface or the TOA atmosphere, were improved. For the outgoing longwave radiation at the TOA, the impact of these corrections is less obvious. The cloud fraction in the cases with improved moisture and shortwave radiation fluxes is slightly decreased (Fig. 26).
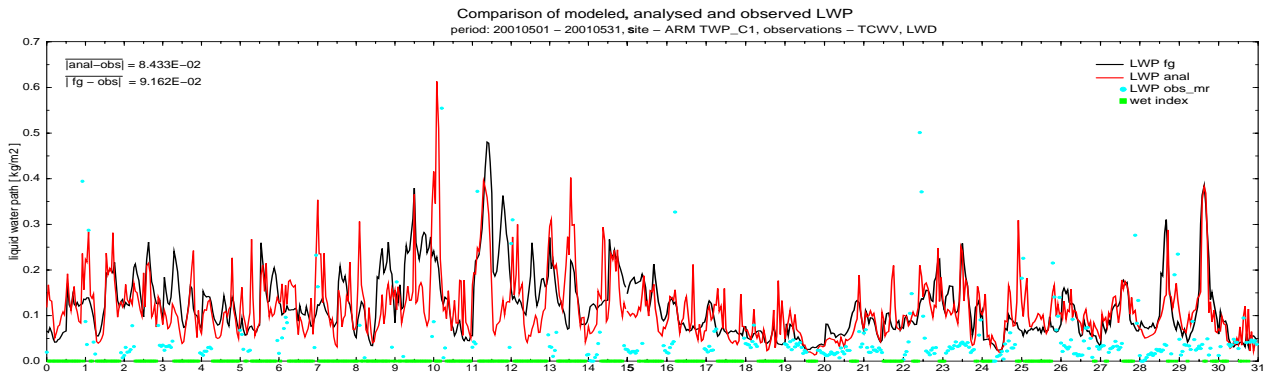
Figure 29: As Fig. 24, but over the ARM-TWP Manus site for the period of May 2001.

Comparison with independent radiosonde observations, when available, indicates that the analyzed profiles of relative humidity are improved compared to the first-guess profiles (Fig. 30). The modification of temperature profiles is small (not shown). Similarly to other ARM sites, it is the specific humidity, which is mainly improved by 1D-Var retrieval.
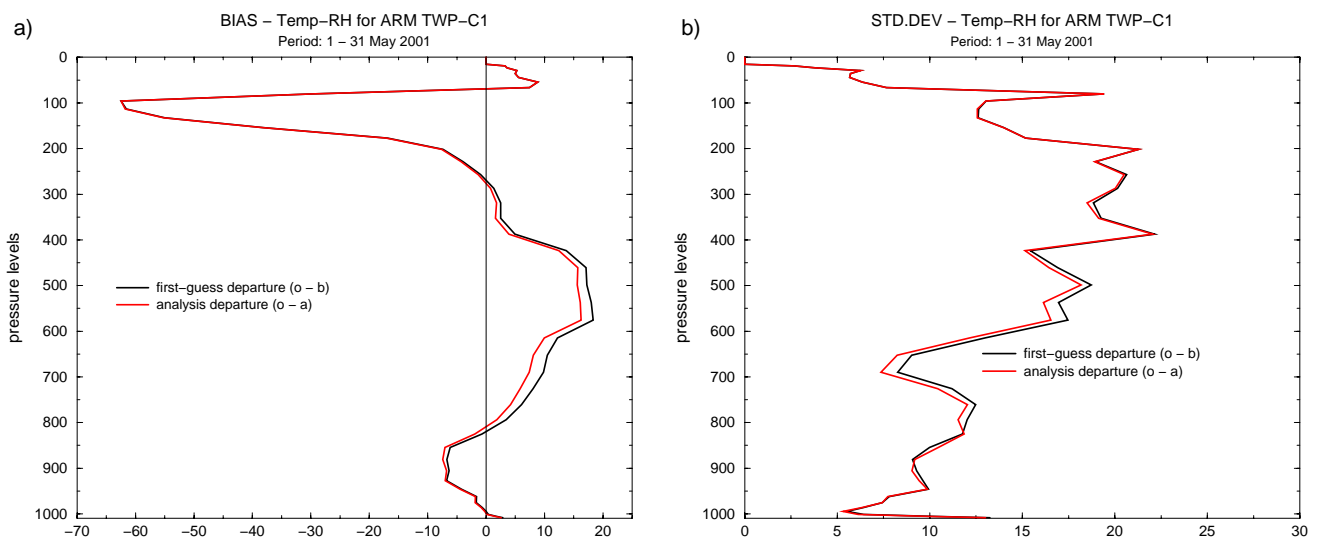
Figure 30: Profiles of relative humidity bias and standard deviation (in %) with respect to radiosounding observations for background (black line) and 1D-Var retrieved profiles (red line) for May 2001 at the TWP Manus site.

The 1D-Var assimilation of observations from the ARM TWP sites has shown a capability to improve the analysis of temperature and specific humidity when using the new moist parametrization schemes for cloud and convection processes in situations when convective clouds are dominant. However, it has also revealed some weaknesses of the 1D-Var system on those sites, such as an ambiguity in the retrieval when the surface humidity observations are not available as well as the lack of complementary observations to the surface observations, such as the cloud radar reflectivities. Feasibility studies in a 1D-Var framework will be carried out for the

4.2 The capability of the 4D-Var system to assimilate cloud affected radiances

Some studies have been done to investigate the capability of 4D-Var systems to assimilate cloud-affected satellite infrared radiances (Chevallier *et al.* 2003). 4D-Var assumes that the forward operator is linear in the vicinity of the background. Observations for which significant non-linearities affect the forward model are discarded. Therefore infrared satellite radiances are currently not assimilated in the presence of clouds. At ECMWF, an observation operator has been developed that computes cloud-affected satellite brightness temperatures from some control variables (profiles of temperature and specific humidity). It contains a diagnostic cloud scheme with a representation of large-scale and convective processes and a radiation model. The possibility of using this operator to assimilate cloud-affected infrared radiances from the narrow-band Advanced Infrared Sounder (AIRS) has been assessed. The study showed that there is a potential benefit in assimilating directly in 4D-Var some of the upper tropospheric channels at 4.5, 6.3 and 14.3 μm in the presence of clouds. Scientific developments to the current 4D-Var systems may still be needed, for instance to improve the estimation of background error statistic, or to harmonize the resolution of the observations and the variable model resolutions within the incremental formulation.

The observation operator developed for this study has also been used for 1D-Var retrievals. In the experiments, observations of AIRS brightness temperature from 35 upper tropospheric channels are used. The retrievals are performed only if clouds are detected in more than 13 channels. Figure 31 (provided by Chevallier, ECMWF 2003) shows the comparison of the retrieved relative humidity against European radiosondes for the period of November 2002 to February 2003. Using 1D-Var of AIRS observations, the root mean square error of relative humidity is reduced.
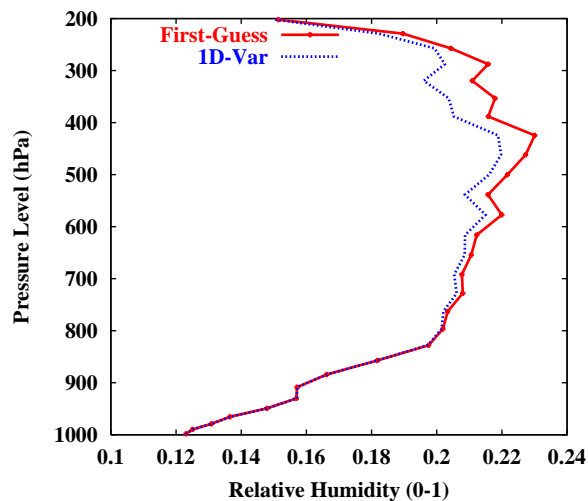
Figure 31: Comparison of the first-guess (red) and retrieved (blue) relative humidity using 1D-Var of AIRS observations against European radiosondes for the period of November 2002 to February 2003. Results are presented as root mean square errors. Relative humidity is defined between zero and one.

Another important result of the mentioned study performed by Chevallier *et al.* (2003) concerns a quality of the new diagnostic cloud scheme (Tompkins and Janisková 2004). It is expected that this scheme does not perform as well as the prognostic scheme in dynamic mode for long long integrations, but in static mode the comparison between model and observations was not very sensitive to whether the diagnostic model or the reference

prognostic cloud scheme is used. Both explain a significant portion of the observation variance, except, for both, in the Tropics at 11 μm. The diagnostic scheme explains a slightly lower portion of the variance, but has smaller biases due to different tuning. Further, the two schemes should have similar sensitivities, since the new diagnostic scheme describes the basic processes of stratiform cloud generation through large-scale motions, convectively generated cloud, precipitation generation and evaporation, which were shown (Fillion and Mahfouf 2003) to dominate the sensitivity of the prognostic scheme. As a consequence, it seems that the diagnostic model could be used in the 4D-Var observation operator in lieu of the prognostic model used in the forecast model, without having to introduce cloud variables in the 4D-Var control vector.

5 Sensitivity studies

5.1 Sensitivity of the radiation scheme to input variables

The adjoint models can be used not only for the data assimilation, but also for sensitivity studies since they enable the computation of the gradient of one output parameter of a numerical model with respect to all input parameters (Le Dimet and Talagrand, 1986). Compared with the standard approaches for evaluating physical parametrization schemes (i.e., sensitivity of all the outputs by modifying one given input quantity), the adjoint is a complementary and very efficient approach for sensitivity studies. A single integration in which one output parameter is modified by unit size perturbations provides the sensitivity of this parameter to all input parameters. When such a technique is applied to a particular physical parametrization scheme, it can provide information on the meteorological variables to which the parametrization scheme are the most sensitive. From a data assimilation point of view, it can give some indications related to the importance and efficiency of particular types of observations in modifying the analysis.

For instance, the vertical extension of the areas showing sensitivity to a given surface radiation observation may support increasing the number of upper-level observations of a certain kind in order to improve this surface radiation flux.

5.1.1 Methodology

The formulation of a sensitivity problem for the radiation scheme can be explained as follows. Using the parametrization schemes for the shortwave and longwave radiation, let $\mathbf{y}$ denote the vector of the outputs (radiation fluxes) from the radiation schemes. It can be expressed as

$$\mathbf{y} = F(\mathbf{x}) \tag{16}$$

where $\mathbf{x}$ is the vector representing an atmospheric state described by temperature T, specific humidity q, surface pressure p_s and cloud characteristics (cloud fraction, liquid water and ice water contents). $F(\mathbf{x})$ is the direct nonlinear operator including the shortwave and longwave radiation schemes with their description of the cloud optical properties and cloud overlap assumption.

A small perturbation $\delta \mathbf{y}$ can be estimated to the first order by the tangent linear equation of the radiation scheme as:

$$\delta \mathbf{y} = \frac{\partial F}{\partial \mathbf{x}} \delta \mathbf{x} \quad \text{or} \quad \delta \mathbf{y} = \mathbf{F_x} \delta \mathbf{x} \tag{17}$$

where $\mathbf{F}$ is the tangent-linear operator of F.

Given the definition of the adjoint of a linear operator for the scalar product:

$$\forall \mathbf{x}, \forall \mathbf{y} \qquad < \mathbf{y} \mid \mathbf{F}.\mathbf{x} > = < \mathbf{F}^T.\mathbf{y} \mid \mathbf{x} > \tag{18}$$

the adjoint $\mathbf{F}^T$ of the linear operator $\mathbf{F}$ provides the gradient of an objective function $\mathscr{J}$ with respect to $\mathbf{x}$ (input variables) given the gradient of $\mathscr{J}$ with respect to $\mathbf{y}$ (output variables):

$$\frac{\partial \mathscr{J}}{\partial \mathbf{x}} = \mathbf{F_x}^T.\frac{\partial \mathscr{J}}{\partial \mathbf{y}} \quad \text{or} \quad \nabla_{\mathbf{x}} \mathscr{J} = \mathbf{F_x}^T.\nabla_{\mathbf{y}} \mathscr{J} \tag{19}$$

In our experiments, the gradient with respect to $\mathbf{y}$ of unit size (i.e. perturbation of some of the radiation fluxes which are output variables of the radiation scheme) is provided to the adjoint of radiation schemes in order

to get the sensitivity of this scheme with respect to its input variables, i.e. temperature, specific humidity and cloud characteristics. This leads to

$$\nabla_{\mathbf{x}} \mathscr{J} = \frac{\partial F}{\partial \mathbf{x}} \tag{20}$$

where $\partial F/\partial \mathbf{x}$ is the corresponding Jacobian matrix.

5.1.2 *Experimental framework*

The method described above has been used in order to examine the sensitivity of the radiation schemes described in Section 3.1 and in more details, in Janisková *et al.* (2002a). To be as close as possible to the full nonlinear radiation schemes used in the forecast model, the linearized shortwave radiation scheme uses the same six spectral intervals as the non-linear scheme, and the linearized longwave radiation scheme is run not using the global mean Jacobian matrices, but using the Jacobian matrices computed at each grid point for each time step of integration. In our experiments, the perturbations of the radiation fluxes with the unity size (± 1 W.m^{-2}) have been used as input for the adjoint of the radiation schemes. The sign was chosen so that an increase in cloudiness (or opacity) will lead to a positive sensitivity. [12] The sensitivity of the downward longwave and shortwave radiation fluxes at the surface, as well as the outgoing longwave (OLR) and shortwave (OSR) radiation fluxes at the top of atmosphere (TOA) has been studied with respect to the input variables. In this report, only the results for the sensitivity of the TOA radiation fluxes are presented.

Two months of integrations were carried out at T159L60 resolution (120 km horizontal resolution and 60 vertical levels) using the ECMWF model for the periods of January 2003 (hereafter the winter case) and July 2003 (the summer case). Each integration was performed up-to 48 hours starting at 12 UTC and the outputs were archived every 3 hours. Clear sky and cloudy conditions are discussed. In the case of clear-sky sensitivities, the time evolution of the nonlinear model is not modified, the cloud characteristics (fraction, cloud liquid and ice water contents) are only set to zero before calling the adjoint of the radiation scheme at each integration step.

The time averaging is performed for sensitivity analysis between 12- and 36-hour of integration, representing a full day, and the sensitivities in that interval are averaged over the whole month. When investigating the diurnal cycle, averaging is done for each 3-hour outputs over the whole month in the same time interval. For the shortwave radiation, to avoid a strong dependence of the sensitivity to the intensity of solar radiation, the sensitivities are weighted, i.e. divided by the actual shortwave radiation flux and multiplied by the mean shortwave radiation at the top of atmosphere.

5.1.3 *Numerical results*

(a) Clear-sky case

The sensitivity of the shortwave upward radiation flux at the top of atmosphere with respect to specific humidity in clear sky conditions is shown on Fig. 32 for the winter (a) and summer (b) cases. The results are presented as zonal means. The shortwave radiation is the most sensitive to humidity at high latitudes in the summer hemisphere, while the tropics is an insensitive region. These latitude dependent features are linked to the surface albedo. Since the tropical surface is mainly characterized by dark oceans, the atmosphere and surface system almost fully absorb the radiation, leading to a small signal in upward (reflected) radiation at TOA. By contrast, the surface at high latitudes is characterized by snow or ice cover with large brightness (a larger albedo), leading to a larger contribution to the upward radiation. Indeed, the sensitivity structure at 700 hPa (Fig. 33), which corresponds to the maximum absorption height illustrates the predominant link to the surface albedo. One

---

[12]Note that the parametrization schemes produce fluxes which are counted positive downwards at the ECMWF model.

can see a large sensitivity over the summer polar areas and lands with a large albedo. Similar results were obtained by Li and Navon (1998) in their study of adjoint sensitivity of the Earth's radiation budget to cloud cover, water vapour, atmospheric temperature and surface temperature in the model of the National Centers for Environmental Prediction (NCEP). They also observed, as in our study, that the sensitivity at high latitudes in the southern summer hemisphere is stronger than that in the northern summer hemisphere.
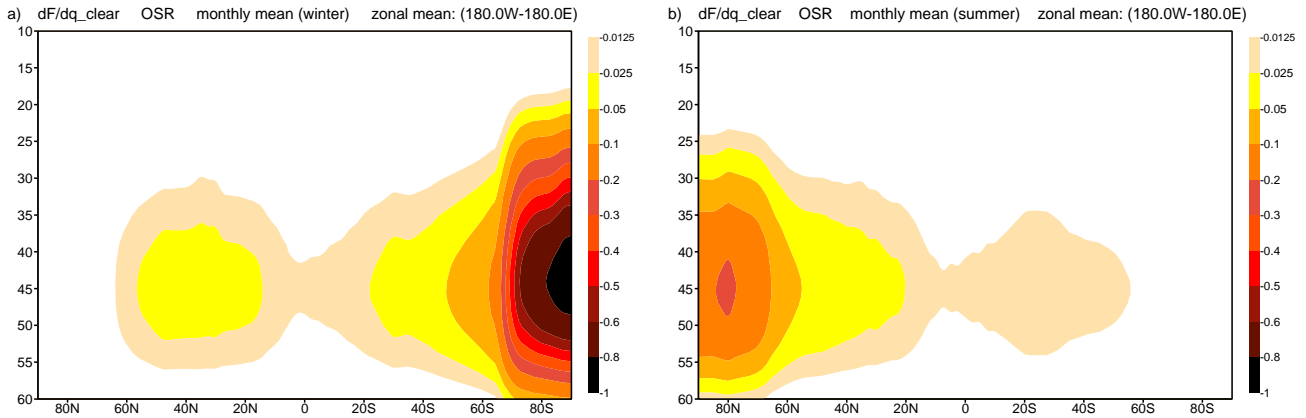
Figure 32: The zonally averaged sensitivity of the upward shortwave radiation flux at the top of atmosphere (TOA) to specific humidity in clear sky conditions. Results are presented for (a) January and (b) July cases. The colour contour intervals are in $Wm^{-2}g^{-1}kg$.
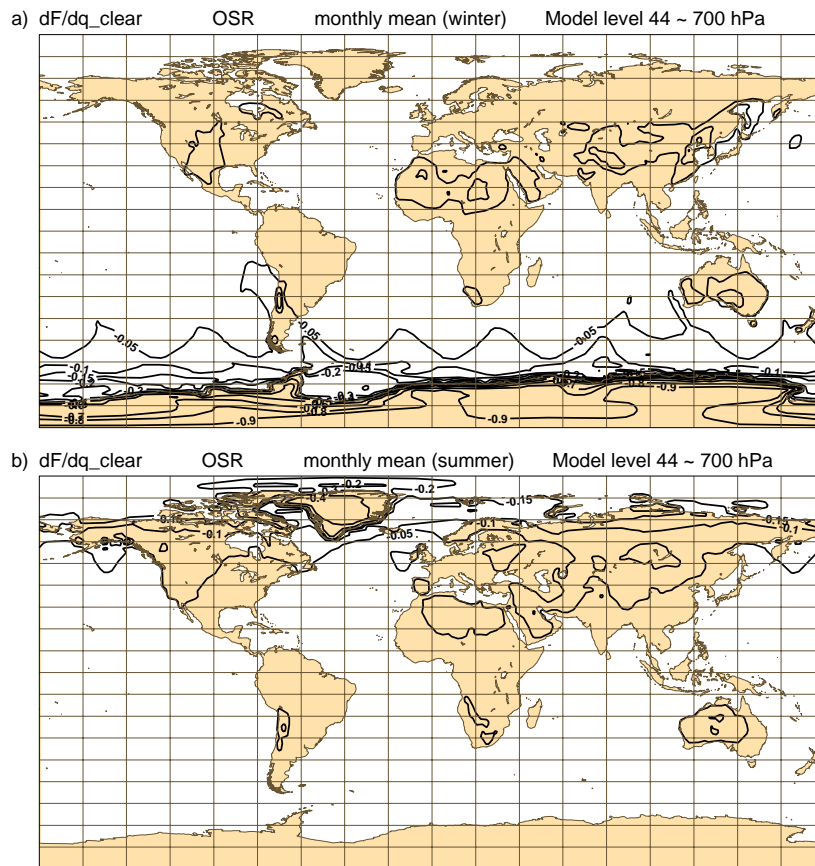
Figure 33: Sensitivity of the upward shortwave radiation flux at the TOA to specific humidity (in $Wm^{-2}g^{-1}kg$) for the model level close to 700 hPa. (a) shows the results for January case and (b) for July one.

Figure 34 illustrates the zonally averaged OLR sensitivity to specific humidity. The largest sensitivity is found near the tropopause in the tropics. The maximum value of sensitivity, which is around 30 W m^{-2} g^{-1} kg, is located in the winter hemisphere. The secondary maxima are over the winter polar areas, between model levels L35 - L40 (corresponding to the pressure levels around 350 - 540 hPa). In the extra-tropics, the sensitivity is larger in the southern winter hemisphere than in the northern one. Moreover, there is a small negative value of sensitivities in the high latitudes in the middle and lower troposphere. This negative value of sensitivity is larger in the southern winter hemisphere, while it is below of the plotting interval in the northern winter hemisphere. Generally, OLR is at least one order of magnitude more sensitive to specific humidity in the upper troposphere than in the middle and lower troposphere.
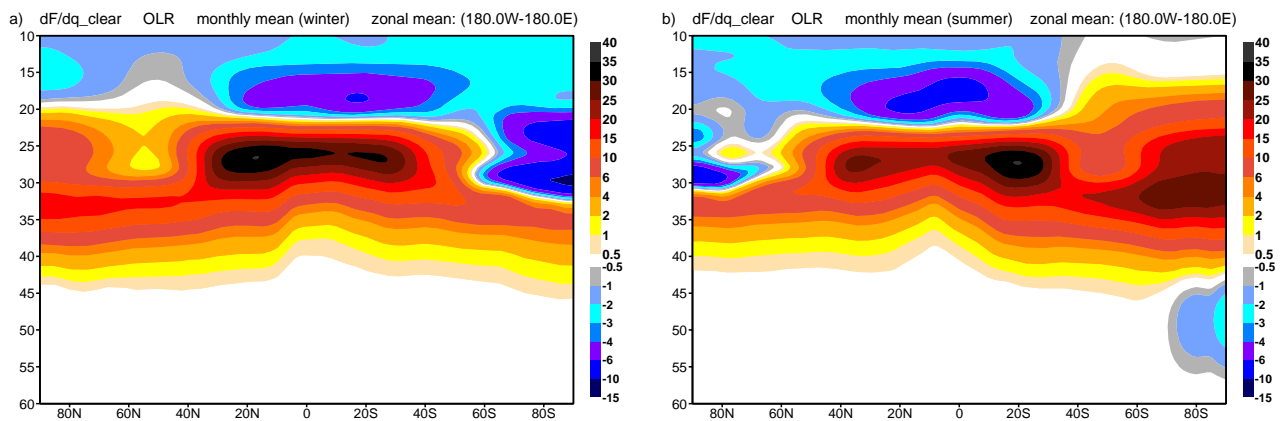
Figure 34: The zonally averaged sensitivity of the upward longwave radiation flux (OLR) at the top of atmosphere (TOA) to specific humidity in clear sky conditions. Results are presented for (a) January and (b) July cases. The colour contour intervals are in $Wm^{-2}g^{-1}kg$.

The sensitivity of OLR to atmospheric temperature in clear-sky conditions is displayed in Fig. 35. One can see that the sensitivity structures are rather symmetric about the equator between the northern and southern winter, though the sensitivity at high latitudes in the northern summer hemisphere is stronger than in the southern summer hemisphere. Generally, the sensitivities are largest over tropical areas and decrease toward the poles. In the vertical, the main maximum stays on the northern hemisphere, at around 500 hPa (model level L39) in the winter case and between 550-650 hPa (L40 - L43) in the summer case. The second maxima are near to 850 hPa (L49) in the winter hemisphere. They are located close to 20N and 20S, respectively.
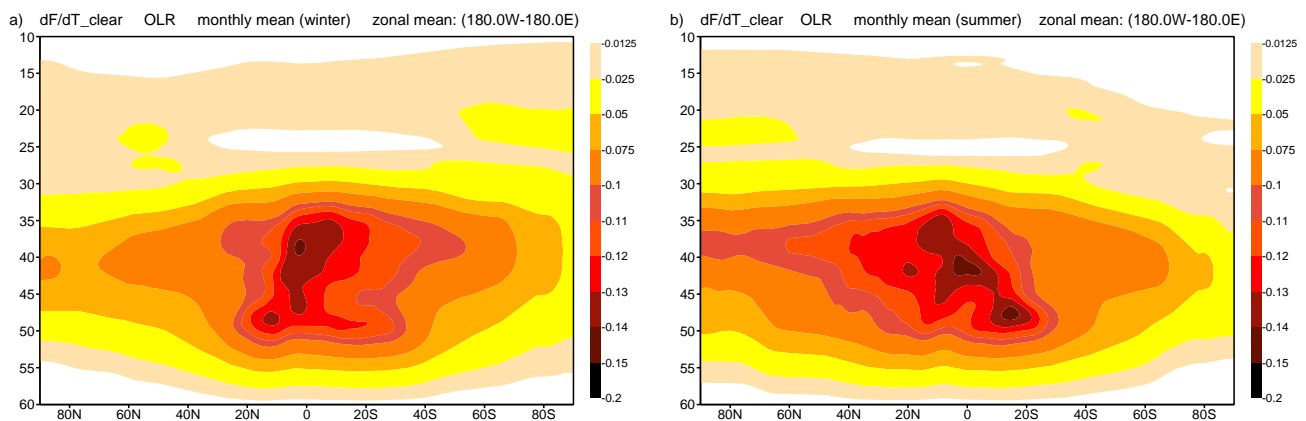
Figure 35: Same as in Fig. 34, but for the sensitivity to temperature. The colour contour intervals are in $Wm^{-2}K^{-1}$.

For illustration, in the maximum OLR sensitivity to temperature (0.15 W m^{-2} K^{-1}), the temperature perturbation of 1 K can produce an OLR increase equivalent to that of a 0.15 g kg^{-1} specific humidity perturbation in the lower troposphere. On the contrary, the maximum sensitivity to specific humidity (30-35 W m^{-2} g^{-1} kg) at high latitudes (the model levels L26-L29 $\sim$ 100 - 180 hPa) leads to an OLR increase, which is similar to what is obtained for a temperature perturbation of about 0.03 K at approximately the same altitudes (the model levels L28-L29 $\sim$ 150 - 180 hPa).

(b) Sensitivity w.r.t. surface temperature

Figure 36 displays the structure of the sensitivity of the OLR to the surface temperature for winter (a) and summer (b) cases in clear sky conditions. The tropical areas together with the hot and humid sub-tropical areas show the smallest sensitivities. The sensitivities tend to increase from the tropics to the polar regions. They reach maximum values over the continents: the regions with high orography and the areas with the dry surface and consequently drier atmosphere, as the Sahara desert. The high values are also observed in the polar regions, especially during summer in the southern hemisphere, where the maximum summer values over the Antarctic are moved over the contiguous oceans during winter. On the northern hemisphere, the sensitivity over the oceans is generally smaller than over the continent. This can be associated with updraft motions in the fronts appearing very often over the oceans.
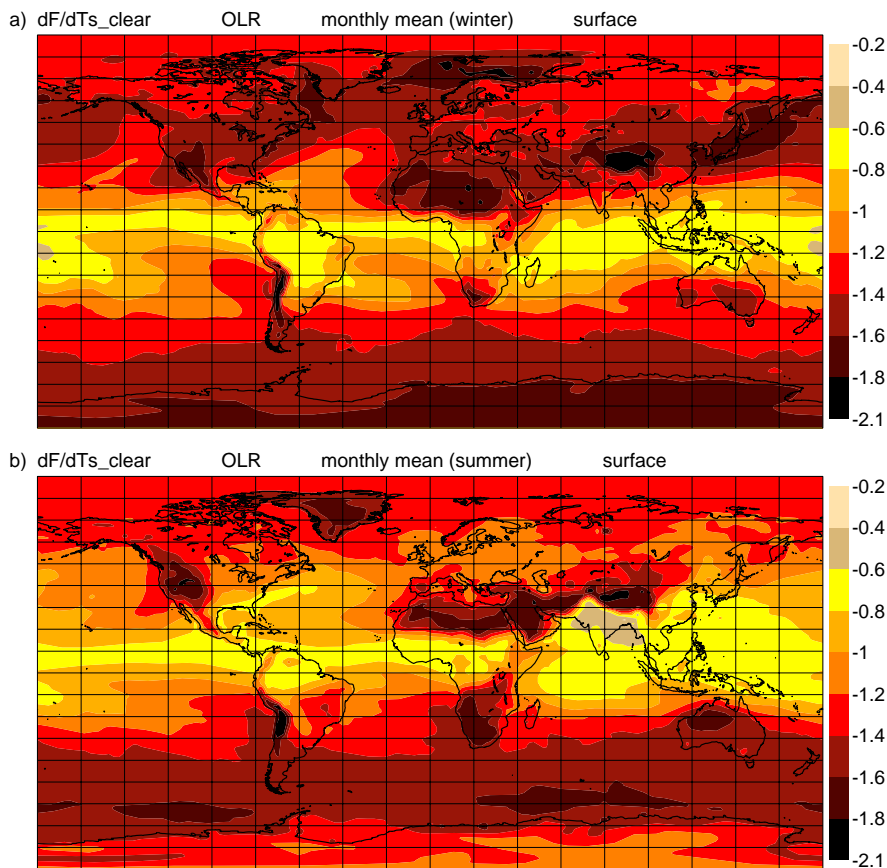
Figure 36: Sensitivity of the upward longwave radiation flux at the TOA (Wm^{-2}K^{-1}) to surface temperature in clear sky conditions. (a) for January and (b) for July.

The areas of relatively small sensitivity correspond to areas with high total column water vapour (ITCZ, South America). On the contrary, areas with high sensitivity are linked to dry areas (Sahara, South West USA, Atacama, Kalahari, Tibet, Australian desert).

Within the range of validity of the tangent-linear approximation for adjoint of the radiation schemes, an increase of OLR at the TOA by 1 W m^{-2} is equivalent to increasing temperature by 1.66 K in the tropics (at sensitivity 0.6 W m^{-2} K^{-1}), by 0.85 K in the mid-latitudes (at sensitivity 1.2 W m^{-2} K^{-1}) and by 0.5 K in the areas of high sensitivities (2 W m^{-2} K^{-1}).

The sensitivity of OLR to the surface temperature for cloudy-sky cases (Fig. 37) is overall smaller than for clear sky conditions. Here the latitude dependence does not play an essential role. The smallest sensitivities are observed not only over the tropics, but also over the mid-latitude oceans. Between these minima over the oceans, there are bands of increased sensitivity over the subtropical oceans. The areas of maximum sensitivity correspond to relatively clear sky areas, so the effect of clouds is simply to screen the high sensitivities seen in Fig. 36. In the southern polar region, the maximum sensitivity for cloudy conditions stays over the continent for both seasons. Similarly, as for clear sky conditions, the sensitivity is large over mountains (the Rocky Mountains, the Tibetan Plateau) and over the dry regions (north Africa, part of Australia, ...).
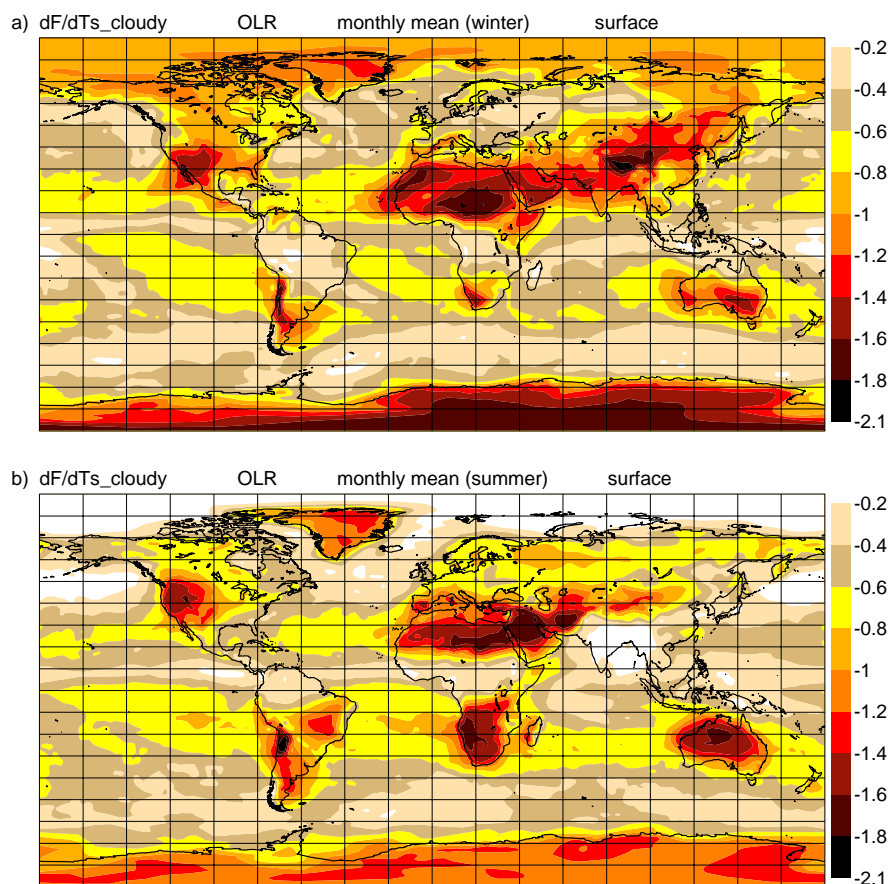
Figure 37: Same as in Fig. 36, but for cloudy conditions.

The adjoint sensitivity technique described in section 5.1.1 is used not only to investigate the spatial patterns of sensitivity, but also to study a diurnal cycle of sensitivity at different geographical locations. Figure 38 shows sensitivity of the longwave upward radiation at the TOA with respect to surface temperature for tropical moist Africa (black line) and dry Sahara (red line). In the dry climate, there is a well pronounced diurnal cycle with the maximum sensitivity at the time of the highest insolation. The minimum is reached close to the sunrise. The sensitivity is thus directly linked to the temperature changes here - the high sensitivity corresponds to the high temperature and the low sensitivity to low one. For the tropical moist Africa, the sensitivity is much smaller as

clouds obscure the surface, and the diurnal cycle of the skin temperature is smaller and has a limited influence on the OLR due to a larger total column water vapour.
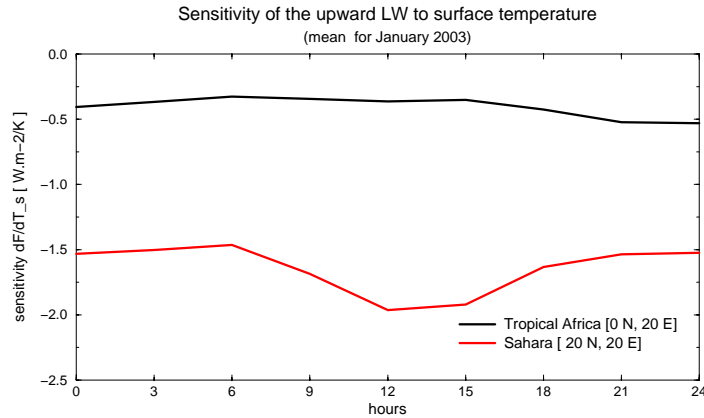
Figure 38: Diurnal cycle of sensitivity of the upward longwave radiation flux at the TOA to surface temperature $(Wm^{-2}K^{-1})$ in the tropical moist Africa (black) and dry Sahara (red) for January case.

(c) Cloudy-sky case

The sensitivity structures in cloudy conditions are more complex since clouds affect radiation by absorption and reflection, and radiation affects clouds through heating and cooling of the atmosphere. Adjoint sensitivity in cloudy conditions is only averaged over the cases where the clouds are present in the basic state.

Sensitivity of the shortwave radiation flux at the TOA with respect to cloud fraction is presented for the winter and summer cases in Fig. 39. The shortwave radiation fluxes are most influenced by the warmer water clouds, particularly in the southern summer hemisphere because of the increased insolation during the southern summer. During the northern summer, the maximum sensitivity in the mid-latitudes is vertically spread between model levels L42-L51 (approximately between 600 and 900 hPa) because of the increased convective activity in this region. High values of sensitivity are also observed at model levels L39-L43 ($\sim$ 500-650 hPa) in the tropics for both cases. The winter time high latitudes are insensitive areas, since an increase in cloud fraction has little additional reflective effect on the outgoing shortwave radiation over snow and ice at those latitudes.
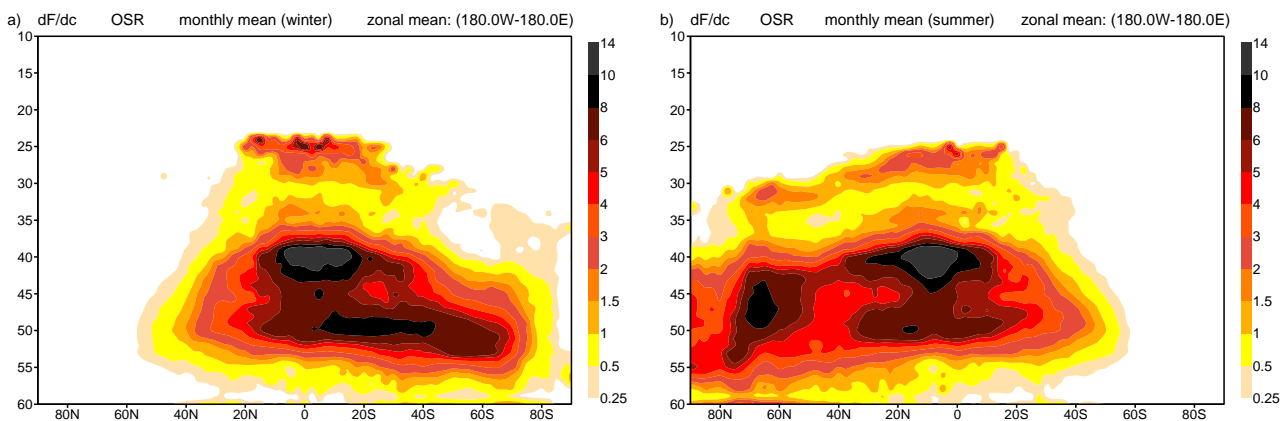
Figure 39: The zonally averaged sensitivity of the upward shortwave radiation flux at the top of atmosphere (TOA) to cloud fraction. Results are presented for (a) January and (b) July cases. The colour contour intervals are in $Wm^{-2}cloud fr^{-1}$.

The longwave sensitivity to cloud fraction is rather different (Fig. 40). Here the greatest sensitivity occurs when changes to the amount of cold high cloud occur, with a subsidiary maximum at the freezing level. The high sensitivity to middle-level clouds is a consequence of the variation in cloud optical thickness at the ice/mixed phase and mixed phase/liquid transitions. The large sensitivities in the tropics are located near the tropopause similarly to the OLR sensitivity w.r.t. specific humidity (Fig. 34). At low altitudes, the clouds do not have a temperature much colder than that of the surface, so their presence has little effect on the upward longwave radiation at TOA.
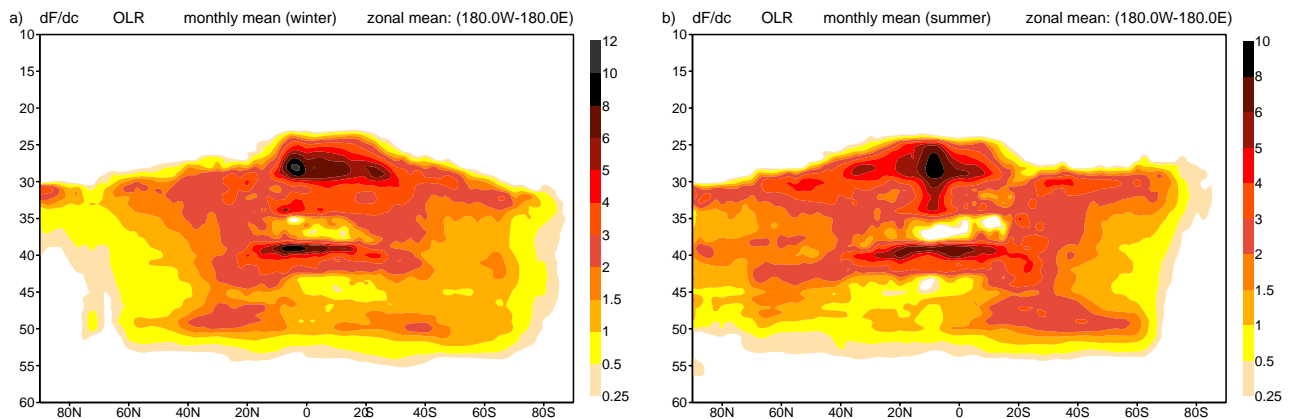
Figure 40: The zonally averaged sensitivity of the upward longwave radiation flux at the top of atmosphere (TOA) to cloud fraction. Results are presented for (a) January and (b) July cases. The colour contour intervals are in $Wm^{-2}cloud fr^{-1}$.

Figures 41 and 42 display the sensitivity of the upward shortwave radiation flux at TOA w.r.t. to cloud liquid and ice water, respectively. Maximum shortwave radiation sensitivity is seen over well-lit areas with a high surface albedo. Given the well-known shape of the dependence of cloud reflectance and cloud emissivity on the cloud water path, the shortwave radiation is mostly sensitive in areas of middle and lower-level clouds, i.e. clouds with relatively large amounts of liquid water.
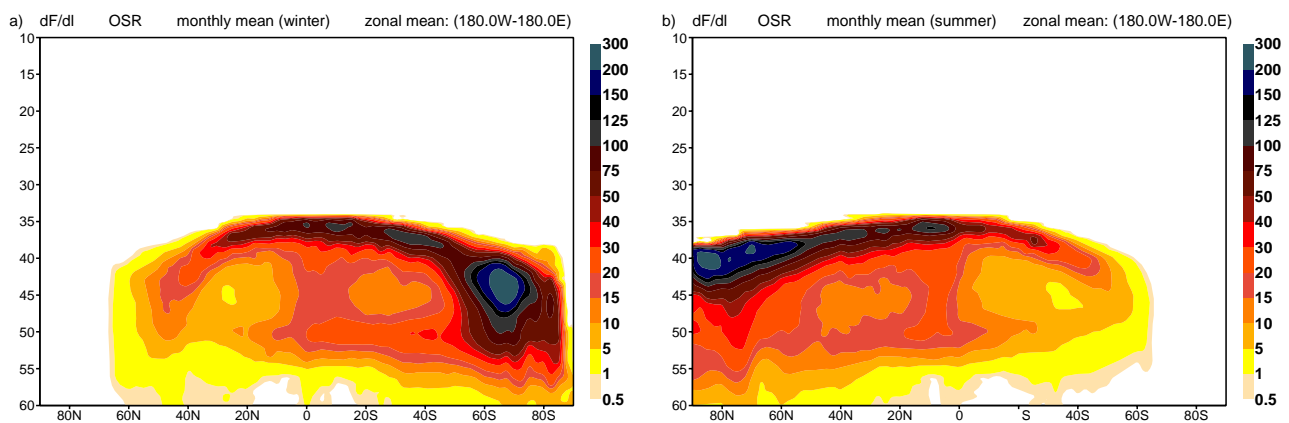
Figure 41: The zonally averaged sensitivity of the upward shortwave radiation flux at the top of atmosphere (TOA) to cloud liquid water content. Results are presented for (a) January and (b) July cases. The colour contour intervals are in $Wm^{-2}g^{-1}kg$.

The longwave radiation is very sensitive to change in the water content of the highest water clouds (Fig. 43). Cloud longwave emissivity saturates much more quickly than cloud shortwave reflectance with increasing integrated cloud water path. For the same water content, liquid water emissivity is higher than ice emissivity.

The OLR sensitivity to cloud ice water content (Fig. 44) has a similar spatial structure as the OLR sensitivity
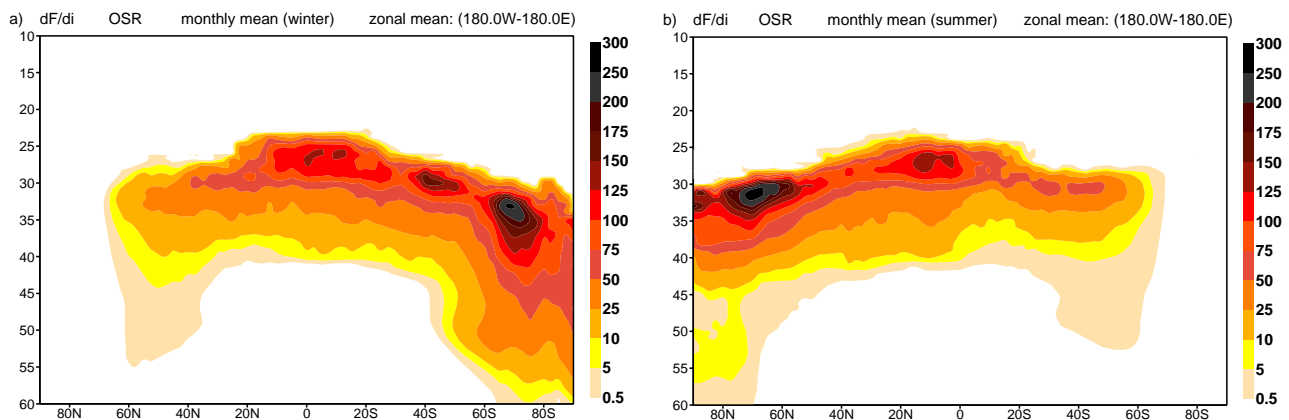
Figure 42: Same as in Fig. 41, but for the sensitivity to cloud ice water content.

to specific humidity (see Fig. 34). Finally, the high sensitivity of OLR to a change in the ice content of ITCZ clouds reflects the larger cloud fraction over this latitude band.
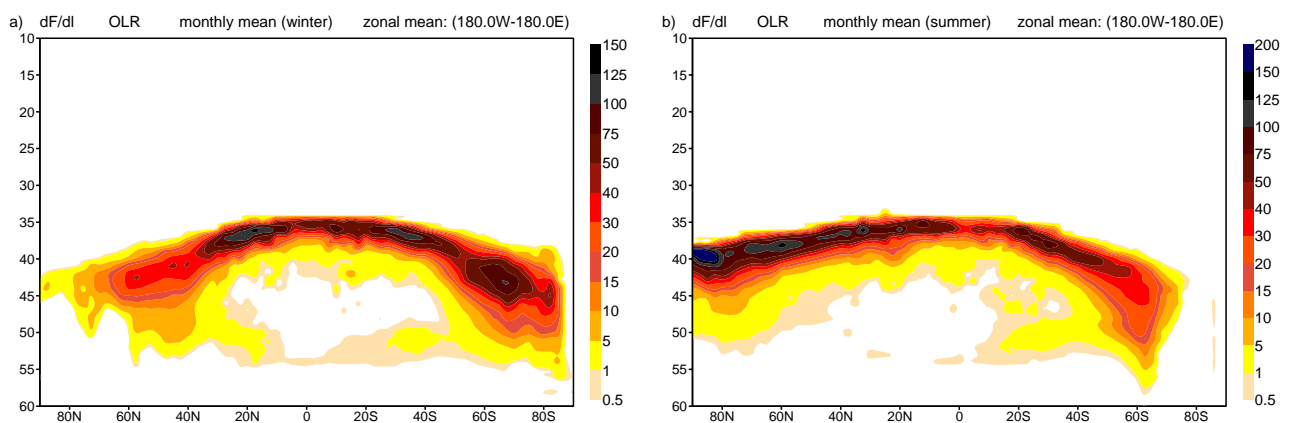
Figure 43: The zonally averaged sensitivity of the upward longwave radiation flux at the top of atmosphere (TOA) to cloud liquid water content. Results are presented for (a) January and (b) July cases. The colour contour intervals are in $Wm^{-2}g^{-1}kg$.
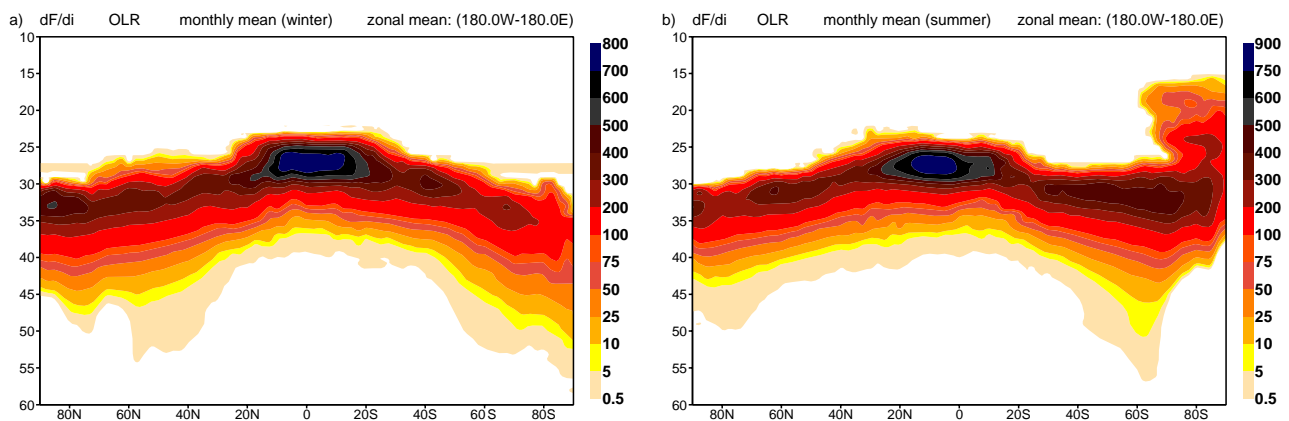
Figure 44: Same as in Fig. 43, but for the sensitivity to cloud ice water content.

To summarize, the evaluation of the Jacobians of radiation fluxes by the adjoint technique has confirmed results usually obtained by more traditional approaches: To decrease the upward longwave radiation flux at the TOA, an increase of cloudiness is required, which may come from an increase in specific humidity and/or a decrease in temperature. The maximum sensitivity is located at the level of the highest clouds. To increase the upward shortwave radiation flux at the TOA, an increase in the radiatively effective cloudiness is required involving increase in some or all of cloud cover, cloud liquid and ice water contents. For shortwave radiation, the sensitivity to specific humidity is much smaller.

This study also shows which variables would be modified and over which vertical extent if observations of the TOA radiation fluxes were used in data assimilation. As shown here, the sensitivity of the OLR is limited to the highest level clouds, and will therefore lead to ambiguity in the retrieval of cloud profiles if OLR is the only observation used. This study further demonstrates the need for additional observations on the vertical structure of clouds that should be provided by future satellite missions (EarthCARE, CloudSat, ...). There are other issues which can play a role in data assimilation. As $\partial F / \partial q \mid_{clear}$ has the same sign as $\partial F / \partial q \mid_{cloudy}$ (not shown), the sensitivity to specific humidity in clear sky conditions can help to trigger new clouds in situations close to cloud formation. On the other hand, if the assimilation system does not succeed in initiating clouds by modifying the control variables in the minimization process and if no other observations are used, such sensitivity could lead to an inadequate modification of the specific humidity in order to get closer to the radiation observations.

The study reported here demonstrates the usefulness of the concept of the adjoint sensitivity in providing the 4-dimensional patterns of sensitivity allowing a detailed analysis of (some of) the interactions between radiation transfer and other atmospheric processes. For the purpose of sensitivity calculations, the adjoint technique is much more efficient than the traditional way of perturbing the input variables one by one. The sensitivity of the shortwave and longwave radiation fluxes in clear-sky and cloudy conditions requires four calculations with the adjoint technique. To deal only with the sensitivity to temperature, surface temperature, specific humidity, cloud cover, cloud liquid and ice water content would require 5 x (number of levels) +1 calculations in the traditional approach. The potential of the technique can be further widened. Simply by considering new parameters as input variables, sensitivity of the TOA and surface radiation fluxes to surface longwave emissivity, surface albedo, concentration of trace gases, distribution and optical properties of aerosols, cloud optical properties including the effective dimension of cloud particles and the liquid/ice water cloud phase can be obtained at minimum cost using the same method. This present study will be extended to these variables in the near future.

6   Conclusions and perspectives

Overview of the ECMWF model performance, model changes and data assimilation experiments related to clouds and radiation have been given in order to emphasize the need for complementary datasets such as those proposed for EarthCARE. The results of the described experiments give an evidence on the potential importance of EarthCARE like mission, which will provide the simultaneous measurements of the vertical structure and horizontal distribution of cloud and aerosol fields together with outgoing radiation, for an improved understanding cloud-radiation interactions, as well as energy and water fluxes in the atmosphere. Such data will be an invaluable source of information for comprehensive model validation, the improvement of physical parametrizations, and could be used as an input for data assimilation systems and their development.

The recent changes related to clouds and radiation in the ECMWF model have been described. The systematic model errors of the ECMWF model have been recently examined for four month atmospheric climate runs in the study of Jung and Tompkins (2003), where an assessment of the ECMWF model in simulating cloud related features of the atmosphere has also been given. In this report, the results of the extended study are presented, when statistics was done for one year experiments, a wider range of up-to-date observations was used, and an impact of the recent improvements and changes in the cloud and radiation parametrizations was indicated. Despite the significant improvements in the recent version of the operational model, a number of problematic aspects, to be still solved, was identified. This underlines the importance for future satellite missions to generate consistent measurements of radiative fluxes, cloud fractional coverage and cloud water/ice contents to allow more comprehensive evaluations of cloud-radiation interactions in NWP models, and hence to improve their parametrization. Uncertainties in the vertical profiles of clouds also limit the accuracy of numerical weather prediction. Observations of cloud profiles over the globe are urgently required for further evaluations of the models and an improvement of their ability to provide reliable weather forecasts.

An important step in the development of the assimilation of cloud-affected observations is introducing the cloud-radiation processes in the assimilating model. Linearized radiation schemes (Janisková *et al.* 2002a) and a linearized cloud scheme (Tompkins and Janisková 2004) have been developed for variational data assimilation of cloud related observations. The shortwave radiation is based on a linearization of the operational ECMWF code. To reduce the computational cost, a combination of artificial neural network and mean Jacobian matrices is used for the linearized longwave radiation scheme.

In the operational ECMWF data assimilation system, the radiation scheme is still combined with the simple diagnostic cloud scheme (Slingo 1987), which has a number of weaknesses. To improve the description of cloud processes in the linearized model, the attempt was made to develop a scheme which retains the most important features of the ECMWF nonlinear prognostic cloud scheme, while removing much of the complexity and as many discrete transitions as possible. The scheme thus retains a simplified link to convective detrainment, and uses a similar formulation for the production of precipitation. A flexible statistical cloud scheme approach is used, where the diagnosis of stratiform cloud fraction and condensate amount depend on assumptions concerning subgrid-scale fluctuations. A novel aspect of the new scheme is the treatment of precipitation evaporation that specifically takes this subgrid distribution of humidity variability into account. When using the prognostic scheme of the ECMWF forecast model as a metric, the new scheme improves on the current assimilation cloud scheme for many parameters such as cloud cover and ice water content, both in the tropics and mid-latitudes. In particular the new diagnostic scheme addresses the overriding weakness of the current diagnostic scheme which produces almost no precipitation in the tropics. Tangent linear and adjoint versions of the new scheme have been constructed and with some regularization to prevent instability, it is demonstrated that the scheme can successfully and robustly perform tangent linear integrations for a 12 hour window, and significantly improves the tangent linear approximation of the simplified linearized model to finite difference calculations using the full nonlinear forecast model. With its physical link between cloud properties and the thermodynamic control

variables of temperature and humidity, the new scheme provides the opportunity to develop a system which can assimilate both cloud and precipitation information. Moreau *et al.* 2004 have used the new cloud scheme in combination with the improved linearized convection scheme of Lopez and Moreau (2004) for rainfall and microwave brightness temperature assimilation. Chevallier *et al.* (2004) discussed the possibility of using the scheme to assimilate AIRS[13] and Meteosat brightness temperatures in a 4D-Var framework, and this will be further investigated.

1D-Var experiments have been carried out using observations from the Atmospheric Radiation Measurement (ARM) Program. Measurements of both cloud properties and radiative fluxes have been used in these feasibility studies. The ARM data sets also offer an ideal platform to study the impact of assimilation of new observations from cloud radars or lidars in preparation for upcoming satellite missions. The aim of these studies has been to show ability of 1D-Var, employing different parametrization schemes, to modify dynamical variables, temperature and humidity, which is important for consistency between cloud parameters and dynamics in order not to lose the analyzed cloud information within a few model time steps. Another purpose of the study has been to examine behaviour of the new moist parametrization schemes (cloud and convection) in 1D-Var assimilation of the cloud related observations and to asses situations when convective clouds are dominant. Assimilation of radar reflectivities over the ARM SGP site appeared to be promising and will be further explored in the near future. Verification with independent observations showed advantages and deficiencies of including profiling versus integrated measurements. It was shown that the synergy of different cloud observations is the most beneficial toward improving the performance of the cloud assimilation system. The 1D-Var assimilation of observations from the ARM TWP sites has shown a capability to improve the analysis of temperature and specific humidity when using the new moist parametrization schemes for cloud and convection processes in convective situations. However, it has also revealed some weaknesses of the 1D-Var system on those sites, such as an ambiguity in the retrieval when the surface humidity observations are not available as well as the lack of complementary observations to the surface observations, such as the cloud radar reflectivities used at ARM SGP.

Feasibility studies in a 1D-Var framework will continue using data from field experiments (e.g. ARM, CLARE[14]) and from some satellites (AIRS, IASI[15], ATOVS - currently available, CloudSat - forthcoming in the near future) in order to assess further how cloud observations can be used for analysis purposes. Data from the cloud radar at Chilbolton (UK), South Great Plains (Oklahoma), North Slope of Alaska and Tropical West Pacific will be used for the periods with available cloud profile observations collocated with radiative measurements in the different meteorological regimes. Moreover, 1D-Var assimilation experiments using either observations from the field experiments or from satellites will represent preparatory studies for the future 4D-Var assimilation of cloud-radiation observations.

Sensitivity of the radiation schemes to temperature, humidity and cloud properties has been investigated using the adjoint technique. The study has shown which variables can be modified when certain observations of the TOA radiation fluxes are used in data assimilation. It has also indicated the vertical extent of the influence of such observations. The limited extension in the vertical of the areas sensitive to cloud properties related to the value of the TOA radiation demonstrated the need for complementary observations of cloud profiles. Such information should be available from future satellite missions, among them EarthCARE. This sensitivity study will be extended to other variables, for instance concentration of trace gases, distribution and optical properties of aerosols, cloud optical properties including the effective dimension of cloud parameters.

---

[13]Atmospheric Infrared Radiometric Sounder
[14]Cloud Lidar and Radar Experiment
[15]Infrared Atmospheric Sounder Interferometer

Acknowledgements

7   References

Beesley, J.A., Bretherton, C.S., Jakob, C., Andreas, E.L., Intrieri, J.M. and Uttal, T.A. ,2000: A comparison of cloud and boundary layer variables in the ECMWF forecast model with observations at the Surface Heat Budget of the Arctic ocean (SHEBA) ice camp. *J. Geophys. Res.*, **105D**, 12337-12350.

Benedetti, A. and Janisková, M. , 2004: Advances in cloud assimilation at ECMWF using ARM radar data. *Abstract from ISSCP.*, 4 pp.

Chevallier, F., Morcrette, J.-J., Chéruy, F. and Scott, N.A. , 2000: Use of a neural network-based longwave radiative transfer scheme in the ECMWF atmospheric model. *Q. J. R. Meteorol. Soc.*, **126**, 761-776.

Chevallier, F., Bauer, P., Kelly, G., Mahfouf, J.-F., Jakob, C. and McNally, T. , 2000: Requirements for the assimilation of cloudy radiances. ECMWF/EuroTRMM Workshop on Assimilation of Clouds and Precipitation. Reading, UK, 6-9 November 2000

Chevallier, F. and Morcrette, J.-J. , 2000: Comparison of model fluxes with surface and top-of-the-atmosphere observations. *Mon. Weather Rev.*, **128**, 3839-3852.

Chevallier, F., Bauer, P., Kelly, G., Jakob, C. and McNally, T. , 2001: Model clouds over oceans as seen from space: comparison with HIRS/2 and MSU radiances. *J. Climate*, **14**, 4216-4229.

Chevallier, F. and Mahfouf, J.-F. , 2001: Evaluation of the Jacobians of infrared radiation models for variational data assimilation. *J. Appl. Meteorol.*, **40**, 1445-1461.

Chevallier, F., Bauer, P., Mahfouf, J.-F. and Morcrette, J.-J., 2002: Variational retrieval of cloud cover and cloud condensate from ATOVS data. *Q. J. R. Meteorol. Soc.*, **128**, 2511-2526.

Chevallier, F. and Kelly, G. , 2002: Model cloud as seen from space: Comparison with SSM/I observations. *Mon. Weather Rev.*, **130**, 712-722.

Chevallier, F., Lopez, P., Tompkins, A.M., Janisková, M. and Moreau, M., 2004: The capability of 4D-Var systems to assimilate cloud-affected satellite infrared radiances, *Q. J. R. Meteorol. Soc.*, **130**, 917-932.

Clothiaux, E.E., Ackerman, T.P., Mace, G.G., Moran, K.P., Marchand, R.T., Miller, M.A. and Martner, B.E. , 2000: Objective determination of cloud heights and radar reflectivities using a combination of active remote sensors at the ARM CART sites. *J. Appl. Meteor.*, **39**, 645-665.

Courtier, P., Thépaut, J.-N. and Hollingsworth, A. , 1994: A strategy for operational implementation of 4D-Var using an incremental approach. *Q. J. R. Meteorol. Soc.*, **120**, 1367-1387.

Derber, J. and Bouttier, F. ,1999: A reformulation of the background error covariance in the ECMWF global data assimilation system. *Tellus*, **51A**, 195-221.

Dubuisson, P.J., Buriez, J.C. and Fouquart, Y. , 1996: High spectral resolution solar radiative transfer in absorbing and scattering media: Application to the satellite simulation. *J. Quant. Spectrosc. Radiat. Transfer*, **55**, 103-126.

Ebert, E.E. and Curry, J.A. , 1992: A parametrization of ice optical properties for climate models. *J. Geophys. Res.*, **97D**, 3831-3836.

European Space Agency , 2004: Reports for mission selection, EarthCARE - Earth Clouds, Aerosols and Radiation Explorer. The six candidate Earth explorer missions. ESA SP-1279(1), 60 pp.

Fillion, L. and Mahfouf, J.-F. , 2003: Jacobians of an operational prognostic cloud scheme. *Mon. Weather Rev.*, **131**, 2838-2856.

Fouquart, Y. , 1987: Radiative transfer in climate models. *Physically Based Modelling and Simulation of Climate and Climatic Changes*, M.E. Schlesinger, Ed., Kluwer Acad. Publ., 223-284.

Fouquart, Y. and Bonnel, B. , 1980: Computations of solar heating of the earth's atmosphere: a new parametrization. *Beitr. Phys. Atmos.*, **53**, 35-62.

Gérard, E. and Saunders, R.W. ,1999: Four-dimensional variational assimilation of Special Sensor Microwave/Imager total column water vapour in the ECMWF model. *Q. J. R. Meteorol. Soc.*, **125**, 3077-3101.

Gilbert, J.-C. and Lemaréchal, C. , 1989: Some numerical experiments with variable-storage quasi-Newton algorithms. *Math. Programming*, **45**, 407-435.

Gregory, D., Morcrette, J.-J., Jakob, C.,Beljaars, A.C.M. and Stockdale, T. , 2000: Revision of convection, radiation and cloud schemes in the ECMWF Integrated Forecasting System. *Q. J. R. Meteorol. Soc.*, **126**, 1685-1710.

Heymsfield, A.J. and Donner, L.J. , 1990: A scheme for parameterising ice cloud water content in general circulation models. *J. Atmos. Sci.*,**47**, 1865-1877.

Hogan, R.J., Jakob, C. and Illingworth , 2001: Comparison of ECMWF winter-season cloud fraction with radar-derived values. *J. Atmos. Sci.*, **40**, 513-525.

Holtslag, A.A.M. and Moeng, C.-H. , 1991: Eddy diffusivity and countergradient transport in the convective atmospheric boundary layer. *J. Atmos. Sci.*, **48**, 407-435.

Jakob, C. , 1999: Cloud cover in the ECMWF reanalysis. *J. Climate*, **12**, 947-959.

Jakob, C. , 2000: The representation of cloud cover in atmospheric general circulation models. Ph.D. thesis, Ludwig-Maximilians-Universität, Munich, Gremany, 193 pp.

Jakob, C. and Klein, S.A. , 2000: A parametrization of the effects of cloud and precipitation overlap for use in general circulation models. *Q. J. R. Meteorol. Soc.*, **126C**, 2525-2544.

Jakob, C. , 2002: Ice clouds in numerical weather prediction models: Progress, problems and prospects. In: D.K. Lynch, K. Sassen, D. Starr and G. Stephens, eds., *Cirrus*, pp. 327-345, Oxford University Press.

Janisková, M. , 2001: Preparatory studies for the use of observations from the Earth Radiation Mission in Numerical Weather Prediction. *Contract report to the European Space Agency*, 79 pp.

Janisková, M., Thépaut, J.-N. and Geleyn, J.-F. , 1999: Simplified and regular physical parametrizations for incremental four-dimensional variational assimilation. *Mon. Weather Rev.*, **127**, 26-45.

Janisková, M., Mahfouf, J.-F., Morcrette, J.-J. and Chevallier, F., 2002a: Linearized radiation and cloud schemes in the ECMWF model: Development and evaluation. *Q. J. R. Meteorol. Soc.*, **128**, 1505-1527.

Janisková, M., Mahfouf, J.-F. and Morcrette, J.-J., 2002b: Preliminary studies on the variational assimilation of cloud-radiation observations. *Q. J. R. Meteorol. Soc.*, **128**, 2713-2736.

Jung, T. and Tompkins, A., 2003: Systematic errors in the ECMWF forecasting system *ECMWF Technical Memorandum*, **422**, 72 pp.

Kessler, E., 1969: On the distribution and continuity of water substance in atmospheric circulation. *Meteorol. Monog.*, **10**, American Meteor. Soc., Boston, Mass.

Klein, S. A. and Jakob, C., 1999: Validation and sensitivities of frontal clouds simulated by the ECMWF model. *Mon. Weather Rev.*, **127**, 2514-2531.

Lalaurette, F., Ferranti, L., Ghelli, A., Saetra, O. and Böttger, H., 2003: Verification statistics and evaluations of ECMWF forecasts in 2001-2992. *ECMWF Technical Memorandum*, **414**

Le Dimet, F.-X. and Talagrand, O., 1986: Variational algorithms for analysis and assimilation of meteorological observations. *Tellus*, **38A**, 97-110.

Li, Z. and Navon, I.M., 1998: Adjoint sensitivity of the Earth's radiation budget in the NCEP medium-range forecasting model. *J. Geophys. Res.*, **103**, 3801-3814.

Lopez, P. and Moreau, E., 2004: A convection scheme for data assimilation purposes: Description and initial tests. *ECMWF Technical Memorandum*, **411**.

Mace, G.G., Jakob, C. and Moran, K.P., 1998: Validation of hydrometeor occurrence predicted by the ECMWF model using millimeter wave radar data. *Geophys. Res. Lett.*, **25**, 1645-1648.

Mahfouf, J.-F., 1999: Influence of physical processes on the tangent-linear approximation. *Tellus*, **51A**, 147-166.

Mahfouf, J.-F. and Rabier, F., 2000: The ECMWF operational implementation of four-dimensional variational assimilation. Part II: Experimental results with improved physics. *Q. J. R. Meteorol. Soc.*, **126**, 1171-1190.

Miller, S.D., Stephens, G.L. and Beljaars, A.C.M., 1999: A validation survey of the ECMWF prognostic cloud scheme using LITE, *Geophys. Res. Lett.*, **26**, 1417-1420.

Mlawer, E.J., Taubman, S.J., Brown, P.D., Iacono, M.J. and Clough, S.A. 1997: Radiative transfer for in-homogeneous atmosphere: RRTM a validated correlated-k model for the longwave. *J. Geophys. Res.*, **102**, 16663-16682.

Morcrette, J.-J., 1989: Description of the radiation scheme in the ECMWF operational weather forecast model. *Research Department Tech.Memo*, **165**, 26 pp.

Morcrette, J.-J., 1991: Radiation and cloud radiative properties in the ECMWF operational forecast model. *J. Geophys. Res.*, **96D**, 9121-9132.

Morcrette, J.-J., 1998: Impact of validated radiative transfer scheme, RRTM on the ECMWF model climate and 10-day forecasts. *ECMWF Technical Memorandum*, **252**, 47 pp.

Morcrette, J.-J., Clough, S.A., Mlawer, E.J. and Iacono, M.J., 1998: Impact of validated radiative transfer scheme, RRTM on the ECMWF model climate and 10-day forecasts. *ECMWF Technical Memorandum*, **252**, 47 pp.

Morcrette, J.-J. and Jakob, C., 2000: The response of the ECMWF model to changes in the cloud overlap

assumption. *Mon. Weather Rev.*, **128**, 876-887.

Morcrette, J.-J. , 2001: Assessment of the ECMWF model cloudiness and surface radiation fields at ARM-SGP site. *ECMWF Technical Memorandum*, **327**, 41pp.

Morcrette, J.-J. , 2002: Assessment of the ECMWF model cloudiness and surface radiation fields at the ARM SGP site. *Mon. Weather Rev.*, **130**, 257-277.

Moreau, E., Lopez, P., Bauer, P., Tompkins, A.M., Janisková, M. and Chevallier, F. , 2004: Variational retrieval of temperature and humidity profiles using rain rates versus microwave brightness temperatures. *Q. J. R. Meteorol. Soc.*, **130**, 827-852.

Ohmura, A., Dutton, E.G., Forgan, B., Frohlich, C., Gilgen, H., Hegner, H., Heimo, A., Konig-Langlo, G., McArthur, B., Muller, G., Philipona, R., Pinker, R., Whitlock, C.H., Dehne, K., and Wild, M. , 1998: Baseline Surface Radiation Network (BSRN/WCRP): New precision radiometry for climate research. *Bull. Amer. Meteor. Soc.*, 79, 2115-2136.

Parrish, D.F. and Derber, J,C. , 1992: The National Meteorological Center's Spectral Statistical Interpolation Analysis System. *Mon. Weather Rev.*, **120**, 1747-1763.

Rabier, F., McNally, A., Andersson, E., Courtier, P., Unden, P., Eyre, J., Hollingsworth, A. and Bouttier, F. , 1998: The ECWMF implementation of three dimensional variational assimilation (3D-Var). Part II: Structure functions. *Q. J. R. Meteorol. Soc.*, **124**, 1809-1829.

Rabier, F., Järvinen, H., Klinker, E., Mahfouf, J.-F. and Simmons, A. , 2000: The ECMWF operational implementation of four-dimensional variational assimilation. Part I: Experimental results with simplified physics. *Q. J. R. Meteorol. Soc.*, **126**, 1143-1170.

Rossow, W.B. and Schiffer, R.A. , 1991: ISCCP cloud data products. *Bull. Amer. Meteor. Soc.*, **72**, 2-20.

Rossow, W.B. and Garder, L.C. , 1993: Cloud detection using satellite measurements of infrared and visible radiances for ISCCP. *J. Climate*, **6**, 2341-2369.

Rossow, W.B. and Schiffer, R.A. , 1999: Advances in understanding clouds from ISCCP. *Bull. Amer. Meteor. Soc.*, **80**, 2261-2287.

Simpson, J. and Wiggert, V. , 1969: Models of precipitating cumulus towers. *Mon. Weather Rev.*, **97**, 471-489.

Slingo, J.M. , 1987: The development and verification of cloud prediction scheme in the ECMWF model. *Q. J. R. Meteorol. Soc.*, **113**, 899-927.

Smith, E.A. and Shi, L. , 1992: Surface forcing of the infrared cooling profile over the Tibetan plateau. Part I: Influence of relative longwave radiative heating at high altitude. *J. Atmos. Sci.*, **49**, 805-822.

Stokes, G.M. and Schwartz, S.E. ,1994: The Atmospheric Radiation Measurement (ARM) Program: Programmatic background and design of the cloud and radiation tested. *Bull. Amer. Soc.*, **75**, 1201-1221.

Sundqvist, H., Berge, E. and Kristjánsson, J.E. , 1989: Condensation and cloud paranetrization studies with a mesoscale numerical weather prediction model. *Mon. Weather Rev.*, **117**, 1641-1657.

Teixeira, J. , 2001: Cloud fraction and relative humidity in a prognostic cloud fraction scheme. *Mon. Weather Rev.*, **126**, 1750-1753.

Teixeira, J. and Hogan, R. , 2002: Boundary layers clouds in a global atmospheric model: Simple cloud cover parametrization. *J. Climate*, **15**, 1261-1276.

Tiedtke, M. , 1993: Representation of clouds in large-scale models. *Mon. Weather Rev.*, **121**, 3040-3061.

Tiedtke, M. , 1996: An extension of cloud-radiation parameterization in the ECMWF model: The representation of sub-grid scale variations of optical depth. *Mon. Weather Rev.*, **124**, 745-750.

Tompkins, A.M. , 2002: A prognostic parametrization for the subgrid-scale variability of water vapor and clouds in large-scale models and its use to diagnose cloud cover. *J. Atmos. Sci.*, **59**, 1917-1942.

Tompkins, A.M. and Janisková, M. , 2004: A cloud scheme for data assimilation purposes: Description and initial tests. *Q. J. R. Meteorol. Soc.*, in press.

Tselioudis, G. and Jakob, C. , 2002: Evaluation of midlatitude cloud properties in a weather and climate model: Dependence on dynamic regime and spatial resolution. *J. Geophys. Res.* **107**, ...

van den Hurk, B.J.J.M., Viterbo, P., Beljaars, A.C.M. and Betts, A.K. , 2000: Offline validation of the ERA40 surface scheme. *ECMWF Technical Memorandum*, **295**, 42 pp.

Webb, M., Senior, C., Bony, S. and Morcrette, J.-J. , 2001: Combining ERBE and ISCCP data to assess clouds in the Hadley Centre, ECWMF and LMD atmospheric climate models. *Clim. Dyn.*, **17**, 905-922.

Wentz, F.J. , 1997: A well-calibrated ocean algorithm for SSM/I. *J. Geophys. Res.*, **102**, 8703-8718.

Wielicki, A.,Barkstrom, B.R., Harrison, E.F., Lee, R. B., Smith, G. L. and Cooper, J. E. , 1996: Clouds and the earth's radiant energy system (CERES): An earth observing system experiment., *Bull. Amer. Meteor. Soc.*, **77**, 853-868.